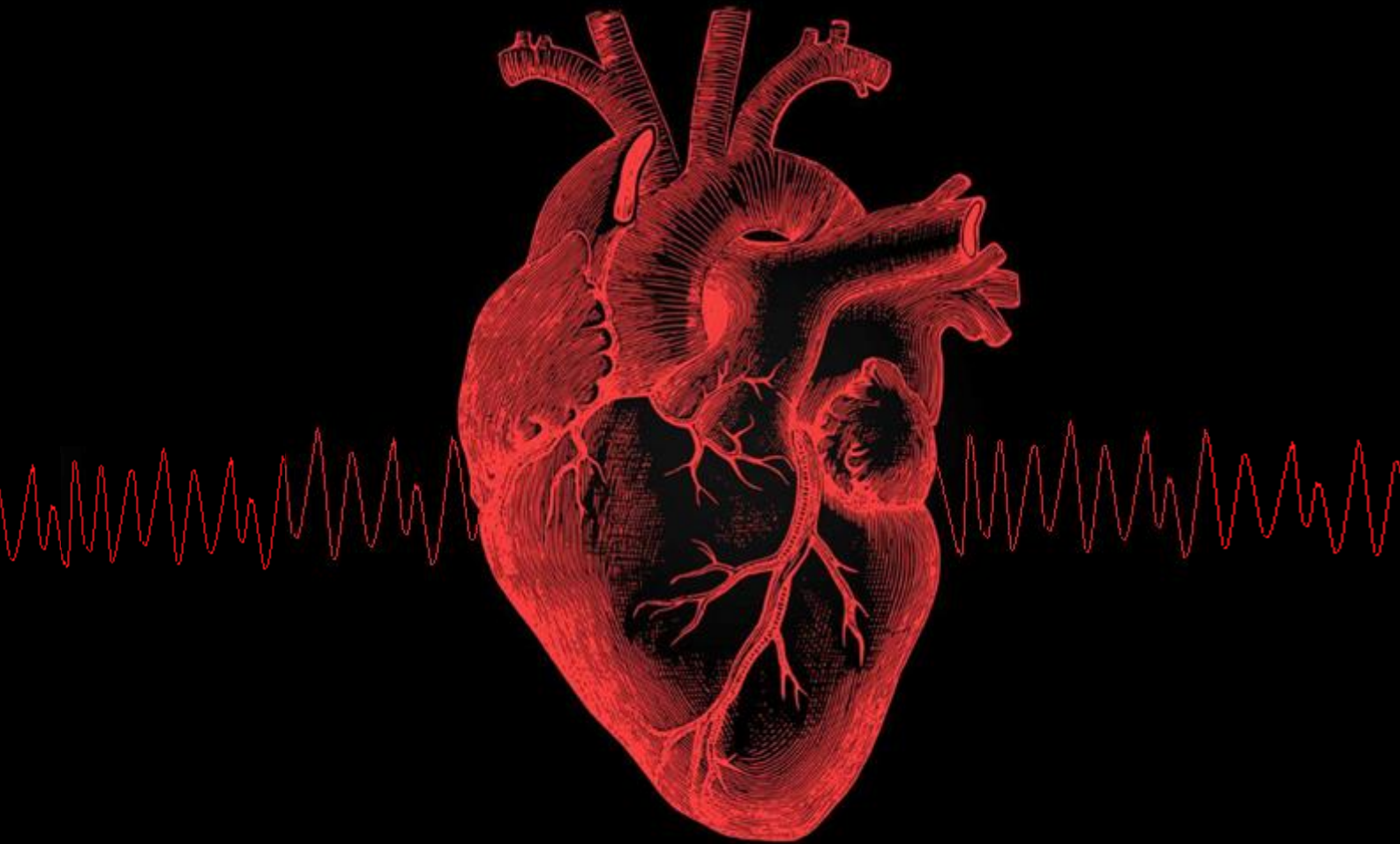


Electrocardiographic analysis of ventricular fibrillation:
a machine learning approach to identify a previous
myocardial infarction



Master's thesis

Technical medicine

S. Gantevoort

General information

Title	Electrocardiographic analysis of ventricular fibrillation: a machine learning approach to identify a previous myocardial infarction
Author	S. Gantevoort
Student number	s1179691
E-mail	serayaa_@hotmail.com
Date	Enschede, 31 August 2018

Organization

Address	Radboud University Medical Centre Geert Grooteplein Zuid 10 6525 GA Nijmegen
Department	Department of Cardiology

Institution

Address	University of Twente Drienerlolaan 5 7522 NB Enschede
Faculty	Faculty of Science and Technology
Master	Technical Medicine <i>Medical Sensing & Stimulation</i>

Committee

Graduation chairman and Technical supervisor	Prof. dr. H.J. Zwart
Medical supervisor	Dr. M.A. Brouwer, J. Thannhauser, MSc
Technical supervisor	Dr. ir. G. Meinsma
Process supervisor	Drs. R.J. Haarman - Linde
External member	Dr. E.J.F.M. ten Berge

Radboudumc

UNIVERSITY OF TWENTE.

Table of contents

Acknowledgements (dankwoord)	4
Summary	5
List of abbreviations	7
1. Introduction	9
2. Clinical Background	
§2.1 Anatomy and physiology of the heart	11
§2.2 Electrical activity in the heart.....	14
§2.3 Ventricular fibrillation	19
§2.4 Current research.....	22
3. Technical background	
§3.1 Introduction to Machine Learning	24
§3.2 Validation	25
§3.3 Support vector machine	27
4. Article: Identification of a previous myocardial infarction using ventricular fibrillation characteristics of the 12-leads electrocardiogram: A single lead model versus a multiple lead model	36
5. Sub-analyses	
§5.1 Gender.....	48
§5.2 Probabilistic outputs	53
§5.3 Infarct sizes.....	54
§5.4 New data	56
§5.5 Statistical approach	58
6. General discussion	61
7. General conclusion	62
8. References	63
Appendix	
A.1 Detrended fluctuation analysis.....	68
A.2 Probabilistic outcomes SVM	70
A.3 ROC curve	72
B.1 Baseline characteristics.....	75
B.2 VF characteristics for two study groups.....	77
B.3 Multiclass lead performances	78
B.4 VF characteristics - Gender	80

Acknowledgements (dankwoord)

Allereerst wil ik Marc Brouwer bedanken voor het mogelijk maken om af te studeren binnen de Cardiologie van het Radboud Universitair Medisch Centrum. Ik ben erg blij dat deze mogelijkheid zich heeft voor gedaan en kijk dan ook terug op een ontzettend leerzaam, maar ook erg gezellig, jaar. Dit jaar heb ik mede door deze afstudeerplek en begeleiding een kritischere en overtuigende houding weten te ontwikkelen en de uitspraak “Weet je het zeker, ook voor 100 euro?” zal ik dan ook zeker niet vergeten.

Hans Zwart en Gjerrit Meinsma wil ik graag bedanken voor de begeleiding vanuit de Universiteit Twente. Het was prettig om ook een blik en feedback van buiten de medische wereld te ontvangen, waarvoor dank.

In het bijzonder wil ik Jos en Joris bedanken voor de dagelijkse begeleiding en de kritische blik met betrekking tot mijn onderzoek. Mede door jullie heb ik het afgelopen jaar erg veel kennis opgedaan binnen de cardiologie en voor het verrichten van gedegen onderzoek. Waarvoor heel veel dank.

Ook wil ik mijn collega-studenten bedanken voor alle discussies, gezelligheid en borrels het afgelopen jaar. Zonder jullie zou het een doodse stilte geweest zijn en onder andere pizza's eten op de afdeling en Sinterklaas waren ontzettend gezellig.

Niet te vergeten dat ook mijn lieve vriendinnen een bijdrage hebben geleverd aan dit alles. Samen met jullie heb ik de afgelopen studiejaren ontzettend veel geleerd en veel plezier gehad. Maar natuurlijk hebben jullie ook support gegeven tijdens de afgelopen stages en ook dit afstudeerjaar. Heel erg bedankt lieve Karin, Kirsten, Marijn, Robin en Suzan. Dat we nog maar veel mooie reisjes mogen maken.

Tevens wil ik mijn lieve ouders, zusjes en schoonfamilie bedanken voor alle oprechte interesse, energie en de gegeven adviezen de afgelopen jaren. Ik waardeer het enorm dat jullie altijd achter mijn keuzes hebben gestaan en het vertrouwen in mij hebben gehad.

Pieter Jan, zonder jouw onvoorwaardelijke steun en positieve energie was dit alles ook zeker niet mogelijk geweest. Aan jou blik op zaken heb ik erg veel gehad. Fijn dat ik altijd bij je terecht kon, en jij altijd uit alles iets positiefs weet te halen.

Seraya Gantevoort

Nijmegen, Augustus 2018

Summary

Out-of-hospital cardiac arrest (OHCA) is one of the main causes of death and carries a poor prognosis. Ventricular fibrillation (VF) as initial rhythm is frequently observed in OHCA cases. Quantitative measures of the VF waveform have been investigated to optimize resuscitation strategies in the OHCA setting. It has already been demonstrated that these VF characteristics are related to arrest duration and shock success. Research has shown that myocardial infarction (MI) influences the VF waveform as well. MI, defined as myocardial cell necrosis due to prolonged ischemia, is the most common cause of VF and can only be diagnosed after restored circulation. Notably, an MI is commonly reversible, but cannot be determined in-field. As MI affects the VF waveform, it might be possible to identify MI using the VF waveform, potentially enabling patient tailored treatment of OHCA patients. Previous research has aimed to detect a previous MI in a controlled setting. In a proof of concept study, the potential of machine learning algorithms to identify an MI using a 12-lead electrocardiogram (ECG) seemed feasible. However, translation to the OHCA setting is limited, because in the acute setting only a single ECG-lead is measured by the defibrillator paddles. In light of the above, we investigated the ability of a single ECG-lead to differentiate between patient with and without a history of MI, in a controlled setting of implantable cardioverter defibrillator (ICD) implantations. In addition, we investigated whether multiple ECG-leads may be superior to the single ECG-lead approach. In follow-up on this analysis, an optimal lead combination for the multiple lead approach was investigated.

We studied a cohort of 189 patients undergoing ICD implantation and induction of VF. Seven VF waveform characteristics of 10 ECG-leads were calculated and used as input features for a support vector machine (SVM) algorithm. Patients were classified according to their history of MI. First, through binary classification (previous MI vs. no MI). Secondly, through multiclass classification, specifying the localisation of an MI (previous inferior MI, anterior MI or no MI). For both cases two models were tested: one using VF characteristics of a single ECG-lead and one using those of multiple ECG-leads. The discriminative ability were assessed by the area under the curve (AUC).

According to the identification of a history of MI: the single lead model had a mean AUC of 0.64, whereas the multiple lead model had a mean AUC of 0.74. In this case, *lead II, V1* and *V6* has shown best performance for the multiple lead approach. Furthermore, looking closer at the localisation of the infarction, either inferior or anterior, the single lead model had a mean AUC of 0.59, 0.73 and 0.59 for the identification of no MI, inferior MI and anterior MI, respectively. The multiple lead model had a mean AUC of 0.70, 0.80 and 0.77. Considering the localisation of an infarct, *lead II, V1* and *V3* has shown best performance for the multiple lead approach.

We are the first to demonstrate that a multiple lead approach results in superior predictive values for the identification of an MI as compared to a single lead approach. This implicates that for the identification of a previous or acute MI in the OHCA setting multiple leads may be recommended instead of a single lead approach. However, translation to the OHCA setting requires further investigation and optimization.

In order to improve our classification model, several other factors have been investigated whether they influence the VF waveform and potentially improve the classification models. First, we investigated whether VF waveform characteristics may differ among gender. In this context, women have shown higher amplitude characteristics in several limb leads, whereas lower amplitudes were seen in several precordial leads, compared to men. This suggests that gender may be a factor to include into the classification algorithm. It follows that the performances of our models slightly increase, suggesting that the inclusion of gender might slightly improve the discriminative ability of the SVM models. Secondly, the relation between the size of infarctions and the recognition of those infarctions has been investigated. We observed lower median values for three cardiac biomarkers, which represents a smaller size of an infarct, in case of unrecognized infarctions. Although, none of these were statistically significant, this might implicate that the identification of smaller

infarctions by the VF waveform is more challenging than larger infarctions. Since these factors might influence the VF waveform, they should be taken into consideration when analysing the VF waveform.

List of abbreviations

<i>AED</i>	Automated external defibrillator
<i>AHA</i>	American Heart Association
<i>AMSA</i>	Amplitude spectrum area
<i>AUC</i>	Area under the curve
<i>AV</i>	Atrioventricular
<i>BMI</i>	Body Mass Index
<i>bpm</i>	Beats per minute
<i>BW</i>	Bandwidth
<i>CAG</i>	Coronary angiography
<i>CC</i>	Chest compression
<i>CK</i>	Creatine kinase
<i>CPR</i>	Cardiopulmonary resuscitation
<i>DFA</i>	Detrended fluctuation analysis
<i>DFT</i>	Defibrillation testing
<i>ECG</i>	Electrocardiogram
<i>EF</i>	Ejection fraction
<i>ESC</i>	European Society of Cardiology
<i>FFT</i>	Fast Fourier transform
<i>Hz</i>	Hertz
<i>ICD</i>	Implantable cardioverter defibrillator
<i>IQR</i>	Interquartile range
<i>LA</i>	Left atrium
<i>LAD</i>	Left anterior descending artery
<i>LCA</i>	Left coronary artery
<i>LV</i>	Left ventricle
<i>MAA</i>	Mean absolute amplitude
<i>MdS</i>	Median slope
<i>MF</i>	Median frequency
<i>MI</i>	Myocardial infarction
<i>ML</i>	Machine learning
<i>mV</i>	Millivolt
<i>NPV</i>	Negative predictive value

<i>OHCA</i>	Out-of-hospital cardiac arrest
<i>PPV</i>	Positive predictive value
<i>PSD</i>	Power spectral density
<i>RA</i>	Right atrium
<i>RCA</i>	Right coronary artery
<i>RCx</i>	Right circumflex artery
<i>RDP</i>	Ramus descendes posterior
<i>ROC</i>	Receiver operating characteristic
<i>ROSC</i>	Return of spontaneous circulation
<i>RV</i>	Right ventricle
<i>SA</i>	Sinoatrial
<i>SD</i>	Standard deviation
<i>SVM</i>	Support vector machine
<i>VT</i>	Ventricular tachycardia
<i>VF</i>	Ventricular fibrillation

1. Introduction

Out-of-hospital cardiac arrest (OHCA) occurs frequently, with a global incidence of around 55 per 100.000 person-years, and carries a poor prognosis [1-3]. Ventricular fibrillation (VF) is the initial rhythm in approximately 23 - 40% of all OHCA cases [2, 4, 5]. The most common cause of VF is acute coronary ischemia, which is commonly reversible and of which the presence can only be diagnosed after restoration of organized rhythm [6-8]. As of yet, the underlying cause of VF, such as myocardial infarction (MI), cannot be determined in-field. In order to optimize treatment of VF to individual needs, more insight is warranted into the aetiology of VF during an arrest. As a first step towards in-field identification of MI, VF waveform analysis of induced VF in a controlled setting is proposed.

A potential tool to identify the underlying aetiology is the VF waveform on the electrocardiogram (ECG). As initially considered a marker for arrest duration and outcome, VF characteristics have been shown to reflect underlying heart disease as well [9, 10]. It has been demonstrated in animal as well as in human studies that underlying MIs causes low-amplitude-low-frequency VF [11-14]. Interestingly, a recent VF study demonstrated that a history of MI causes regional differences on the 12-lead ECG, related to the area of infarction [12].

However, to identify the presence of a (previous) MI using the VF waveform remains a clinical challenge. Rebergen (2016) was the first to explore the potential of machine learning (ML) based algorithms to discriminate between the presence and absence of a previous MI, using VF waveform characteristics. In this proof of concept study, ML models using 12-lead ECG characteristics of induced VF were demonstrated to be a feasible method to identify a previous MI.[15] Although these results were promising, in the setting of an OHCA only a single ECG lead is routinely measured by the defibrillator paddles, and there is no time for attaching a full 12-lead ECG. This may limit translation to the OHCA setting. In the current setting of an OHCA, the defibrillation system makes use of two paddles, resulting in only one recording lead, which roughly reflects *lead II*.

To narrow the gap between the experimental setting of induced VF and clinical practice, more insight is required into the ability of the VF waveform to identify a previous MI. The controlled setting of defibrillation testing (DFT) after implantable cardioverter defibrillator (ICD) implantations provides an ideal setting to investigate this topic. To mimic the current OHCA setting, we investigated the ability of a single ECG-lead to identify a previous MI using a machine learning method. Furthermore, this study will focus systematically on the additional value of multiple ECG-leads compared to a single ECG-lead to identify a previous MI using these machine learning methods. We hypothesized that adding more ECG-leads increases the discriminative ability of these ML models. Therefore, secondary aims were to assess the optimal combination of ECG-leads and to compare this multiple lead model to our initial single lead model.

To elaborate study results and potentially improve classification models, further sub-analyses on these results has been performed. Previous studies have shown that during sinus rhythm ECG voltages may differ between men and women [16-18]. Therefore, we investigated whether these gender related differences were present during VF, by comparing the VF waveform characteristics and evaluating their impact on the classification models. Furthermore, studies have shown that the number of involving ECG-leads is proportional to the size of an infarct. Hence, we investigated in another sub-analysis whether unrecognized infarctions could be explained by the size of an infarct. In order to investigate this topic, the release of cardiac biomarkers, the ejection fraction and left ventricular mass were analysed.

Outline of the thesis

The research reported in this thesis is performed at the Department of Cardiology at the RadboudUMC, Nijmegen and is divided into 8 chapters. After the preface on page 4, an overall summary is given on page 5. The abbreviations used in this thesis are listed on page 7. The research question of this thesis is introduced in **Chapter 1**.

The next two chapters describe the background information. **Chapter 2** clarifies the clinical background, describing to the anatomy, physiology, electrical activity of the human heart, followed by an introduction of ventricular fibrillation. The technical background is clarified in **Chapter 3**, describing the support vector machine approach and multiclass classification. Note that Chapter 3 has its own reference list, included on page 34 and 35.

In **Chapter 4** we study our main research question: What is the value of using multiple ECG-leads compared to a single ECG-lead for the identification of a previous myocardial infarction using ventricular fibrillation waveform characteristics? In order to answer this question, this chapter is divided into three sub-questions:

- What is the performance of a single ECG-lead to identify a previous myocardial infarction based on ventricular fibrillation waveform analysis?
- Would the performance increase when more ECG-leads were added?
- What is the optimal lead combination of ECG-leads to identify a previous myocardial infarction based on ventricular fibrillation waveform analysis?

Thereafter, **Chapter 5** focuses on several sub-analyses. These sub-analyses include gender-related differences of ventricular fibrillation waveform characteristics, probabilistic outputs, an analysis according to the size of infarctions and the analysis of data of a new cohort. Besides, statistical classification is performed, in order to compare both the machine learning and statistical approach.

A general discussion is given in **Chapter 6**, after which a general conclusion is recapitulated in **Chapter 7**.

Finally, used references are shown in **Chapter 8** and the Appendix is included by *Part A* and *Part B*.

2. Clinical background

§ 2.1 Anatomy and physiology of the heart

Circulatory system

The human heart is about the size of a clenched fist and is located within the thoracic cavity between the two lungs [19]. The heart functions as a circulatory pump that pumps blood through the human body. There are two circuits in the circulation of blood, the pulmonary circulatory system and the systemic circulatory system, see Figure 1.

The right side of the heart receives deoxygenated blood from regions superior to the diaphragm and inferior to the diaphragm from the superior vena cava and inferior vena cava, respectively. The right side of the heart is responsible for pumping deoxygenated blood into the lungs via the pulmonary artery. In the lungs, oxygen and carbon dioxide are exchanged. Specifically, oxygen is delivered to blood, whereas carbon dioxide is absorbed for exhalation. Oxygenated blood is returned to the left side of the heart. This circuit is known as the pulmonary circulation. The left side of the heart pumps blood through the aorta to the rest of the body, where the cells of the body consume this oxygen. Subsequently, deoxygenated blood is collected into the veins and returned to the right side of the heart. This circuit is known as the systemic circulation. In that way, the systemic circulation transports oxygenated blood into rest of the body and returns deoxygenated blood back to the pulmonary circulation where it is pumped into the lungs again. The pulmonary and systemic circulation together is known as the circulation of blood. [19]

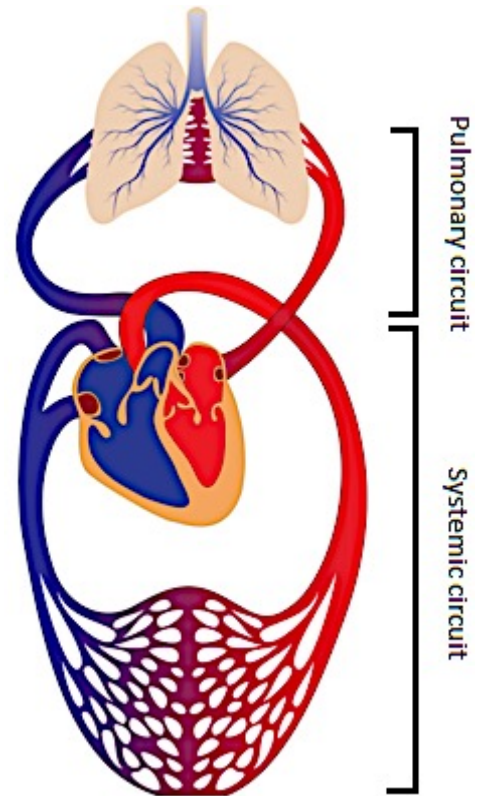


Figure 1. Schematic representation of the circulation of blood (anterior view). Adapted from [20].

The anatomy of the heart

The human heart is made up of four chambers: the right atrium (RA), right ventricle (RV), left atrium (LA) and left ventricle (LV). The RA and LA act as receiving chambers and contract to pump blood into the RV and LV, respectively. The ventricles function as pumping chambers, to pump blood into the pulmonary artery or the aorta. Although both ventricles pump the same amount of blood, the muscular layer of the LV is much thicker compared to the RV. In order to perfuse all body organs, a sufficient driving force of the LV is necessary and therefore a thick wall is required [21].

In order to sustain the circulation of blood, the heart contracts and relaxes. The part of the cardiac cycle in which the two ventricles contract is called the systole, whereas the part of the cardiac cycle where the two ventricles relaxes and fills with blood is called the diastole. The maximum pressure of the left ventricle, generated by the contraction of the left ventricle is known as systolic blood pressure, whereas the diastolic blood pressure is known as the minimum pressure of the left ventricle during relaxation of the ventricles.

The heart contains four heart valves to ensure unidirectional blood flow through the heart. The right atrium and right ventricle are separated by the tricuspid valve. The left atrium and left ventricle are separated by the mitral valve. The pulmonary valve is located between the right ventricle and pulmonary artery, whereas the aortic valve is located between the left ventricle and aorta. During systole the tricuspid and mitral valve are closed to prevent backflow from the right and left ventricle into the right and left atrium, while the pulmonary and aortic valve are open. In contrast, during diastole the tricuspid valve and mitral valve are open, while the pulmonary valve and aortic valve are closed to prevent backflow of blood from the pulmonary arteries and aorta into the right and left ventricle, respectively. [22]

Conducting system

The heart contraction is triggered by electrical currents in the heart muscle cells. The heart muscle cells are also known as myocytes or cardiomyocytes. Electrical activation is conducted through the cardiac conduction system. The elements of this system include the sinoatrial (SA) node, the atrioventricular (AV) node and the ventricular conduction pathway including the bundle of His, the right and left bundle branch and the Purkinje fibers, see Figure 2. The SA node consists of a cluster of cells that is located in the high wall of the right atrium near the superior vena cava. The SA node functions as the natural pacemaker of the heart; it generates electrical impulses. These impulses are propagated via the atrial myocardium to the AV node, which is located at the base of the right atrium. The AV node delays the conducted impulses from the atria to the ventricles [23]. Electrical impulses from the AV node are propagated to the ventricular pathway via the fast-conducting His bundle. The His bundle conducts impulses to the left and right bundle branches and the Purkinje fibers, which enables activation (depolarisation) of ventricular myocardium. [24]

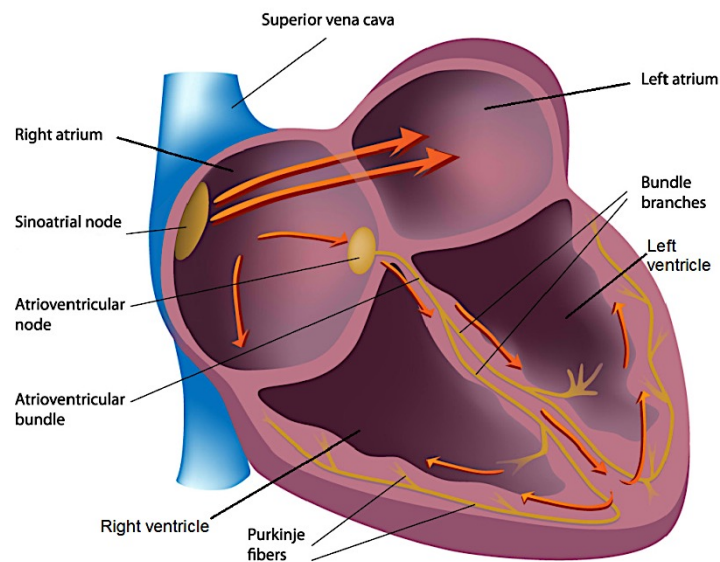


Figure 2. Elements of the cardiac conduction system. Adapted from [25].

Coronary arteries

The heart itself receives oxygenated blood via the coronary arteries to function properly. The coronary arteries arise from ostia in the ascending aorta, shortly above the aortic valve. There are two main coronary arteries: the right coronary artery (RCA) and the left coronary artery (LCA), see Figure 3. Both arteries split in numerous smaller arteries.

The LCA bifurcates into two branches: the right circumflex artery (RCx) and the left anterior descending artery (LAD). The LAD descends into the interventricular groove (the groove that separates the ventricles), whereas the RCx descends into the left atrioventricular groove (the groove that separates the left atrium and ventricle). The LAD gives rise to one or two diagonal branches, that may arise and descend across the anterior surface of the LV and to the septal branches. The LAD and its branches supply blood to the anterior and lateral wall of the left ventricle and the intraventricular septum. The RCx can be considered as the artery that supplies blood to the left atrium and lateral wall of the left ventricle and in some cases the inferior wall of the left ventricle.

The RCA descends into the right atrioventricular groove (the groove that separates the right atrium and ventricle) and bifurcates into the ramus posterolateral (RPL) and often the ramus descendens posterior (RDP) [26]. The RCA supplies blood to the right atrium, right ventricle, the posterior wall and in most cases the inferior wall of the left ventricle.

In general, there are variants regarding to the vascular supply to the inferior wall. The artery that supplies the RDP and a posterolateral branch determines the coronary dominance. If the RCA supplies the RDP, it is called right dominance (85% of the population). In contrast, if the RCx supplies the RDP (15% of the population), it is called a left dominant system. [27]

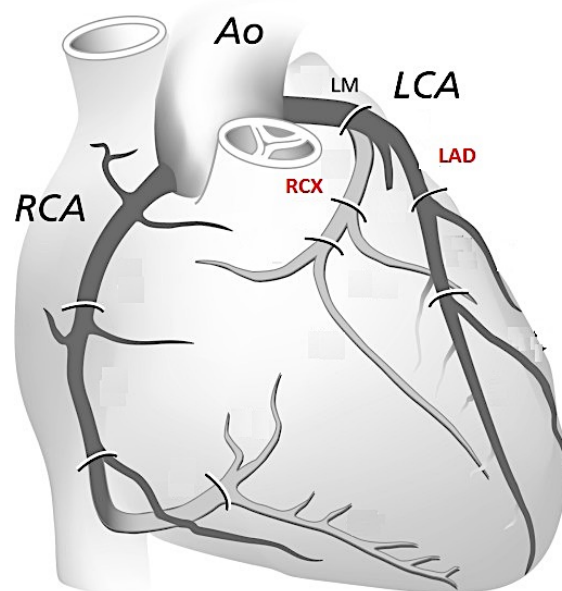


Figure 3. Coronary artery segments according to the American Heart Association (AHA) classification (anterior view). Adapted from [28].

§ 2.2 Electrical activity in the heart

Cardiac action potential [29]

The cardiac cycle describes the mechanical and electrical events during cardiac contraction and relaxation. The cardiac action potential is defined as the voltage difference across the cell membrane of myocardial cells. This voltage difference is caused by the movement of electrical charged particles (ions) through ion channels. The Na^+ , K^+ and Ca^{2+} ions are the most important charge carriers of the cardiac action potential.

The inside of the cardiac cell has a negative electrical charge compared to the outside of the cell. The resulting voltage difference across the cell membrane is called the transmembrane potential and lies between -80 and -90 mV. Cardiac cells are excitable, as they possess tiny channels in the cell membrane, which can open and close sequentially. This latter allows the voltage across the cell membrane to change. The voltage changes in time are represented by the cardiac action potential.

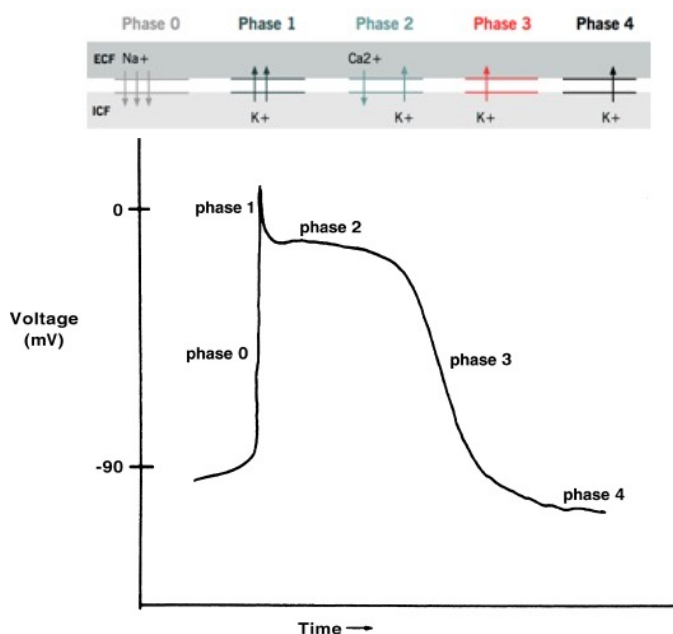


Figure 4. The cardiac action potential. Na^+ , K^+ and Ca^{2+} represents sodium, potassium and calcium ions, respectively. ECF = extracellular fluid and ICF = intracellular fluid. [29, 30]

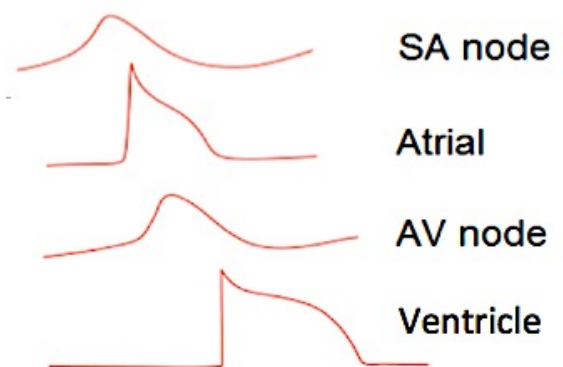


Figure 5. Specific cardiac action potential for several cardiac cells. Adapted from [31].

As can be seen in Figure 4, the cardiac action potential can be divided into the following five phases:

Phase 0 occurs when the rapid sodium channels in the cell membrane are stimulated to open. When this happens, positively charged sodium ions enter the cell, causing a rapid positively directed change in the transmembrane potential. This voltage spike is called *depolarization*. Once a cardiac cell is stimulated to depolarize, the wave of depolarization (the electrical impulse) is propagated across the myocardium, cell by cell. Once a cell is depolarized, it cannot be depolarized again until the ions are back to where they started, which is known as the refractory period.

Phase 1 begins with rapid inactivation of the sodium channels, reducing the movement of sodium channels into the cell. Simultaneously, the potassium channels open and close rapidly, creating a flow of potassium out of the cell. This is called *repolarisation* and charges the membrane more negative in order to return the cardiac action

potential to the resting membrane potential. During **phase 2** of the cardiac action potential, positively charged calcium ions slowly enter the cell, thus interrupting repolarisation and prolonging the refractory period. This is called the plateau phase and is unique to cardiac cells.

Phase 3 represents rapid repolarisation, where the calcium channels are closed and the potassium channels remain open.

During **phase 4** (resting phase) there is no net movement of ions across the cell membrane. In some cardiac cells, there is leakage of ions back and forth in the resting phase, in such a way to cause a gradual increase of the transmembrane potential. When this transmembrane potential reached the voltage threshold, appropriate channels are stimulated to cause the cell to depolarize and another action potential is generated. This spontaneously generated electrical impulse propagated across the heart is called *automaticity*. Automaticity is the mechanism by which the sinus rhythm of the heart is generated. The pacemaker cells of the SA node usually have the fastest phase 4 activity within the heart, generating a sinus rhythm.

The cardiac potential varies in different cell types within the heart (e.g. SA node, AV node, atrial muscle, Purkinje fibers and ventricular muscle), see Figure 5. Specifically, cardiomyocytes can be divided into pacemaker cells and non-pacemaker cells. The pacemaker cells of the SA and AV node have smaller unstable resting potentials and are able to depolarize spontaneously, see Figure 5. On the other hand, the non-pacemaker cells (e.g. atrial and ventricular cardiomyocytes) have a larger stable resting potential. In Figure 4 the specific cardiac potential of a typical Purkinje fiber is shown. Moreover, if the SA node will fail, there are usually other cells (e.g. in the AV node or ventricular myocardium) to take over the pacemaker function of the heart, but at a slower rate. This is known as an escape rhythm.

Electrocardiography (ECG)

Cardiac cycle

The cardiac action potential represents the electrical activity of one single cardiac cell. The electrocardiogram (ECG) detects the electrical activity of the heart recorded from electrodes placed on the surface of the skin. So the surface ECG represents the sum of all action potentials of all cardiac cells of the entire heart, see Figure 6.

The electrical impulse generated by the SA node is conducted to the left and right atria and leads to depolarization of the atrial cardiomyocytes, which is visualized on the ECG by the P wave. Ventricular depolarization is reflected by the QRS complex. The repolarisation of the atria is not visible because it occurs simultaneously as the depolarisation of the ventricles, which generates substantially larger electrical potentials and therefore dominates. The T-wave represents the ventricular repolarisation.

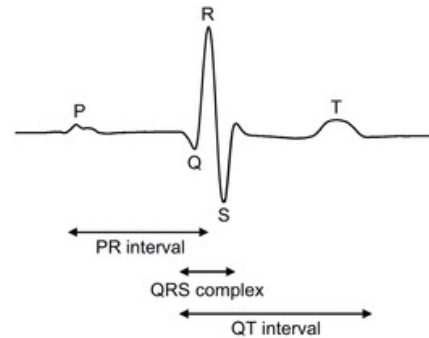


Figure 6. One cardiac cycle of the surface electrocardiogram (ECG). [21]

Lead vectors

A vector is a physical quantity, which has both a magnitude and a direction. Movement of electrically charged ions (Na^+ , K^+ and Ca^{2+}) during the cardiac action potential generates an electrical vector. The electrical vector is the average direction and magnitude of an impulse*. Hence, the ECG represents the electrical vectors of the electrical activation in time. By placing electrodes on the human skin, it is possible to detect the currents of these electrical vectors. In particular, these currents can be measured either bipolar (i.e. using a positive and negative electrode) or unipolar (i.e. using a positive electrode and an indifferent electrode**). A vector towards the positive electrode yields a positive deflection on the ECG and a vector away from the positive electrode yields a negative deflection. The voltage difference between two electrodes on the body is referred as a lead.

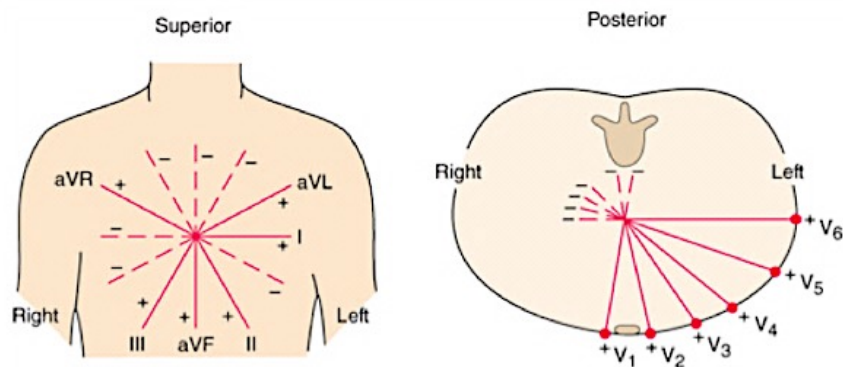


Figure 7. Representation of the conventional 12-lead reconstruction. [32]

* An impulse is defined as the excitation wave over a nerve or muscle fiber, having either a stimulating or inhibitory effect. ** The indifferent electrode is defined as the "reference" electrode and is supposed to contribute minimally to the recording electrode.

The conventional 12-leads ECG is acquired using ten electrodes on patient's limb and chest, see Figure 7. Six unipolar electrodes ($V1-V6$) are placed on the patient's chest and called the precordial leads. The four other electrodes are placed on the right arm (RA), left arm (LA), right leg (RL) and left leg (LL). The electrode placed on the RL functions as a ground electrode to prevent electrical interference on the ECG recording. The overall magnitude is measured to 12 different directions, which are known as the 12 leads.

The 12-leads ECG consist of 6 limb leads and 6 precordial leads. The standard limb leads are lead I , II and III , which form a "closed" equilateral triangle. According to Kirchhoff's law the potential difference of a closed circuit is zero, due to the following relationship: $V_I + V_{III} = V_{II}$. The relationship of these standard limbs is based on the principle that the sum of the electrical current in *lead I* and *lead III* equals the sum of the electrical current in *lead II*. This resulting principle is called the *Einthoven's law*. [33]

The three bipolar limb leads are numbered with Roman numerals I, II and III and defined as follow

$$\begin{aligned} \text{lead } I &= V_{LA} - V_{RA} \\ \text{lead } II &= V_{LL} - V_{RA} \\ \text{lead } III &= V_{LL} - V_{LA} \end{aligned} \tag{1}$$

The 'augmented' limb leads are aVR , aVL , and aVF , and are unipolar. Because these resulting electrical currents on the ECG are quite small, the signals are augmented. The three augmented unipolar limb leads use a mean of two limb leads as the negative pole. These leads are defined as follow

$$\begin{aligned} aVR &= \frac{2V_{RA} - V_{LA} - V_{LL}}{2} \\ aVL &= \frac{2V_{LA} - V_{RA} - V_{LL}}{2} \\ aVF &= \frac{2V_{LL} - V_{RA} - V_{LA}}{2} \end{aligned} \tag{2}$$

In order to measure the unipolar precordial leads, the potentials of the three limb electrodes at RA , LA and LL are used. The average potential of the three limb leads is known as the central terminal (V_C) and functions as the virtual reference point [34, 35]. With this point, individual precordial leads can be measured with the same reference point as negative pole. These precordial leads are defined following formula (3).

$$V_i = V_i - V_C \tag{3}$$

where i is referred as the precordial leads 1 to 6 and $V_C = \frac{1}{3}(V_{RA} + V_{LA} + V_{LL})$.

The three standard (I, II and III) and the three augmented limb (aVL , aVR and aVF) leads record the electrical cardiac activity in the two-dimensional frontal plane. The six precordial leads ($V1 - V6$) record the electrical cardiac activity in the horizontal plane. [33]

Rhythm disorders on the ECG

An abnormal heart rhythm can be diagnosed by analysing the ECG. During normal sinus rhythm the impulse begins in the sinus node at rates between 60 and 100 beats per minute (bpm). As described in **Section §2.1**, the normal sequence of electrical activation of the heart is from the SA node through the atria to the AV node and His-Purkinje system and to the ventricular myocardium. Abnormalities in the electrical system of the heart can result in cardiac arrhythmias, such as bradycardia (<60 bpm) or tachycardia (>100 bpm) [36].

When the action potential arises from the ventricular myocardium, the arrhythmia is called a ventricular arrhythmia. A tachycardia of >100 bpm derived from the ventricles is known as a ventricular tachyarrhythmia and is a life-threatening arrhythmia [37]. Ventricular tachyarrhythmias take two major forms; ventricular tachycardia (VT) and ventricular fibrillation. These arrhythmias often result in symptoms as dizziness, palpitations, syncope and sudden cardiac death. [29]

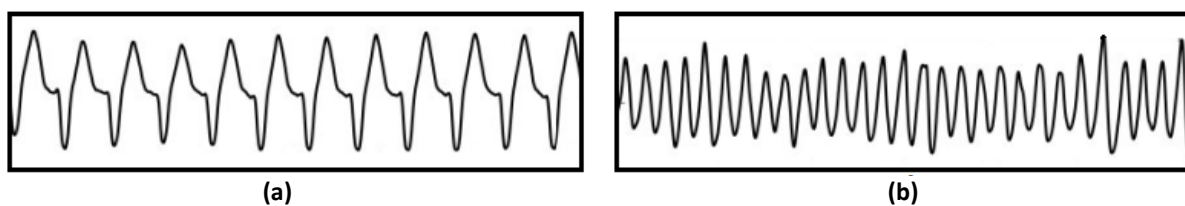


Figure 8. In (a), a regular ventricular tachyarrhythmia is shown on the electrocardiogram (ECG), representing ventricular tachycardia (VT). In (b), an irregular ventricular tachyarrhythmia is shown on the ECG, representing ventricular fibrillation (VF).

Ventricular tachycardia

VT is defined as a relatively organized tachyarrhythmia with the presence of QRS complexes, see Figure 8a. In general, a VT has a rate faster than 120 bpm. Depending on the duration, a VT can be classified in either non-sustained or sustained. A non-sustained VT is referred when at least three consecutive VT beats are seen, which spontaneously converts to sinus rhythm within 30 seconds. [38] In contrast, a sustained VT lasts at least 30 seconds (or less if treated by cardioversion within 30 seconds). Moreover, a VT can be either monomorphic or polymorphic. In a monomorphic VT, all QRS complexes are similar in morphology, whereas in polymorphic VT beat to beat changes in QRS morphology are seen [29]. Generally, a monomorphic VT does not cause significant hemodynamic instability, whereas a polymorphic VT does often cause hemodynamic instability [39]. Moreover, VT can deteriorate to VF, where VT commonly precedes the onset of VF.

Ventricular fibrillation

VF is defined as a mainly disorganized tachyarrhythmia with the absence of recognizable QRS complexes, see Figure 8b. This arrhythmia causes instant hemodynamic instability and rapid loss of consciousness. VF is the initial rhythm in 23 - 42% of the out-of-hospital cardiac arrest cases [2, 4, 5]. OHCA is one of the main causes of death, with a global incidence of around 55 per 100.000 person-years [1, 4]. In general, VF rarely terminates spontaneously and secondary prevention is necessary to prevent recurrences. Therefore, an implantable cardioverter defibrillator (ICD) have become the cornerstone of chronic therapy in patients at continued risk for VT or VF, see **“Prevention”** in **Section §2.3** [40]. Since, VF is the most observed arrhythmia in cardiac arrest patients, this arrhythmia will be discussed in further detail in the next section.

§ 2.3 Ventricular fibrillation

Definition

Ventricular fibrillation is a rapid (>250 bpm), uncoordinated and mainly disorganized ventricular tachyarrhythmia, without meaningfully contractions [29]. On the ECG VF is characterized by a chaotic signal with varying amplitude and frequency, in the absence of recognizable QRS complexes [41, 42]. Because of the absence of contractions, oxygen supply to the brain and other organs stops. Moreover, it may lead to irreversible damage of the brain, which causes instant hemodynamic collapse and rapid loss of consciousness.[43]

Mechanism of ventricular fibrillation

The basic electrophysiological mechanisms leading to ventricular tachyarrhythmias (e.g. VT and VF) can be divided into three groups: 1. abnormal automaticity, 2. triggered activity and 3. re-entry. Re-entry accounts for the majority of ventricular arrhythmias and is most often associated with underlying heart disease. Previous experimental and simulation studies have suggested that VF is maintained solely by re-entry [40]. Re-entry requires the following criteria to be met. First, two conducting pathways (A and B in Figure 9a) must be connected proximally and distally, forming a potential electrical circuit. Second, one of the pathways must have a longer refractory period (B) than the other pathway (A). Third, the pathway with the shorter refractory period (A) must conduct electrical impulses more slowly than the other pathway (B), see Figure 9a. [29]

Re-entry can be initiated when a timed premature impulse has entered the circuit, see Figure 9b. This premature impulse must enter at a time when pathway B is still refractory, while pathway A is not refractory any longer and is able to conduct the premature impulse. Pathway A conducts the premature impulse slowly, while pathway B is recovering. By the time the impulse reaches pathway B from the opposite direction, pathway B is no longer refractory and able to conduct the impulse in retrograde direction. If this retrograde impulse reaches pathway A, it will be conducted antegradely. From this, a continuously circulating impulse is established, which is spinning around and known as a re-entry loop. [29]

Furthermore, a re-entry can be terminated by a premature impulse as well, see Figure 9c. This premature impulse should enter the circuit during a re-entry tachycardia at an appropriate time to collide and terminate the re-entry impulse.

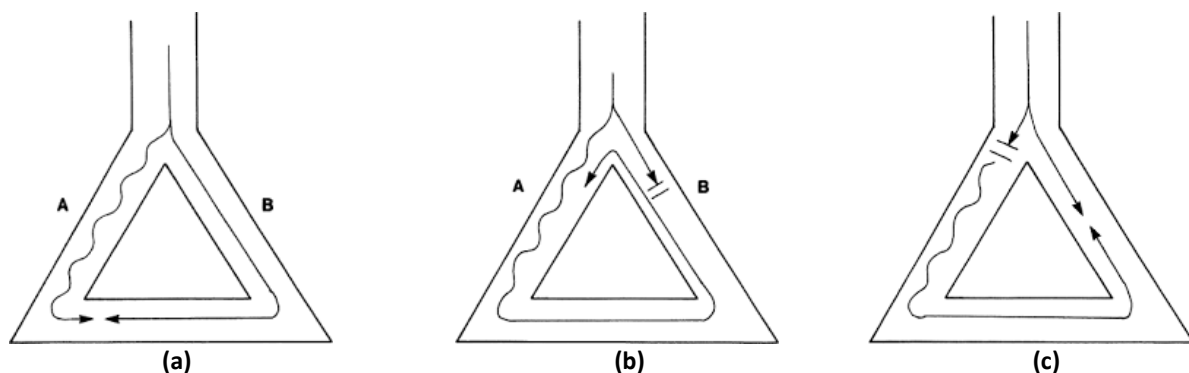


Figure 9. Principle of a re-entry. In (a) the prerequisites for a re-entry are shown by a slow conduction pathway A and a fast conduction pathway B. In (b) the initiation of a re-entry is presented by a premature impulse, whereas as in (c) the termination of a re-entry is shown [29].

Re-entrant circuits within the ventricle usually do not express until patients develop a form of heart disease which often causes scarring in the ventricular myocardium. [29] Approximately 50% of the cardiac arrests occur in individuals without a known heart disease, but most have a concealed ischemic heart disease [8].

Causes of ventricular fibrillation

Firstly, the most common cause of ventricular fibrillation is acute coronary ischemia (75-80%) [39]. During acute ischemia, the leakage of potassium results in increased extracellular potassium that depolarizes the myocardial cells around the ischemic border zone. This depolarization leads to heterogeneity of conduction and refractoriness, which enclose a substrate for re-entry. [7]

Secondly, scar formation after myocardial infarction (MI) represents another important prerequisite for re-entry, creating unidirectional blocks and areas of slow conduction [39, 40]. The most common cause for scar is a previous infarction, see text box "**Myocardial infarction**". VF can occur in nonischemic cardiomyopathies as well, including dilated cardiomyopathy, hypertrophic cardiomyopathy, valvular disease, arrhythmogenic right ventricular cardiomyopathy (ARVC) and inflammation (e.g. sarcoidosis). ARVC is associated with fatty and fibrous replacement of right ventricular myocardium, leading to dysfunction of the right ventricle. [7]

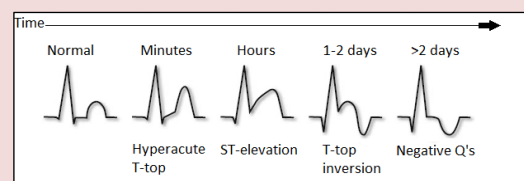
Thirdly, ventricular arrhythmias can also be caused by genetic disorders even in the absence of visible structural heart disease. Currently known disorders are ion channel abnormalities, such as long QT syndromes and Brugada syndrome. Long QT syndromes affect the repolarisation and often manifest as a prolonged QT interval on the resting ECG. In patients with Brugada syndrome abnormalities involving the sodium channels are found. [7] These channelopathies enclose a substrate for re-entry and may therefore provoke ventricular arrhythmias.

Moreover, ventricular arrhythmias can incidentally occur in patients with conduction disorders, such as bundle branch blocks and the Wolff-Parkinson-White syndrome [50, 51].

Finally, ventricular fibrillation that occurs in the absence of a known structural heart disease, inherited disorder or electrolyte disorder is referred as idiopathic ventricular fibrillation and accounts for 5 – 10 % of the OHCA survivors [40, 52, 53].

Myocardial infarction (MI) is defined in pathology as myocardial cell necrosis due to prolonged ischemia. Ischemia results from an imbalance between oxygen supply and demand.

According to the Third Universal Definition of Myocardial Infarction; an MI is defined by the rise and fall of cardiac biomarkers and at least one of the following: clinical symptoms of ischemia, ECG changes and/or imaging evidence by echocardiography or coronary angiography [44]. For instance in an acute ST-elevated MI (STEMI), ECG changes evolve through the following typical sequence:



In the Netherlands, in 2009 the incidence of an acute MI was estimated at 2.9 per 1000 men and 1.7 per 1000 women. In 2010, 6823 acute MI related deaths were registered. Moreover, the rate of MI rises for both men and women with increasing age. [45]

It is estimated that approximately 75 to 90% of all MIs affect the inferior and/or anterior myocardium [46, 47]. To localise the ischemic area by using the ECG, ECG changes (e.g. ST-elevations or Q-waves) can be examined. Generally, the ECG leads which show ECG changes reflect the ischemic area. For instance, ST elevation in lead II, III and aVF are due to transmural ischemia located in the inferior wall of the ventricle, caused by an occlusion of the RCA or RCx. To discriminate between the involvement of the RCA or RCx, it should be approved that when ST-elevation in lead II is higher than in lead III the RCx is involved and when ST-elevation in lead III is higher than in lead II the RCA is involved. [42] ECG changes in V1-V6 are caused by ischemia located in the anterior wall, caused by an occlusion of the LAD. More specifically, ECG changes in V1-V3 involve the anteroseptal wall and ECG changes in V4-V6 the anterolateral wall. [42]

Furthermore, it is estimated that 1-5% of all patients with a previous MI and 2-20% of all patients with acute MI will develop episodes of VT/VF [48, 49].

Treatment

Studies have described initial VF rhythm in approximately 23 – 42 % of the OHCA cases [2, 4, 5]. OHCA is one of the main causes of death, with a global incidence of around 55 per 100.000 person-years [1, 4]. In view of the above, early cardiopulmonary resuscitation (CPR) in combination with defibrillation is a key point in the chain of survival for OHCA patients. The general goals are to restore the cardiac rhythm to one that is hemodynamically effective and to maintain and support the restored circulation. As the first priority, the patient's cardiac rhythm is promptly defibrillated. A period of chest compressions is followed and an intravenous line is established to administer medications. Since the probability of the success of defibrillation is inversely proportional to the duration of VF, the chain of survival should be initiated as soon as possible. Every minute lost of initiating CPR results in a 10% decrease in survival rates. [54]

Prevention

In order to prevent sudden cardiac death in patients at risk for VF, implantation of an implantable cardioverter defibrillator (ICD) is generally considered as the standard of care. An ICD is a device that monitors and responds to dangerous cardiac arrhythmias. In order to terminate a ventricular arrhythmia, the ICD can give anti-tachypacing or deliver a shock to restore a normal rhythm. When an ICD is offered to a patient with a history of sustained ventricular arrhythmia, this is known as *secondary prevention*. When medical conditions may lead to an increased risk for ventricular arrhythmias and the associated risk of sudden cardiac death, but without an episode of a ventricular arrhythmia, this is known as *primary prevention*.

Inherent to the mortality reduction is the expectation that the ICD can terminate the arrhythmia successfully. For this reason, defibrillation testing (DFT) has long been a traditionally part of the ICD implantation. Until recently, routine DFT testing was performed after ICD implantation to test the ability of the implanted device to sense, detect and terminate VF appropriately. After sedation with propofol, VF was induced using T-wave shock, direct current pulses or 50 Hz burst pacing. The T-wave period has been described as a vulnerable phase during the cardiac cycle, because electrical stimulation during this phase may evoke another action potential. During T-wave shock, a shock is given during the vulnerable period of the T-wave (so ventricular depolarisation is superimposed on the T-wave). This is known as the R-on-T phenomenon and may induce VF [55].

However, the current generations of ICDs have a high success rate of successful defibrillation. Given this success rate and the risks associated with induction of VF, many centres have changed their practice on routinely inducing VF. [56]

Furthermore, anti-arrhythmic drugs are commonly used as adjuvant treatment in ICD recipients. These drugs may suppress VT/VF episodes and slow the rate of VT episodes, and therefore may reduce the incidence of ICD shocks and hospitalizations related to the cardiac arrhythmia. Amiodarone, beta-blockers and sotalol are recommended drugs as therapy for the management of ventricular arrhythmias and the prevention of sudden cardiac death. However, the efficacy of these current anti-arrhythmic drugs has been limited in many patients, resulting in recurrent VT/VF episodes. [8, 57]

§ 2.4 Current research

Over the last decades, there has been large interest in studying VF waveform characteristics. The morphology of VF can be quantified by continuous VF waveform measures based on amplitude, frequency and non-linear dynamics of the signal. Studies have shown that when VF starts, the ECG often shows a coarse electrical pattern, see Figure 10a. When time passes over a period of a few minutes, the heart become less viable, causing lower amplitude of fibrillation waves seen on the ECG (fine VF), see Figure 10b. [14, 29, 58-60]

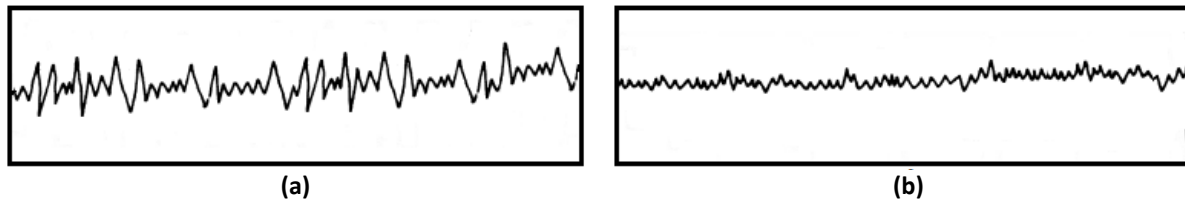


Figure 10. In (a), a representation of coarse ventricular fibrillation (VF) on an electrocardiogram (ECG) is shown. In contrast, (b) shows a representation of fine VF on an ECG. Adapted from [29].

Prior studies based on retrospective data have shown that higher VF amplitudes are associated with higher success of defibrillation [61, 62]. In addition, it was assumed that coarse VF (> 0.2 mV) is present early after the onset of cardiac arrest and is more likely to be converted into return of spontaneous circulation (ROSC). In contrast, when time passes fine VF (0.1-0.2 mV) occurs and is less likely to be converted into ROSC. [10, 29]

Moreover, it has been shown that chest compressions (CC) can cause increasing VF characteristics, potentially increasing the chances of a successful defibrillation [63]. Given that, two randomized trials hypothesized that a brief period of CC prior to shock delivery may be beneficial in patients with prolonged response times, it has been proposed to use the VF waveform to optimize the timing of defibrillation [64, 65]. However, a randomized trial investigating such a waveform-guided protocol as compared to a standard shock-first protocol did not show any differences in outcome after OHCA [66]. A possible explanation for this study outcome is that the study did not account for underlying heart diseases. Studies have shown that, not only time but, underlying heart disease may influence the VF waveform as well. It has been demonstrated in animal studies as well in human studies that underlying MI, both acute and previous MI, can cause VF with lower amplitudes and frequencies, already at the onset of VF [11-13, 67], see Figure 11.

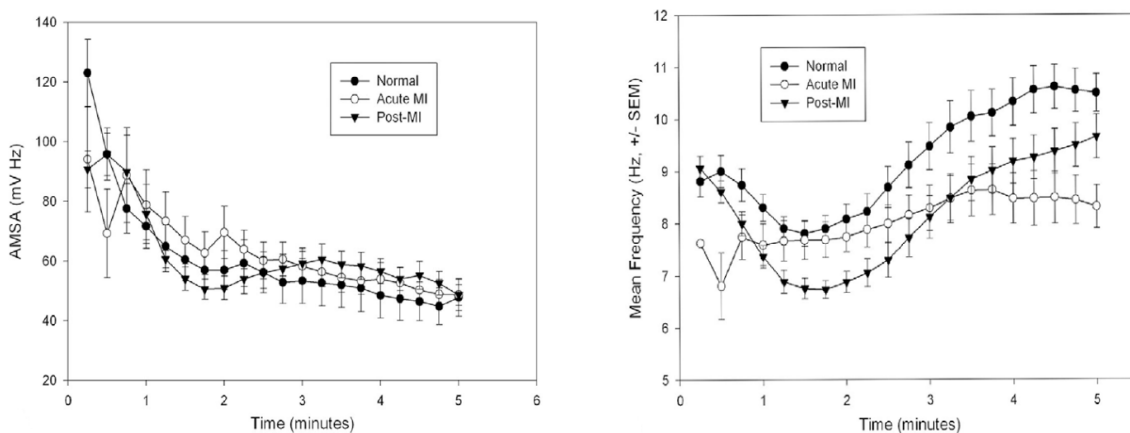


Figure 11. Amplitude and frequency characteristics of the ventricular fibrillation waveform over time for normal (control) (n=16), acute myocardial infarction (n=11) and post myocardial infarction (n=10) in swine. [59]

Particularly, differences were most outspoken in the leads adjacent to the area of the infarct location. A human study on induced VF showed that the VF waveform may also be affected by other structural abnormalities of the left ventricle, such as mass and dilatation [9]. Differences were found already in the early onset of VF, suggesting that not only the duration of VF is important, but underlying heart disease as well. All in all, it may occur that an OHCA patient with relatively short arrest duration, still reflects fine VF due to an expression of a previous or acute MI.

Information on the presence of a (previous) MI may be useful for two reasons. From one point of view, for the timing; one could account for lower amplitudes in case of a (previous) MI and therefore adjust the threshold value for shock success. From the other point of view, assuming that an acute MI is a common reversible cause of VF, the identification of an acute MI during resuscitation might help in choosing the best resuscitation strategy.

Unfortunately, the widely known typical ECG changes that suggest myocardial infarction can be observed especially during sinus rhythm and not during ventricular fibrillation. In **Section §2.3** it has already been described that a common cause of VF is an MI, either an acute or a previous MI. In case of this ventricular tachyarrhythmia the electrical activity of the heart is mainly disorganized. Therefore, during VF, caused by an MI, the observation of typical ECG changes is quite challenging, see Figure 12. Nevertheless, characteristics of the VF waveform on the ECG might be a potential tool to identify an acute or previous myocardial infarction.

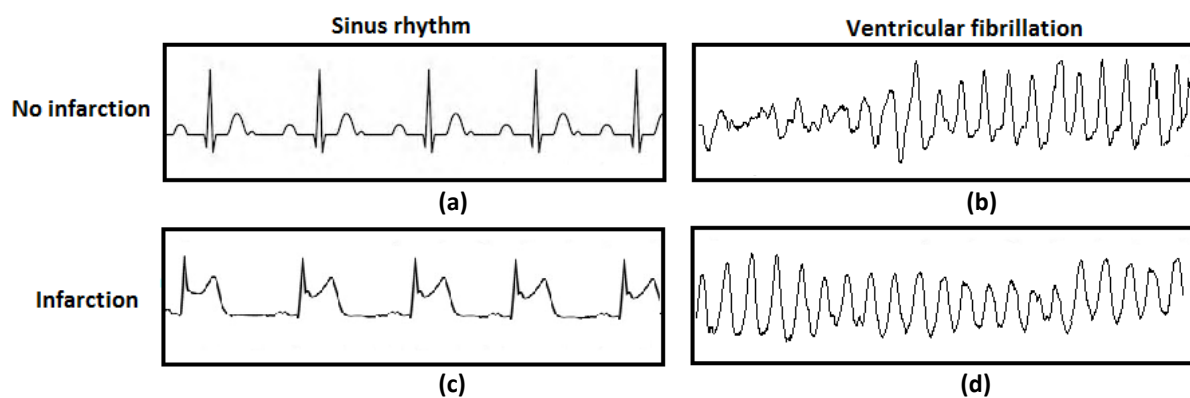


Figure 12. A rough representation of the electrocardiogram (ECG) in case of no myocardial infarction (MI) versus MI, for both sinus rhythm and ventricular fibrillation (VF). Generally, in healthy subjects no ECG changes will be observed in the absence of an MI (a), whereas ST-elevations will be observed in the presence of an MI (c). In case of VF, expression of an MI on the ECG cannot be easily observed visually, (b) versus (d). The mean absolute amplitude of (b) and (d) are both 0.10 mV.

To identify the presence of a (previous) MI using the VF waveform remains a clinical challenge. The identification of a previous MI using machine learning (ML) was explored in a master's thesis of Rebergen (2016). To our knowledge, he was the first who explored the potential of ML based algorithms to discriminate between the presence and absence of a previous myocardial infarction, using VF waveform characteristics of induced VF. He found that with the use of ML a previous myocardial infarction could be moderately identified out of the VF waveform of a 12-leads ECG, with a maximum area under the curve (AUC) of 0.710. [15]

The next chapter "**Technical background**" describes some basics of ML and the theory of one of the most widely-known classifiers.

3. Technical background*

§3.1 Introduction to Machine Learning

Over the last decade, data availability has increased and it might be seen as an infinite process. Intelligent analyses of data is a valuable resource. Data analyses may give new insights and better decision making [1]. Nowadays, machine learning (ML) is a popular term and these techniques teaches the computer to do what comes naturally to human and animals: learn from experience [2].

Using computational methods, ML algorithms can learn directly from data, within the absence of predetermined equations as a model. In fact, when the number of samples increases, the ML algorithms will adaptively improve their performances. [2]

ML is a method based on computer science and statistics. However, statistics primarily focuses on the conclusions of data, whereas ML focuses on the algorithms to effectively capture, store, retrieve and merge these data to arrange multiple learning subtasks [3]. The aim of ML is to build and train a model that makes predictions in the presence of uncertainty. One of the applications of the ML approach is to create a classifier that is able to separate subjects into two or more classes. ML algorithms can be distinguished, based on how they learn about data to make predictions, into two different approaches; supervised learning and unsupervised learning. Supervised learning algorithms take a set of input data and known responses as output data and train a model to generate predictions for the response of new "unseen" data. In contrast, unsupervised learning algorithms make use of unlabelled data in order to find hidden patterns or intrinsic structures in input data. [2]

ML provides methods and tools that support solving diagnostic and prognostic problems in the medical field. One potential of ML is to use a classifier to analyse biomedical data and detect or diagnose a disease. Moreover, ML methods can help the implementation of computer-based systems in the health care, creating opportunities to facilitate and improve the work of medical experts. However, there have been several discussion on the ethical implication of ML in health care. One of the major concerns people are having is that it will minimize the requirement of human intellect in several job sectors, resulting in a more presenting role of robotics [4].

Several ML algorithms have been described in literature. Support vector machine (SVM) algorithms are developed in the sixties by Vapnik, Lerner and Chervonenkis [5, 6]. A few years later, SVM have been applied successfully to tasks as optical character recognition [7] and in regression and time series predictive applications [8, 9]. In order to answer our research question we apply SVM algorithms and cross-validation. In the following sections an introduction is addressed how the support vector classifier functions and to the used parameters. First of all, the principle of cross-validation will be described.

* This chapter has its own reference list, included on page 34 and 35.

§3.2 Validation

A poor performance of a model can often be explained by the optimization problem of "underfitting" or "overfitting". A model that has learned the noise instead of the signal is considered as "overfitted" because it fits the training dataset well, but has a poor fit with the new dataset. Conversely, insufficient model complexity or few data implies that information in the training data cannot be completely exploited, so the model will be "underfitted". In general, a simple model is often caused by too few input features, resulting in inflexible learning from the data set and therefore an underfitted model, see Figure 13.

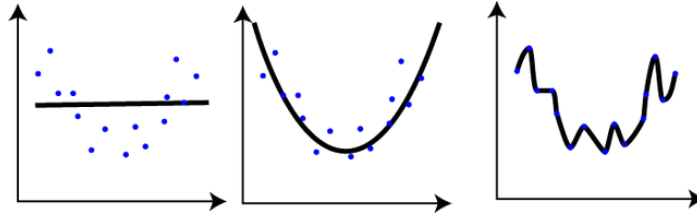


Figure 13: Principles of fitting. On the left an underfitted model, in the middle a good fitted model and on the right an overfitted model were shown. [10]

A key challenge in under- and overfitting and ML in general, is that we are not able to know how well our model will perform on new data until we actually test it. To address this, there are options available to split an initial dataset into separate training and test subsets and thereafter using cross-validation or hold-out validation. The cross-validation principle will be explained in the next section.

Cross-validation

Ideally, when enough data is available, a validation set will be put aside to assess the performance of a prediction model. This latter is known as hold-out validation. Since data is often scarce, this is not desired. To overcome this problem, cross-validation is introduced. Cross-validation is a method for predictive performance evaluation of a model. In particular for small data sets, cross-validation is recommended [11, 12]. The main purpose of cross-validation is to achieve a stable and reliable estimate of the model performance [13]. In k -fold cross-validation, the dataset X is randomly split into k mutually exclusive subsets, the folds: $\{X_1, X_2, \dots, X_k\}$ of approximately equal sizes. Typical choices for k are 5 or 10 [14]. For example, when $k = 10$ the scenario corresponds to Figure 14. Data is split into two parts, on one part training is done ($k - 1$ parts) while the predictive performance is tested on the other, test, part. The principle of cross-validation is based on the fact that a model is trained using some instances of the dataset and leave some instances out of it, to test the model after it has been trained. [15]

The cross-validation accuracy is the overall number of correct classifications, divided by the number of instances in the dataset. The accuracy obtained in each iteration k is then averaged to get the model accuracy. An important thing that should be taken into account is that data should be stratified before being split into k segments. Stratification is the principle that data is rearranged in such a way that each fold is a good representative of the whole [1, 15]. This is performed by randomisation. Implementing cross-validation in the training algorithm, may avoid overfitting, because the training samples are independent from the test samples. However, the size of the folds may be critical, since this may lead to under- or overfitting. In general, higher values of k (small test sets) may result in higher accuracy. However, this may lead to overfitting. [15]

It must be noted that the data actually being hold-out is different every iteration, i.e. it is random in k -fold cross-validation. Therefore, the performance measures may slightly vary every time the model has been running; however, in generally these changes are small.

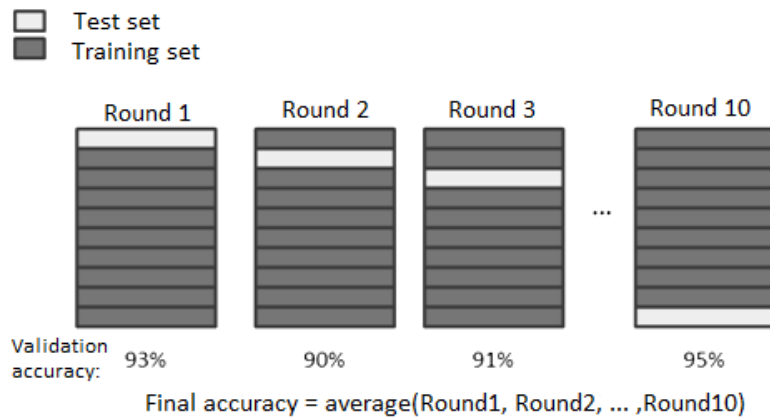


Figure 14: Principle of cross-validation for $k = 10$.

§3.3 Support Vector Machine

The goal of support vector machine (SVM) is to find a discriminative function, that calculates on which side of the decision boundary an unknown data point is located. SVM algorithms classify data by finding the decision boundary that separates all data points of one class from those of the other class, see Figure 15. The decision boundary is also known as the hyperplane. The optimal hyperplane is the one with the largest margin between the two classes. This will be further explained in a next section. Moreover, the support vectors are the data points on which the decision boundary is based. In most cases, data classes are not linearly separable by a hyperplane. If data is not linearly separable, a loss function is used to penalize points on the wrong side of the hyperplane. A kernel is introduced to transform non-linearly separable data into higher dimensions where a linear decision boundary can be found and described in the section "Kernel scale".

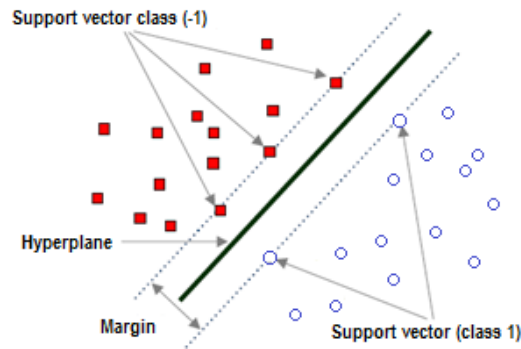


Figure 15: Principle of SVM with linear separable data, $x \in \mathbb{R}^2$

3.3.1 SVM classifier

Given the following training data:

$$(x_1, y_1), (x_2, y_2), \dots, (x_n, y_n), \quad x_i \in \mathbb{R}^p, \quad y_i \in \{-1, +1\} \quad (4)$$

where x is the input, n is the number of training samples, y the output, where $y = -1$ for class 0 and $y = +1$ for class 1 and p the number of inputs per sample (dimensions). Suppose two classes that are linearly separable. This training data can be separated by a decision boundary, which is called the hyperplane. The hyperplane separates all data points of one class from those of the other class. The approach when data should be classified into two classes is known as "binary classification". The hyperplane is defined by a function, where w is a vector and β_0 a bias, that can separate the classes without error

$$\{x \mid f(x) = w \cdot x + \beta_0 = 0\} \quad (5)$$

To find such a hyperplane, w and β_0 should be estimated in a way that

$$\begin{cases} w \cdot x_i + \beta_0 > 1 & \text{if } y_i = 1 \quad (\text{class1}) \\ w \cdot x_i + \beta_0 < -1 & \text{if } y_i = -1 \quad (\text{class0}) \end{cases} \quad (6)$$

The data points which define the optimal hyperplane are called the support vectors. The support vectors lie on the two margins of the hyperplane and are parallel to the optimal hyperplane and are given by

$$w \cdot x_i + \beta_0 = \pm 1 \quad \equiv \quad y_i(w \cdot x_i + \beta_0) = 1 \quad (7)$$

The distance between the support vectors to the hyperplane is defined as the margin, M . The optimal hyperplane is the one with the largest margin between the two classes. Based on vector principles, the distance d (known as the norm) to the hyperplane can be described by

$$d(x, f(x)) = \frac{|x \cdot w|}{\|w\|} \quad (8)$$

The width of the hyperplane is $2M$, hence the largest margin $2M = 2/\|w\|$, see Figure 16a. To maximize the margin, the smallest $\|w\|$ is chosen (equal to $\min\|w\|$). This gives the following optimization problem:

$$\min\|w\| \quad \text{subject to } y_i(w \cdot x_i + \beta_0) \geq 1 \quad \forall i, \quad (9)$$

Once this optimization problem was solved, the pair (w, β_0) were found for the smallest $\|w\|$. Thereafter, the equation of the optimal hyperplane can be found.

The signed distance from a data point x to the hyperplane is given by the classification rule $G(x)$. Depending of the sign of $G(x)$, a data point is classified to either class 0 or class 1. $G(x)$ is defined by

$$G(x) = \text{sign}[w \cdot x_i + \beta_0] \quad (10)$$

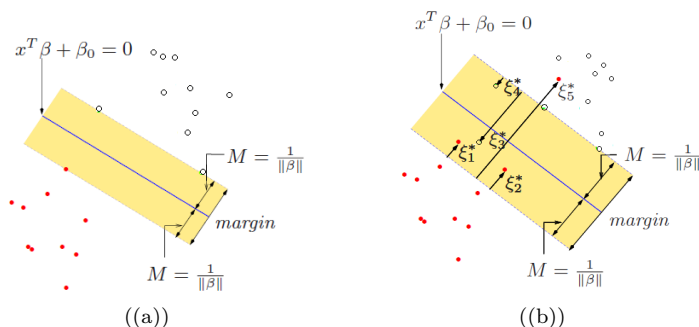


Figure 16: Separation of SVM classifier, where β is equal to w in the above formulations. The red filled dots represent one class, while the other class is represented by the black outlined dots. Adapted from [14].

3.3.2 SVM parameters

Regularization parameter C

Suppose that the classes overlap in the input feature space $x \in \mathbb{R}^p$, see Figure 16b. One way to deal with the overlap is to allow for some points to be on the wrong side of the margin. Define the slack variables $\xi = \{\xi_1, \xi_2, \dots, \xi_n\}$ [16]. These ξ variables contain the distance from its corresponding training sample x to their correct decision region. The support vectors will lie on the edge of the margin ($\xi_i = 0$). Now we are modifying the regularization parameter in the optimization problem to modify a constraint, which is called regularization:

$$y_i(w \cdot x_i + \beta_0) \geq 1 - \xi_i \quad (11)$$

where ξ_i are the samples by which the classification, derived from formula 7, is on the wrong side of its margin ($\xi_i > 1$), also known as misclassifications [14].

By taking the sum $\sum \xi_i$, the total number of misclassifications can be limited by formula (12).

$$\min \|w\| \quad \text{subject to} \quad \begin{cases} y_i(w \cdot x_i + \beta_0) \geq 1 - \xi_i \quad \forall i, \\ \xi_i \geq 0, \quad \sum \xi_i \leq \text{constant} \end{cases} \quad (12)$$

This formula can be "re-written" in the equivalent form:

$$\begin{cases} \min \|w\|^2 + C \sum_{i=1}^N \xi_i \\ \text{Subject to} \quad \xi_i \geq 0, \quad y_i(w \cdot x_i + \beta_0) \geq 1 - \xi_i \quad \forall i, \end{cases} \quad (13)$$

where the regularisation parameter C replaces the constant in formula (12).

It is obvious that the chosen value of C should be based on how the training data is distributed. Although, it can be taken into account that a small regularisation parameter C means that the classifier is able to accept more misclassifications. In that case, minimization of formula (13) does not consider the small term of the "regularization" sum and therefore, the margin of the hyperplane will be the widest as possible. In contrast, a larger regularisation C parameter will accept less misclassifications, resulting in a smaller margin, see Figure 17.

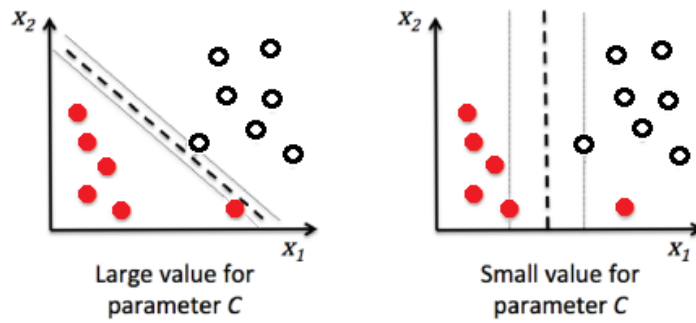


Figure 17: Choices of parameter C . The red filled dots represent one class, while the other class is represented by the black outlined dots. On the left a large value for C is chosen, regularising no misclassifications and therefore resulting in a small hyperplane margin. On the right a small value for C is chosen, regularise misclassifications and therefore resulting in a larger hyperplane margin.

The support vector classifier has been described so far for finding a linear boundary in the input feature space, either with or without allowing misclassifications. In the next section the optimization problem is given in case of non-linear separable data, in a special way that the input features are involved via inner products.

Kernel scale

Consider the case where x is not linearly separable, thus there exist no hyperplane that divides the data correctly in two classes. In that case, there exist a transformation (called feature mapping) $\phi : \mathbb{R}^p \rightarrow \mathbb{R}^{p^+}$, for some $p^+ > p$ that maps all $x \in \mathbb{R}^p$ into a higher dimensional space such that the transformed data $\phi(x)$ is linearly separable through a hyperplane in \mathbb{R}^{p^+} [14]. In this extended feature space the optimal hyperplane is constructed, with previously mentioned maximized margin. It would be considered that mapping into a high-dimensional feature space will add extra complexity to the problem. We can represent the optimization problem by the input features via inner products. The method of directly computing the inner products is called *kernel function* or *kernel trick* [14]. The transformation requires only knowledge of the kernel function, which measures the inner products in the transformed feature space [14]:

$$K(x, x') = \langle \phi(x), \phi(x') \rangle \quad (14)$$

where ϕ is a function that project the vectors x into a new feature space. The kernel function K measures the inner-products between two vectors.

One of the most familiar kernels used in machine learning is the Radial Basis Function (RBF). The kernel K of the Gaussian RBF kernel is expressed as follow [14, 17]:

$$K(x, x') = \exp(-\gamma \|x - x'\|^2) \quad (15)$$

As can be seen in formula (15), a smaller γ results in a kernel scale that don't descend rapidly as the point x' move away from x . This suggests that data points far away from the hyperplane will be involved as well, resulting in a more 'smooth' or 'coarse' classifier. In order to this large kernel scale, it will contribute to high variance and small bias*. In contrast, higher gamma results in a kernel that descend rapidly as the point x' moves away from x , and is therefore known as a 'fine' classifier, see Figure 18.

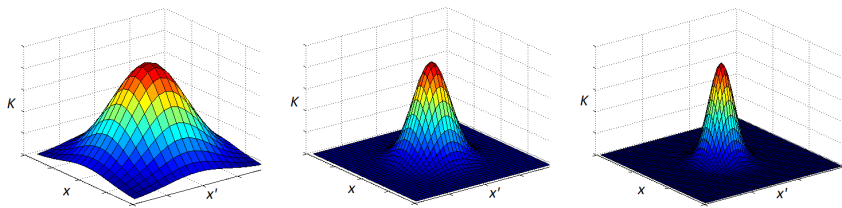


Figure 18: Choices of parameter γ . On the left the kernel scale for a small γ is represented, resulting in smooth classifier where a large variance of data points are involved. On the right the kernel scale is presented for a large γ , resulting in a fine classifier where only data points close to the hyperplane will be involved. In the middle the intermediate is shown. Adapted from [18].

*Bias is known as the average difference between the expected and true outcome, whereas variance is known as the variability of the model for a given data point by creating the model several times [68].

Depending on the kernel scale, a Gaussian kernel can be assumed as a fine, medium or coarse classifier. In our main research question we have optimized this parameter according to the suggested kernel scales of the Classification learner app*. In general, if the number of input features increase, this will result in a higher dimensional space, where data is distributed further away from each other. Therefore, the choice of a kernel is related to number of input features. A fine Gaussian kernel makes fine distinction between classes using a kernel scale commonly set to $K = \sqrt{P}/4$, where P is the number of input features. An example of a fine Gaussian kernel can be seen in Figure 18 on the right. Medium Gaussian kernels make relatively fewer distinction between classes with a kernel scale set to $K = \sqrt{P}$. In contrast, coarse Gaussian kernels make coarse distinction between classes using a larger kernel scale, commonly set to $K = \sqrt{P} \cdot 4$. [15] An example of this coarse Gaussian kernel can be seen in Figure 18 on the left.

3.3.3 Cost function

To describe how well the responses of the model fit the true data, a cost function approach is proposed. To this end, a hypothesis function $h_\theta(x) = \hat{y}$ is introduced, which describes the relation between the input $x \in \mathbb{R}^p$, and the output $\hat{y} \in \{-1, +1\}$, where h_θ is described by the used transformation method, depending on the chosen ML algorithm. In ML cost functions are used to estimate how models are performing. Thereby the main goal of ML is to find parameters and weights that minimizes the cost function (16)

$$J(\theta) = \sum_{i=1}^n [y_i - \hat{y}_i]^2 \quad (16)$$

where $J(\theta)$ is defined as the cost, y as the true output and \hat{y} as the predicted output. The best model is defined as the model that minimizes the residual errors of the cost function. A residual error is defined as the difference between the predicted output \hat{y} and the true output y . Therefore, a perfect model, succeeding from minimized residual errors set to $[y_i - \hat{y}_i]^2 = 0$, predicts all output values correct.

The cost function is minimized using the gradient descent algorithm. The gradient descent approach has been described by several authors [19]. In short, gradient descent is the optimization algorithm that finds the (local) minimum of a function and therefore (locally) minimizing the error $J(\theta)$.

* The Classification learner app is implemented in Matlab 2017 and is used to train (supervised) models to classify data.

3.3.4 Multiclass classification

As stated before, classifying data into one of two classes is called binary classification (with classes $Z = 2$). SVM was originally developed for binary classification [20]. However, the real-world often require discrimination of more than two classes, known as multiclass classification [21]. Basically, multiclass classification problems ($Z > 2$) are commonly partitioned into a series of binary classification problems, such that SVM can be directly applied. Multiclass classification can be categorized into the one versus one (one-vs-one) and one versus all (one-vs-all) approach. Both approaches decompose the multiclass problem into a predefined set of binary problems and forms the basis of the multiclass feature selection method to be presented [22].

One versus one

The one-vs-one strategy evaluates all possible pairwise classifiers and thus trains $Z(Z - 1)/2$ individual binary classifiers, see Figure 19. Every classifier assigns the input to one of the other classes, while discarding the rest of the classes. Given a data set x of training data, one-vs-one learns $Z(Z - 1)/2$ SVM classifiers $f_{ij}(x) := \text{sign}[w_{ij} \cdot x + \beta_0]$ that classify Z_i (positive class) against Z_j (negative class). Notice that for each f_{ij} there is no f_{ji} , thus there are no duplicates. For an input feature $x \in \mathbb{R}^p$, one-vs-one determines all $f_{ij}(x)$ and votes for Z_i if $f_{ij}(x) > 0$, otherwise for Z_j . Finally, x is classified as that Z with the most votes. This latter is called the "Max Wins" voting strategy. [22–24]

One versus all

The one-vs-all strategy constructs Z separate binary classifiers. The binary classifier is trained using data from one class as the positive class and the remaining classes ($Z - 1$) as the negative class, see Figure 19. Given a data set x of training data, one-vs-all learns a SVM classifier $f_i(x) : w \cdot x_i + \beta_0$ for each Z_i (positive class) against all other $Z_j \neq i$ (negative class). An input feature $x \in \mathbb{R}^p$ is now classified as Z_i where $i = \text{argmax}_i f_i(x)$. This latter is called the "Winner takes all" strategy. [22, 23]

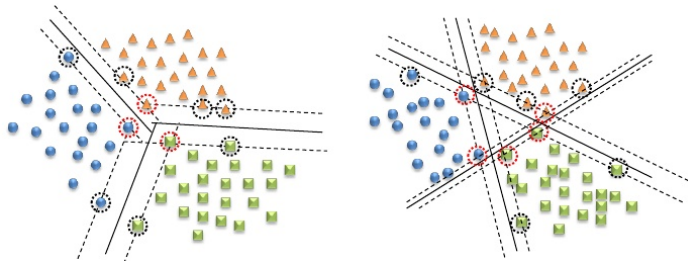


Figure 19: Multiclass classification strategies for three classes ($Z = 3$). Classes are represented by the blue dots, orange triangles and green squares. On the left the one-vs-one approach is shown and on the right the one-vs-all approach [25].

References

- [1] H. Wi and F. Eibe. Practical machine learning tools and techniques. *United State: Morgan Kauffman*, 2011.
- [2] Mathworks. What is machine learning? 3 things you need to know. 2018.
- [3] T.M. Mitchell. *The discipline of machine learning*, volume 9. Carnegie Mellon University, School of Computer Science, Machine Learning Department, 2006.
- [4] Michael Anderson and Susan Leigh Anderson. Machine ethics: Creating an ethical intelligent agent. *AI Magazine*, 28(4):15, 2007.
- [5] V. Vapnik. Pattern recognition using generalized portrait method. *Automation and remote control*, 24:774–780, 1963.
- [6] V. Vapnik. A note one class of perceptrons. *Automation and remote control*, 1964.
- [7] P.B. Schiilkop, C. Burgest, and V. Vapnik. Extracting support data for a given task. In *Proceedings of the 1st international conference on knowledge discovery & data mining*, pages 252–257, 1995.
- [8] V. Vapnik, S. E. Golowich, and A. J. Smola. Support vector method for function approximation, regression estimation and signal processing. In *Advances in neural information processing systems*, pages 281–287, 1997.
- [9] K.R. Müller, A. J Smola, G. Rätsch, B. Schölkopf, J. Kohlmorgen, and V. Vapnik. Predicting time series with support vector machines. In *International Conference on Artificial Neural Networks*, pages 999–1004. Springer, 1997.
- [10] J. Johnson. General shape of data. general regression and over fitting. 2013.
- [11] T. S. Furey, N. Cristianini, N. Duffy, D. W. Bednarski, M. Schummer, and D. Haussler. Support vector machine classification and validation of cancer tissue samples using microarray expression data. *Bioinformatics*, 16(10):906–914, 2000.
- [12] S. Wold. Cross-validatory estimation of the number of components in factor and principal components models. *Technometrics*, 20(4):397–405, 1978.
- [13] Z. Reitermanova. Data splitting. In *WDS*, volume 10, pages 31–36, 2010.
- [14] J. Friedman, T. Hastie, and R. Tibshirani. *The elements of statistical learning*, volume 1. Springer series in statistics New York, 2001.
- [15] S. Yadav and S. Shukla. Analysis of k-fold cross-validation over hold-out validation on colossal datasets for quality classification. In *Advanced Computing (IACC), 2016 IEEE 6th International Conference on*, pages 78–83. IEEE, 2016.

- [16] C. Cortes and V. Vapnik. Support-vector networks. *Machine learning*, 20(3):273–297, 1995.
- [17] B. Scholkopf, K.K. Sung, C. J.C. Burges, F. Girosi, P. Niyogi, T. Poggio, and V. Vapnik. Comparing support vector machines with gaussian kernels to radial basis function classifiers. *IEEE transactions on Signal Processing*, 45(11):2758–2765, 1997.
- [18] Stackoverflow. 2d/3d plot of image processing filters. 2016.
- [19] X.M. Dong and D.R. Chen. Learning rates of gradient descent algorithm for classification. *Journal of Computational and Applied Mathematics*, 224(1):182–192, 2009.
- [20] F. Schwenker. Hierarchical support vector machines for multi-class pattern recognition. In *Knowledge-based intelligent engineering systems and allied technologies, 2000. Proceedings. Fourth international conference on*, volume 2, pages 561–565. IEEE, 2000.
- [21] Z. Wang and X. Xue. Multi-class support vector machine. In *Support Vector Machines Applications*, pages 23–48. Springer, 2014.
- [22] D. Wu, C. Li, J. Chen, D. You, and X. Xia. A novel multi-class support vector machines using probability voting strategy and its application on fault diagnosis of gearbox. *International Journal of Performability Engineering*, 10(2):173–186, 2014.
- [23] M. Aly. Survey on multiclass classification methods. *Neural Netw*, 19:1–9, 2005.
- [24] S.W. Lee and A. Verri. Pattern recognition with support vector machines first international workshop, svm 2002 niagara falls, canada, august 10, 2002 proceedings. 2002.
- [25] S. Herrero. Multiclass classification using massively threaded multiprocessors. 2010.

4. Article

Identification of a previous myocardial infarction using ventricular fibrillation characteristics of the 12-leads electrocardiogram: A single lead model versus a multiple lead model

S. Gantevoort¹, J. Thannhauser¹, J. Nas¹, H.J. Zwart², G. Meinsma², M.J. de Boer¹, N. van Royen¹, J.L. Bonnes¹, M.A. Brouwer¹

¹ Department of Cardiology, Radboud University Medical Center, Nijmegen, The Netherlands

² Department of Applied Mathematics, University of Twente, Enschede, The Netherlands

Introduction: Myocardial infarction (MI) is a common cause of ventricular fibrillation (VF) in the setting of out-of-hospital cardiac arrest (OHCA). Identification of underlying etiology in VF-patients remains challenging. As a first step towards in-field identification of an MI, we investigated the ability of support vector machine (SVM) algorithms to differentiate patients with and without a previous MI in a controlled setting after implantable cardioverter defibrillator (ICD) implantations.

Method: We studied patients who underwent defibrillation testing at the Radboud University Medical Center, Nijmegen (2010-2013) from a registry of first ICD implantations. Seven VF waveform characteristics were calculated from 4.1 second VF-segments of ten surface electrocardiogram (ECG) leads. VF characteristics were used as input predictors for SVM models. Patients were classified according to their history of MI, either through binary (previous MI vs. no MI) or multiclass classification (previous inferior MI, anterior MI or no MI). Model performances were assessed by receiver operating characteristic (ROC) analysis in terms of area under the curve (AUC). Two models were tested: one using VF characteristics of a single lead (*lead II*) and one using VF characteristics of multiple leads (three leads).

Results: We studied 189 patients, of whom 101 had a history of MI. Specifically, 54/101 had an inferior MI and 47/101 an anterior MI. *Binary classification:* The single lead model demonstrated a mean AUC of 0.64 ± 0.01 . The optimal multiple lead model (*lead II*, *V1* and *V6*) demonstrated a mean AUC of 0.74 ± 0.01 . *Multiclass classification:* The AUCs of the single lead model were 0.59, 0.73 and 0.59 for the identification of no MI, inferior MI and anterior MI, respectively. The optimal multiple lead model (*lead II*, *V1* and *V3*) demonstrated AUCs of 0.70, 0.80 and 0.77 for the identification of no MI, inferior MI and anterior MI, respectively.

Conclusion: We demonstrated that identification of underlying etiology using VF-waveform characteristics seems feasible using a single lead model of VF-characteristics. A multiple lead approach improved the discriminative ability compared to the single lead approach. In follow-up on this experimental study, in-field studies are eagerly awaited.

Keywords: ventricular fibrillation – myocardial infarction – out-of-hospital cardiac arrest – machine learning – support vector machine

§ 4.1 Introduction

OHCA occurs frequently, with a global incidence of around 55 per 100.000 person-years, and carries a poor prognosis [1-3]. VF is the initial rhythm in approximately 40% of all OHCA cases [2, 4]. The most common cause of VF is acute coronary ischemia, which is commonly reversible and of which the presence can only be diagnosed after restoration of organized rhythm [6-8]. As of yet, the underlying cause of VF, as myocardial infarction, cannot be determined in-field. In order to optimize treatment of VF to individual needs, more insight is warranted into the aetiology of VF.

A potential tool to identify the underlying aetiology is the VF waveform on the electrocardiogram (ECG). As initially considered a marker for arrest duration and outcome, VF characteristics have been shown to reflect underlying heart disease as well [9, 10]. It has been demonstrated in animal as well as in human studies that underlying MIs causes low-amplitude-low-frequency VF [11-14]. Interestingly, a recent VF study demonstrated that a history of MI causes regional differences on the 12-lead ECG, related to the area of infarction [12].

However, to identify the presence of an MI using the VF waveform remains a clinical challenge. As a first step towards in-field identification of MI, VF waveform analysis of induced VF in a controlled setting is required. Rebergen (2016) was the first to explore the potential of machine learning (ML) based algorithms to discriminate between the presence and absence of a previous MI, using VF waveform characteristics. In this proof of concept study, ML models using 12-lead ECG characteristics of induced VF were demonstrated to be a feasible method to identify a previous MI.[15] Although these results were promising, in the setting of an OHCA only a single ECG lead is routinely measured by the defibrillator paddles, and there is no time for attaching a full 12-lead ECG. This may limit translation to the OHCA setting.

To narrow the gap between the experimental setting and clinical practice, more insight is required into the ability of the VF waveform to identify an MI. The controlled setting of defibrillation testing (DFT) after implantable cardioverter defibrillator (ICD) implantations provides an ideal setting to investigate this topic. To mimic the current OHCA setting, our primary aim was to investigate the ability of a single ECG-lead ML model to identify a previous MI. Furthermore, we hypothesized that adding more ECG leads increases the discriminative ability of these models. Therefore, secondary aims were to assess the optimal combination of ECG-leads and to compare this multiple lead model to our initial single lead model.

§ 4.2 Methods

Study population

We identified all patients who underwent defibrillation testing at the Radboud University Medical Center, Nijmegen between June 2010 and December 2013 from a registry of first ICD implantations. We studied patients of whom the 12-lead ECG with induced VF was analysable and in whom the history of a previous MI was known prior to the ICD implantation. Since most infarctions involve the inferior and/or anterior wall, solely these infarctions were included, corresponding to a study of Bonnes et al. [12]. Exclusion criteria were the following: age <18 years, congenital heart disease and right-sided ICD implant. In addition, patients were excluded in case of a history of MI that did not involve the anterior or inferior wall. Given the observational design of the study, informed consent was not necessary to obtain according to the Dutch Act on Medical Research involving Humans Subjects.

ICD implantation

The devices implanted are Medtronic (Minneapolis, Minnesota, USA), St Jude Medical (St. Paul, Minnesota, USA), Boston Scientific (Marlborough, Massachusetts, USA) or Biotronik (Berlin, Germany) ICDs or cardiac resynchronization therapy defibrillator (CRT-D) systems with transvenous single coil leads. Routine defibrillation testing was performed after ICD implantation to test the ability of the implanted device to sense, detect and terminate VF appropriately. After sedation with propofol, VF was induced using T-wave shock, direct current pulses or 50 Hz burst pacing. The presence of VF, defined as a rapid (around 300 bpm) grossly irregular ventricular rhythm with marked variability of QRS cycle length, morphology and amplitude, was confirmed on 12-lead surface ECG recordings. Sequential shocks were delivered (15 – 25 – 35 Joule) until VF was terminated. In case of persisting VF after the third shock, external defibrillation was performed.

Data acquisition

Data regarding demographic, clinical and echocardiographic parameters were collected from patient records. During DFT testing, conventional 12-lead ECG data were recorded and digitalized using BARD Electrophysiology 16 bit D/A converter with a sample frequency of 1000 Hz. The signals were filtered using a second order Butterworth high-pass filter with a 2 Hz cut-off frequency and a low-pass filter with a 48 Hz cut-off frequency to remove artifacts produced by external sources. In total 10 leads were selected for VF analysis, as these represent the inferior (*II, III and aVF*), anterior (*V2-V6*), and right part of the heart (*V1 and aVR*).

VF waveform

Waveform characteristics were calculated from the surface ECG leads, using a time segment of 4.1 seconds (= 4096 samples) prior to the first delivered shock to terminate VF. Calculations were performed using Matlab (Version 2014b, The Mathworks Inc., Natick, MA). For mathematical descriptions, see Table 1. The following VF characteristics were measured:

- Mean absolute amplitude (MAA), which is determined from the ECG signal in time-domain.
- Amplitude spectrum area (AMSA). First, the signal is converted into frequency domain using a Fast Fourier Transform (FFT). The AMSA is calculated as the summed product of the amplitude and corresponding frequency over an interval of 2 to 20 Hz.
- Median frequency (MF), is calculated from the power spectrum as the frequency that divides the integrated power signal in two equal areas.
- Median slope (MdS), which is the median slope of the amplitude per second in time domain.
- Bandwidth (BW), is calculated as the difference in frequency corresponding to the first and third quartile of the total power.
- Detrended fluctuation analysis (DFA), is calculated from the original unfiltered ECG signal in time domain. DFA corresponds to long-range correlations of the signal. In short, time series to be analysed are first integrated. Thereafter, integrated time series are divided into boxes of equal length, n . In each box n a root mean square line is fitted into the data, representing the trend. Next, the integrated time series are detrended by subtracting the trend in each box n . This is repeated over several time scales to characterize the relationship between the average fluctuation and the box size n . Finally, the DFA slope is divided into two separated slopes, DFA α_1 and DFA α_2 . For further explanation, see **Appendix A.1**.

Table 1. Overview of the ventricular fibrillation (VF) waveform characteristics and their calculations. Abbr = abbreviation.

Waveform characteristic	Abbr.	Mathematical description	Unit
Mean absolute amplitude	MAA	$\frac{1}{N} \sum_{i=1}^N x_i $	mV
Amplitude spectrum area	AMSA	$\frac{2}{N} \sum_{2 \leq f_k \leq 20} \hat{x}_k f_k$	mV . Hz
Median frequency	MF	f_m such that $\sum_{i=1}^m PSD(f_k)$ $= \frac{1}{2} \sum_{i=1}^N PSD(f_k)$	Hz
Median slope	MdS	$median(x_2 - x_1 , \dots, x_n - x_{n-1}) f_s$	mV s ⁻¹
Bandwidth	BW	f_a such that $\sum_{i=1}^a PSD(f_k)$ $= \frac{1}{4} \sum_{i=1}^N PSD(f_k)$ f_b such that $\sum_{i=1}^b PSD(f_k)$ $= \frac{3}{4} \sum_{i=1}^N PSD(f_k)$ $BW = f_b - f_a$	Hz
Detrended fluctuation analysis	DFA α_1 DFA α_2	See description in Appendix A.1	-

$x_i \in \{i=1,2,\dots,N\}$ are samples of VF segment $x(t)$ in time-domain with sampling rate f_s . The unit of x_i is millivolts (mV). The frequency characteristics were calculated for frequency band $[2,20]$. $|\hat{x}_k|$ is the amplitude of Fourier transform of x_i at frequency f_k , with $f_k = \frac{k}{N} f_s$. The power spectral density (PSD) function describes the power of the signal as a function of frequency f_k and was calculated as $PSD(f_k) = |\hat{x}_k|^2$. m , a and b are the minimal sample numbers at which the power of the signal is at least 50%*, 25%* and 75%*, respectively. * For the minimal sample numbers that not exactly align these powers of the signal, the first subsequent sample number is selected.

Study groups

We defined the following study groups for binary classification; patients with a previous MI (either an inferior or anterior MI) and without a history of MI. For multiclass classification we defined the following three study groups; patients with a previous inferior MI, patients with a previous anterior MI and patients without a history of MI. Evidence for the presence or absence of a previous MI was based on reports in the medical files. MI was defined according to the European Society of Cardiology (ESC) criteria [44]. The finding and localisation of an MI were based on a combination of information from ECG findings and/or coronary angiographies and was confirmed by imaging reports (i .e. magnetic resonance imaging (MRI), echo or nuclear scan) [12].

Discriminative models

VF waveform characteristics were calculated for the surface ECG-leads and used as input features for the discriminative models. We divided a single lead model and multiple lead models:

- Single lead model: For the single lead model, we used VF-waveform characteristics of *lead II*
- Multiple lead model: The multiple lead model consisted of VF-waveform characteristics of three ECG-leads, reflecting the inferior, anterior and right side of the heart:
 - one of the leads which reflects the inferior part of the heart (*II, III or aVF*)
 - one lead which reflects the anterior/lateral part of the heart (*V2 to V6*)
 - one lead which reflects the right side of the heart (*V1 or aVR*)

Machine Learning

Machine learning (ML) was performed using the Classification learner App in Matlab (Version 2017b, The MathWorks Inc., Natick, MA). As predictor input the VF waveform characteristics were selected. As response output the presence or absence of a previous MI was selected and divided in two groups (previous MI vs. no previous MI) and three groups (no previous MI, inferior previous MI or anterior previous MI). Automated training was applied to search for the best support vector machine (SVM) model. The developed classification model is thereafter adapted in the editor of Matlab to calculate the performance measures. To validate model performance 5-fold cross-validation has been applied, in compliance with [68]. 5-Fold cross-validation refers to “**Cross-validation**” described in **Section §3.3**. To minimize the bias of one time running, the models have been run 100 times and the average of performance was used for evaluation, according to other studies [69, 70]. The required parameters for SVM are *K* and *C* and were selected according to the highest area under the curve (AUC). The parameter *K* refers to the parameter for “**Kernel scale**” described in **Section §3.3**. This parameter *K* for a Gaussian SVM was examined following the values: [$\sqrt{P}/4$; \sqrt{P} ; $\sqrt{P} \cdot 4$], where *P* represents the number of input features. Parameter *C* was examined following the values: [0.1; 1; 2; 5; 10; 20; 40; 50; 100], which refers to the parameter for “**Regularisation**” described in **Section §3.3**.

Performance measures

To assess the performance of the different models, receiver operating characteristic (ROC) curves were calculated. The principle and the requirement of the ROC curve has been described in **Appendix A.3**. From the ROC-curve, the area under the curve was calculated. The optimal operating point on the ROC curve was obtained as described in “**Optimal operating point**” in **Appendix A.3**. From this optimal operating point a confusion matrix (2x2 table) was achieved. From the confusion matrices, we assessed the accuracy, sensitivity, specificity, positive predictive value (PPV) and negative predictive value (NPV):

$$Accuracy = (TN + TP)/(TN + TP + FN + FP).$$

$$Sensitivity = TP/(TP + FN) \qquad PPV = TP / (TP + FP)$$

$$Specificity = TN/(TN + FP) \qquad NPV = TN / (TN + FN)$$

where TP represents the true positives, TN the true negatives, FP the false positives and FN the false negatives.

Statistical analysis

Categorical data were expressed as frequencies (percentages) and analysed using the Chi-square test. Continuous data was firstly tested for normal distribution, reported as mean \pm standard deviation (SD), or median \pm interquartile range* (IQR), whichever appropriate, and then analysed using the Student t-test or the Mann-Whitney U test, whichever appropriate.

* The interquartile range is the difference between 75th and 25th percentiles.

Multiclass classification was analysed using the non-parametric Kruskal-Wallis test. The additional value of multiple leads was analysed using the paired t-test. For the statistical analyses, Microsoft Excel (Version 2007, Microsoft) and SPSS Statistics (Version 2007, IBM) were used. A p-value of <0.05 was considered to be statistically significant.

Outcome measures and study aims

The primary outcome measure was the area under the ROC-curve (AUC). Secondary outcome measures were the accuracy, sensitivity, specificity, PPV and NPV. The following study aims were addressed: First, performance of the single lead model was assessed. Secondly, of the multiple lead model, the optimal combination was investigated, after which the optimal multiple lead model was compared to the single lead model.

§ 4.3 Results

Baseline characteristics

Patient characteristics

A total of 189 patients were studied, of whom 101 (53%) had a history of MI. Specifically, of the 101 patients with a history of MI, 54 (53%) had an inferior MI and 47 (47%) had an anterior MI. The overall mean age was 63 ± 13 years and 141 (75%) were men. In 67 (35%) of the patients an ICD was implanted for secondary prevention. Furthermore, it is shown that there is a significant difference in distribution of gender and age between the two study groups, $p=0.001$ and $p<0.001$, respectively. Baseline characteristics of the two study groups are presented in supplementary Table 15 in **Appendix B.1** on page 75.

VF waveform characteristics

VF waveform characteristics for the two study groups are presented per lead in supplementary Figure 31 on page 77. VF waveform characteristics for the three study groups are presented per lead in Figure 21 on page 44.

4.3.1 Binary classification

Single lead model

For the identification of a previous MI using a single lead (*lead II*), the SVM model have shown a mean AUC of 0.64 ± 0.01 and a mean accuracy of $60.1\pm 0.9\%$. The selected (optimized) SVM parameters *C* and *K* are set to 1 and 11, respectively. Using the output scores for the classification (as described in **Appendix A.2**) the performance for classifying the presence of a previous MI is shown in Figure 20. Thereafter the optimal operating point was performed (**Appendix A.3**), resulting in a confusion matrix. According to the confusion matrices the mean sensitivity was $86.8\pm 1.5\%$, the mean specificity $29.4\pm 2.2\%$, the mean PPV = 0.59 ± 0.01 and the mean NPV = 0.66 ± 0.03 .

Optimal lead combination

The performances of all lead combinations for the multiple lead model were obtained and given in Table 2. It is shown that a lead combination consisting of *lead II*, *V1* and *V6* turns out to be the best combination for the identification of a previous MI using VF waveform characteristics. Furthermore, it is remarkable that *lead II* as ‘inferior lead’ led to more frequently higher AUCs compared to *lead III* and *aVF*. Likewise, more frequently higher AUCs applies to *V5* and *V6* for the ‘anterior lead’ and *V1* for the ‘right side lead’.

Multiple lead model

For the identification of a previous MI using the multiple leads (*lead II*, *V1* and *V6*), the SVM model have shown a mean AUC of 0.74 ± 0.01 and a mean accuracy of $67.5 \pm 0.8\%$. The selected SVM parameters *C* and *K* are set to 1 and 18, respectively. The performance for classifying the presence of a previous MI is shown in Figure 20. Thereafter the optimal operating point was performed, resulting in a confusion matrix. According to the confusion matrices the mean sensitivity was $84.4 \pm 1.1\%$, the mean specificity $48.2 \pm 1.5\%$, the mean PPV 0.65 ± 0.01 and the mean NPV 0.73 ± 0.01 .

Additional value

It is shown that the AUC significantly increases in case of the multiple lead model (0.74 ± 0.01) compared to the single lead model (0.64 ± 0.01), $p < 0.001$. Thereby, a significant increase in the accuracy has been observed for the multiple lead model ($67.5 \pm 0.8\%$) compared to the single lead model ($60.1 \pm 0.9\%$), $p < 0.001$. Furthermore, using the optimal operating points the specificity increases in case of the multiple lead model, while the sensitivity remain almost unchanged.

Table 2. Performances of all lead combinations.

Inferior lead	Anterior lead	Right side lead	Mean AUC
II			0.64
II	V2	V1	0.65
	V2	aVR	0.67
	V3	V1	0.70
	V3	aVR	0.67
	V4	V1	0.68
	V4	aVR	0.66
	V5	V1	0.71
	V5	aVR	0.69
	V6	V1	0.74
	V6	aVR	0.71
III	V2	V1	0.61
	V2	aVR	0.66
	V3	V1	0.62
	V3	aVR	0.65
	V4	V1	0.67
	V4	aVR	0.66
	V5	V1	0.70
	V5	aVR	0.69
	V6	V1	0.74
	V6	aVR	0.70
aVF	V2	V1	0.65
	V2	aVR	0.65
	V3	V1	0.67
	V3	aVR	0.66
	V4	V1	0.69
	V4	aVR	0.66
	V5	V1	0.70
	V5	aVR	0.70
	V6	V1	0.73
	V6	aVR	0.71
10-Lead			0.72

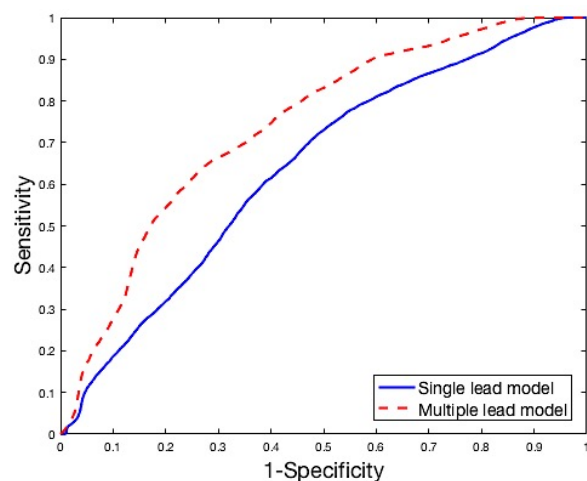


Figure 20. Receiver operating characteristic (ROC) curves for both the single lead model (blue straight line) and multiple lead model (red dotted line).

4.3.2 Multiclass classification

SVM model

For multiclass classification a linear and Gaussian SVM classifier turns out to be the best classifier for the identification of the three study groups. We tested a linear and Gaussian SVM classifier for all lead combinations. According to “**Multiclass classification**” in **Section §3.3**, we investigated both, the one-vs-one and one-vs-all approach for both classifiers. The performances for all lead combinations for both the one-vs-one and one-vs-all approach were obtained and given in **Appendix B.3** in Table 17 and Table 18 (on page 78 and 79), respectively.

Performances

We observed that the one-vs-one approach overall performs better than the one-vs-all approach, on nearly all lead combinations. According to the one-vs-one approach, the identification of a previous MI using the *single lead* model (*lead II*) led to a mean AUC of 0.64. Specifically, the AUC was 0.59 ± 0.02 , 0.73 ± 0.01 and 0.59 ± 0.02 for the identification of no MI, an inferior MI and an anterior MI, respectively, see Figure 22. The mean accuracy was $48.9 \pm 1.7\%$. The selected SVM parameters C and K were set to 1 and 3, respectively.

In Table 17 on page 78 it is shown that a lead combination consisting of *lead II*, $V1$ and $V3$ turns out to be the best combination for the identification of a previous MI using VF waveform characteristics. Furthermore, it is remarkable that *lead II* as ‘inferior lead’ led to more frequently higher AUCs compared to *lead III*. Moreover, the performances of *lead II* and *aVF* are substantially equal. Likewise, frequently higher AUCs applies to $V3$ for the ‘anterior lead’ and $V1$ for the ‘right side lead’.

According to the one-vs-one approach, the identification of a previous MI using the *multiple lead* model (*lead II*, $V1$ and $V3$) led to a mean AUC of 0.76. Specifically, the AUC was 0.70 ± 0.02 , 0.80 ± 0.02 and 0.77 ± 0.01 for the identification of no MI, an inferior MI and an anterior MI, respectively, see Figure 22. The mean accuracy was $57.0 \pm 1.8\%$. The selected SVM parameters C and K were set to 1 and 5, respectively.

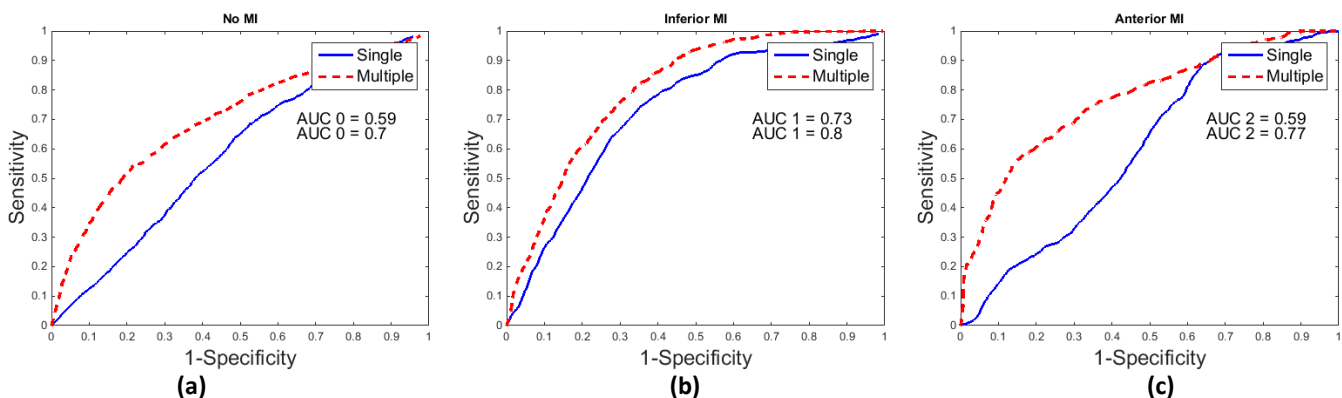
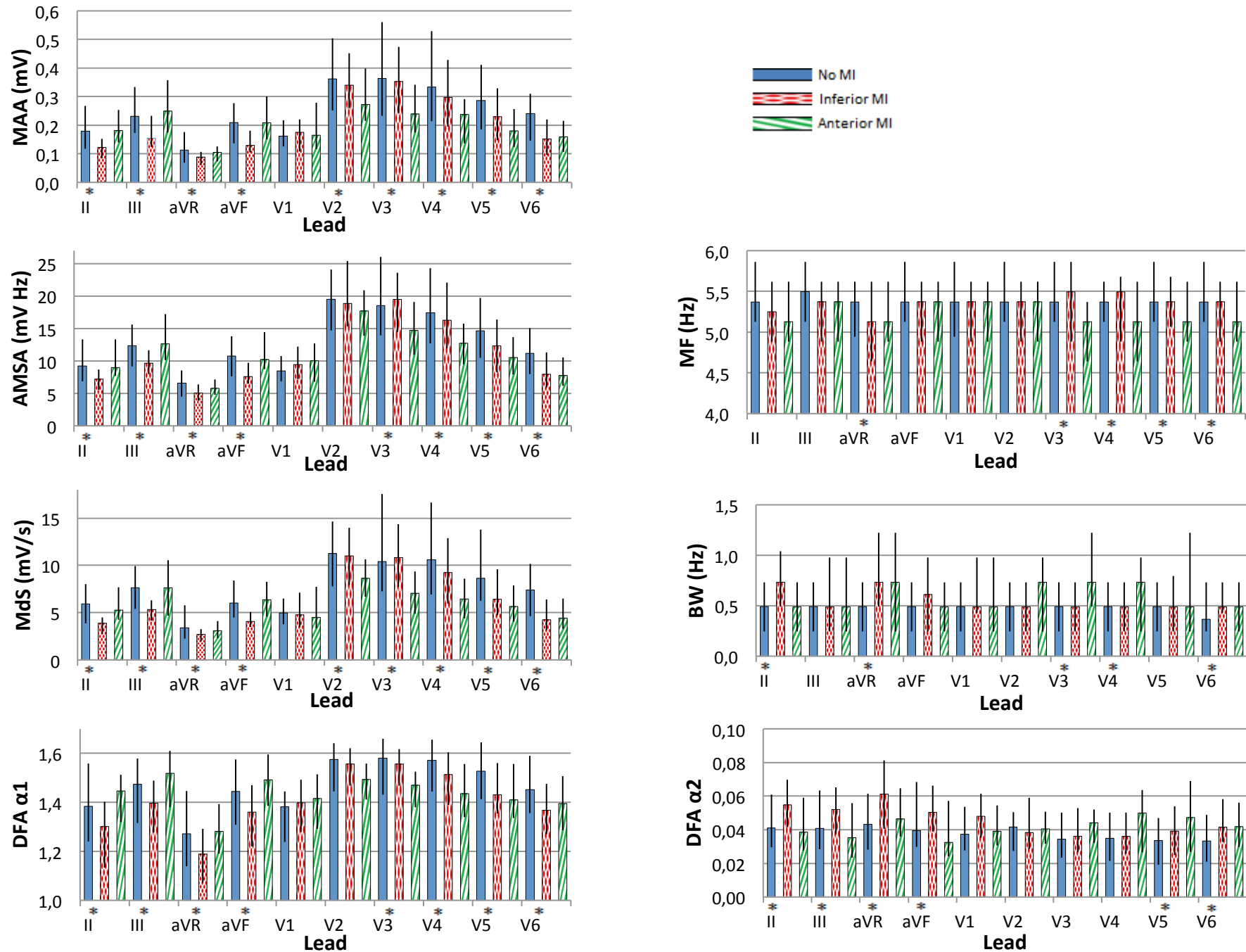


Figure 22. Area under the curve (AUC) for all three classes, for both the single lead model (blue straight line) and multiple lead model (red dotted line). In (a) the AUC is shown to identify “no myocardial infarction (MI)”, in (b) to identify an “inferior MI” and in (c) to identify an “anterior MI”.

Figure 21. VF characteristics of all 10 leads for the three study groups. Values are presented as median (IQR). Differences between the groups were tested using a Kruskal-Wallis H test. * = P<0.05



§ 4.4 Discussion

To our knowledge, this is the first study in ICD patients investigating the single ECG-lead approach versus a multiple ECG-lead approach for the identification of a previous MI. Discriminative predictive values for the identification of a previous MI were lower in the single lead approach compared to the multiple lead approach. The optimal multiple lead combination to identify a previous MI were *lead II, V1 and V6*. To localise the infarctions more specifically, either inferior or anterior, *lead II, V1 and V3* might be seen as the optimal lead combination.

Previous studies

This study was carried out to demonstrate the identification of a previous MI based on VF waveform characteristics using a machine learning approach. Over the last decades there has been large interest in studying VF waveform characteristics in both animal and human studies.

Animal studies

It has already been demonstrated in animal studies that VF waveform characteristics are related to arrest duration and shock success [71, 72]. Likewise, animal studies have shown that underlying MI, both acute and previous MI, can cause VF with lower amplitudes and lower frequencies, already at the onset of VF [59, 67, 73, 74]. However, in another study analysing the AMSA and slope, it was described that in untreated VF, the AMSA and slope were significantly lower in acute MI compared to the control group, whereas in a previous MI these characteristics were similar to controls [75]. In our study we observed lower amplitude-related characteristics and lower median frequencies in several leads in patients with a history of MI.

Human OHCA studies

In retrospective OHCA studies it has been shown that the median slope and AMSA in patients with an acute MI were lowered compared to patients without an acute MI, regardless of call-to-initial-ECG time. On the contrary, it was examined that a previous MI was not associated with a significantly lower AMSA. [11, 76] This might confirm the indication that identification of a previous MI is more challenging than identification of an acute MI.

To date, no studies have been performed that focused on the identification of underlying heart disease with the use of the VF waveform. Moreover, in several animal and OHCA studies it has been demonstrated that a previous MI was not significantly associated with lower amplitude characteristics, while significance has been observed for the setting of an acute MI. This might indicate that the identification of a previous MI is more challenging than the identification of an acute MI. Notwithstanding, the conflicting results of VF waveform characteristics between a previous and acute MI, we observed that the identification of a previous MI based on the VF waveform characteristics seems feasible. Therefore, we expect that the identification of an acute MI seems feasible as well and might be even less challenging.

Human controlled studies

A study of Bonnes et al. on patients with induced VF during DFT testing after ICD implantation, demonstrated that a previous MI was associated with lower amplitude characteristics, but only in the leads adjacent to the area of the infarction [12]. In contrast, frequency characteristics were lower only in the presence of a previous anterior MI. They suggest that this finding may be explained the fact that anterior MIs are larger infarctions, which may affect a larger extent of the VF waveform characteristics than smaller inferior MIs. Assuming that a larger infarction affects more ECG-leads, it follows that the identification of an anterior might be achieved more frequently than the identification of an inferior MI. In our study we observed that anterior MIs are correctly identified in 79% of the total anterior MI cases and inferior MIs in 89% of the total inferior MI cases.

Machine learning studies

Nowadays, machine learning algorithms have been widely implemented in rhythm detection and resuscitation optimization [77-81]. Although machine learning algorithms have been used for both previous and acute myocardial infarction detection, this was accomplished in the absence of ventricular fibrillation [82-84]. Accordingly, detection was based on ECG abnormalities in different segments of the well-known PQRST-pattern. To date, no studies were published which have focused on the detection of a previous MI based on the VF waveform using machine learning algorithms.

To summarize, previous studies have shown conflicting results on the VF waveform characteristics between animals or patients with and without a history of MI. This might be explained by the fact that studies differ in the way they measured the ECG (i.e. the number of ECG-leads). If we presume our observations that multiple ECG-leads led to superior predictive values compared to a single ECG-lead; studies which have observed no differences in the VF waveform, could possibly be explained by the fact they measured only a single ECG-lead.

Paddle ECG

Several studies, both animal and human studies, have analysed the VF characteristics of paddle ECGs. On the contrary, we have analysed the VF characteristics of varying number of ECG leads, either a single lead or three leads. This may be of interest for two reasons. From one point of view, one should consider incomparable quantitative VF characteristics when different recording leads are measured. From the other point of view, a single lead reflects the cardiac activity from only one direction. The single lead roughly corresponds to the paddle ECG lead and reflects the inferior part of the heart. Bonnes et al. already found that differences in VF characteristics were most outspoken in the leads adjacent to the area of the infarction [12]. Therefore, the single lead, *lead II*, may neglect an anterior MI when it was classified to a previous MI according to the binary classification.

Optimal lead combination

Our observations show that in case of binary classification the investigated optimal lead combination is *lead II*, *V1* and *V6*, while in case of multiclass classification the optimal combination is *lead II*, *V1* and *V3*. When inferior and anterior MIs are taken together in one group it is believed that precordial lead *V6* might be essential. This can be explained by the fact that this lead usually captures the activity of the lateral part of the heart, and it is assumed that this part is involved in both inferior and anterior MIs [85]. In contrast, to differentiate these inferior and anterior infarctions, precordial lead *V3* might be seen as the essential recording lead. With regard to these involved leads, Bonnes et al. reported the same findings [12]. They also supposed that involvement of the lateral wall occurred in both groups with a previous MI.

Implications

The first implication of our findings is that identification of a previous MI using the VF waveform characteristics of a single lead model is possible, but only to a limited extent. The performance of the identification seems to improve with the use of the multiple leads, reflecting additional recording directions of the electrical activity of the heart. This latter is driven by the fact that an MI affects particular myocardial areas and therefore has effect on specific leads that reflect these particular areas. Apparently, measuring multiple recording directions leads to a better discriminative ability of the model than measuring a single recording direction.

It should be further investigated whether our findings on induced VF also apply to the OHCA setting. However, several studies have shown that differences in VF characteristics were even more outspoken in the acute setting compared to the controlled setting of induced VF [75, 76]. Once the benefit of using multiple leads for

the identification of a previous MI by VF waveform analysis has been proven, the use of the VF waveform in OHCA could be recommended. Nowadays, defibrillation systems make use of two paddles, resulting in only one recording lead. Secondly, our observations implicate that for the identification of an MI in the OHCA setting in future, multiple ECG-leads might be recommended instead of the current single ECG-lead. It is implicated that by the use of multiple leads, more etiological information of the electrical activity of the heart will be provided and therefore a potential previous or acute MI could be identified more frequent.

Limitations

There are several limitations that need to be addressed for this study. First, the most important limitation is the retrospective design of the study. The retrospective aspect may provoke selection bias. However, a case-control study could not be executed, because nowadays DFT testing is rarely performed during ICD implantations. Nevertheless, this is the data at our disposal and patient records were scrutinized to determine the presence or absence of a previous MI.

Secondly, patients' demographics and medical history were collected from patients records. In the presence of a previous MI, the localisation was checked using ECGs and imaging reports, as described in **Section §4.2**. For the collection of these records human interpretation need to be addressed. Therefore, it should be acknowledged that an aberration of these records could not be excluded and actual results could somewhat differ.

Thirdly, the duration of the VF waveform that used to be analysed is different from several other studies. Besides, it should be considered that induced VF in the hospital setting is not similar to VF in the OHCA setting. Induced VF tends to be more organized than spontaneous VF. Moreover, in the controlled setting short-duration VF is assessed, whereas VF in the acute setting might be seen as longer-term VF. Therefore, quantitative values of the VF characteristics could not be directly compared to each other. Quite apart from the observed differences in VF characteristics in the controlled setting of a previous MI, we expect the VF waveform to be even more aberrant in the setting of an acute MI.

§ 4.5 Conclusion

We are the first to demonstrate that a multiple lead approach led to superior predictive values for the identification of an MI as compared to a single lead approach. Following on a previous study on this induced VF, we confirmed that identification of underlying aetiology using VF-waveform characteristics seems feasible. The use of multiple leads seems to have an added value for the identification of a previous MI based on VF waveform characteristics. The optimal multiple lead combination to identify a previous MI were *lead II, V1* and *V6*. To localise the infarctions more specifically, either inferior or anterior, *lead II, V1 and V3* might be seen as the optimal lead combination. This might implicate that for the identification of a previous or acute MI in the OHCA setting multiple leads may be recommended instead of a single lead approach. However, translation to the OHCA setting requires further investigation and optimization.

5. Sub-analyses

Several studies have reported that the appearance of the VF waveform on the ECG-leads depends on multiple factors. In order to improve our classification model, several other factors have been investigated whether they influence the VF waveform and potentially improve the classification models.

§ 5.1 Gender

Introduction

Baseline characteristics have shown that previous MIs were more frequently seen in men than in women, in 60% of total men and in 33% of total women. Furthermore, patients' demographics of correct and incorrect predictions based on the multiple lead model were analysed. It was remarkable that more women were observed in the incorrect group compared to men, 35% versus 28%, respectively. This suggests for example that the amplitude characteristics of these women were lower than the those for the absence of a previous MI. Probably, (proportional) more women will be incorrectly classified as having a MI than men. Looking closer to the gender-related characteristics, obvious differences were observed.

Several studies demonstrated gender-related ECG differences in healthy subjects, where women have lower ECG voltage [16, 17]. Simonson et al. found that in general, sex amplitude differences in limb leads are small although some are statistical significance [18]. He found that differences were found especially in precordial leads, where smaller amplitudes of the QRS complex were found in women. The reason for these differences can be explained by the amount of breast adipose tissue or the smaller vectors of the QRS complexes in women due to smaller hearts and body weight [18].

From this point of view, it would interesting to know whether underlying pathology, as MI, alter these ECG-differences related to gender. Mieszcandka et al. found that QRS voltages were higher in men than in women ($p=0.04$) even in the setting of recent MI [17]. However, studies based on gender-related differences in case of VF are limited.

Method / Results

5.1.1 Binary classification

In our study we found no significant differences in amplitude characteristics between men and women in healthy subjects (no MI), see Table 3 and Table 19 on page 80. However, in case of a previous MI gender-related differences were certainly observed. An overview of the amplitude related VF characteristics of all 10 leads for men and women is given in Table 19 on page 80. Interestingly, in all limb leads (*lead II, III, aVR, aVF*) median amplitude characteristics were higher in women than in men, while in the precordial leads (*V1 to V6*) all leads have shown lower median amplitudes in women than in men, except the MAA in *V2*. With regard to these differences, statistical significance was observed in *lead II, III, aVF* and *V3 to V5*. From the results of "**Binary classification**" described in **Section §4.3** it has been concluded that the optimal lead combination for two study groups is *lead II, V1* and *V6*. It therefore follows that this lead combination is examined for this sub-analysis. In Table 3 we show the differences only for the selected leads according to binary classification.

Moreover, in women several limb leads (*II, III, aVF*) have shown even higher median amplitudes in case of a previous MI compared to no previous MI, whereas in men all leads have shown lower median amplitudes in case of a previous MI except *lead V1*. However, in women significant differences in amplitude characteristics between no previous MI and a previous MI were only observed in precordial leads *V3 to V6* (except the AMSA

in V3). Likewise, for men these significant differences were observed in the same leads, but in addition in the limb leads *lead II*, *aVR*, *aVF* and the MAA in *lead III*.

Since, less obvious differences were observed in amplitude characteristics in women in either the absence or presence of a previous MI, it may suggest that the identification of a previous MI in binary classification based on amplitude related characteristics is more challenging in women than in men.

Table 3. Amplitude characteristics of the three leads for the two study groups for both men and women. Differences were analysed using Mann-Whitney U-test. Values are presented as median (IQR). * = P<0.05.

Amplitude characteristics – Binary						
Study groups						
	No MI			MI		
	Men (n=56)	Women (n=32)	p-value	Men (n=85)	Women (n=16)	p-value
	Median	Median		Median	Median	
MAA_II	0.18 (0.11-0.27)	0.19 (0.14-0.27)	.319	0.14 (0.10-0.18)	0.21 (0.12-0.27)	.048*
AMSA_II	8.89 (6.74-13.08)	11.01 (7.92-13.85)	.182	7.70 (6.40-9.54)	10.85 (7.65-13.29)	.009*
MAA_V1	0.17 (0.13-0.22)	0.16 (0.12-0.22)	.931	0.18 (0.11-0.25)	0.14 (0.11-0.19)	.324
AMSA_V1	8.48 (7.06-10.27)	7.85 (6.69-11.09)	.555	9.74 (7.11-13.54)	8.82 (6.95-10.14)	.367
MAA_V6	0.24 (0.15-0.32)	0.24 (0.14-0.31)	.696	0.16 (0.10-0.23)	0.14 (0.09-0.16)	.104
AMSA_V6	11.61 (8.14-15.29)	10.27 (7.63-14.17)	.302	8.01 (6.09-11.31)	7.16 (5.36-8.67)	.213

Inclusion of gender

Since, we observed gender-related amplitude differences in case of a previous MI, we may take gender into account for our binary classification algorithm. Therefore, we have added gender as categorical input feature to the given SVM models, for both the single lead model and multiple lead model, see Figure 23.

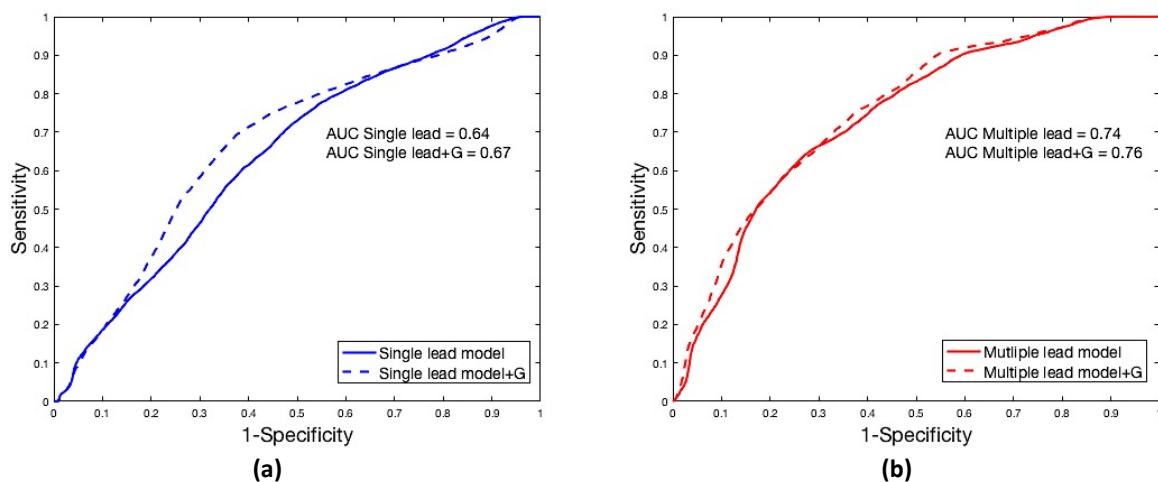


Figure 23. Performances of classification when taking gender into account for both the single lead model (a) and multiple lead model (b). The lines represent the model without the inclusion of gender (straight lines) and with the inclusion of gender (dotted lines).

The AUC slightly increases when gender was taken into consideration for both the single and multiple lead model, 0.03 and 0.02, respectively. According to the following confusion matrix of the single lead model, the sensitivity is 82.2%, specificity is 39.8%, PPV is 0.61 and NPV is 0.66. According to the following confusion matrix of the multiple lead model, the sensitivity is 85.1%, specificity is 51.1%, PPV is 0.67 and NPV is 0.75.

5.1.2 Multiclass classification

In *Subsection 5.1.1* gender related differences in VF characteristics have been described for binary classification so far. It has been observed that in women significant differences between the presence or absence of a previous MI is only significant in some precordial leads, whereas in men several limb leads were affected as well. This may hypothesize that in women more anterior MIs were seen and may overshadow results of *Subsection 5.1.1*.

In previous mentioned analysis, the group of previous MI contains both the presence of inferior MIs and anterior MIs. However, it would be more precise to discriminate between these two groups as well. Therefore, the same analysis has been performed for three study groups, known as the multiclass classification. From the results of “**Multiclass classification**” described in **Section §4.3** it has been concluded that the optimal lead combination for three study groups is *lead II, V1* and *V3*. It therefore follows that this lead combination is examined for this sub-analysis. An overview of the amplitude related VF characteristics all 10 leads for men and women is given in Table 20 and Table 21 on page 81 and 82, respectively. In Table 4 and Table 5 we show these differences only for the selected leads according to multiclass classification.

Table 4. Amplitude characteristics of the three leads for the three study groups in men. Values are presented as median (IQR). α = p-value between No MI and Inferior MI (column 1 versus column 2) using a Mann-Whitney U-test; β = p-value between No MI and Anterior MI (column 1 versus column 3) using a Mann-Whitney U-test. * = $p < 0.05$

Amplitude characteristics – Multiclass - Men					
	Study groups			α	β
	No MI (n= 56)	Inferior MI (n=50)	Anterior MI (n=35)		
	Median (IQR)	Median (IQR)	Median (IQR)	p-value	p-value
MAA_II	.18 (.11-.27)	.12 (.09-.15)	.18 (.14-.25)	.000*	.877
AMSA_II	8.89 (6.74-13.08)	7.20 (5.59-8.64)	8.98 (7.70-13.29)	.002*	.870
MAA_V1	.17 (.13-.22)	.18 (.11-.22)	.17 (.12-.28)	.879	.387
AMSA_V1	8.48 (7.06-10.27)	9.44 (7.28-11.88)	10.03 (6.79-12.67)	.172	.123
MAA_V3	.37 (.24-.56)	.35 (.24-.47)	.24 (.17-.34)	.578	.001*
AMSA_V3	19.92 (14.44-27.16)	19.49 (14.41-23.56)	14.71 (10.97-19.10)	.835	.002*

Table 5. Amplitude characteristics of the three leads for the three study groups in women. Values are presented as median (IQR). α = p-value between No MI and Inferior MI (column 1 versus column 2) using a Mann-Whitney U-test; β = p-value between No MI and Anterior MI (column 1 versus column 3) using a Mann-Whitney U-test. * = $p < 0.05$

Amplitude characteristics – Multiclass - Women					
	Study groups			α	β
	No MI (n=32)	Inferior MI (n=4)	Anterior MI (n=12)		
	Median (IQR)	Median (IQR)	Median (IQR)	p-value	p-value
MAA_II	.19 (.14-.27)	.10 (.07-.13)	.24 (.17-.30)	.010*	.317
AMSA_II	11.01 (7.92-13.85)	7.11 (5.88-7.28)	12.25 (9.33-14.21)	.035*	.370
MAA_V1	.16 (.12-.22)	.12 (.10-.16)	.15 (.11-.23)	.208	.693
AMSA_V1	7.85 (6.69-11.09)	8.16 (6.16-9.32)	9.34 (7.37-11.01)	.725	.562
MAA_V3	.32 (.21-.58)	.26 (.16-.39)	.18 (.14-.29)	.365	.008*
AMSA_V3	16.74 (12.30-22.20)	16.04 (10.29-22.15)	12.16 (9.53-16.75)	.615	.040*

Among the group of inferior MIs, no significant differences in VF characteristics were observed between men and women, except the MAA and MdS in V4, (0.15 (0.11-0.24) versus 0.30 (0.20-0.43) mV, $p=0.043$) and (9.40(6.19-13.03) versus 4.71 (3.29-7.68) mV/s, $p=0.039$), respectively. However, a minority of women have been observed in the inferior MI group ($n=4$) compared to the anterior MI group ($n=12$). Among the group of anterior MIs, significant differences in VF characteristics between men and women were observed in the AMSA of lead II, III and aVF and the MAA in V4, $p=0.014$, $p=0.022$, $p=0.013$ and $p=0.045$, respectively.

Inclusion of gender

We took gender into account for the multiclass classification algorithm for both the single lead model and multiple lead model, see Figure 24 and Figure 25, respectively.

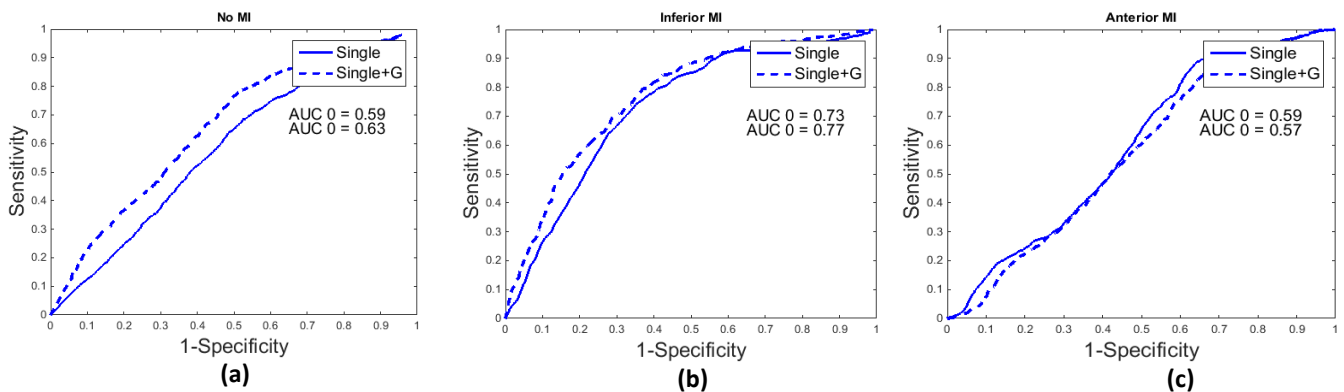


Figure 24. Area under the curve (AUC) for all three classes for the single lead model (straight blue line) and when gender is added (dotted blue line). In (a) the AUC is shown to identify “no myocardial infarction (MI)”, in (b) to identify an “inferior MI” and in (c) to identify an “anterior MI”. G = gender.

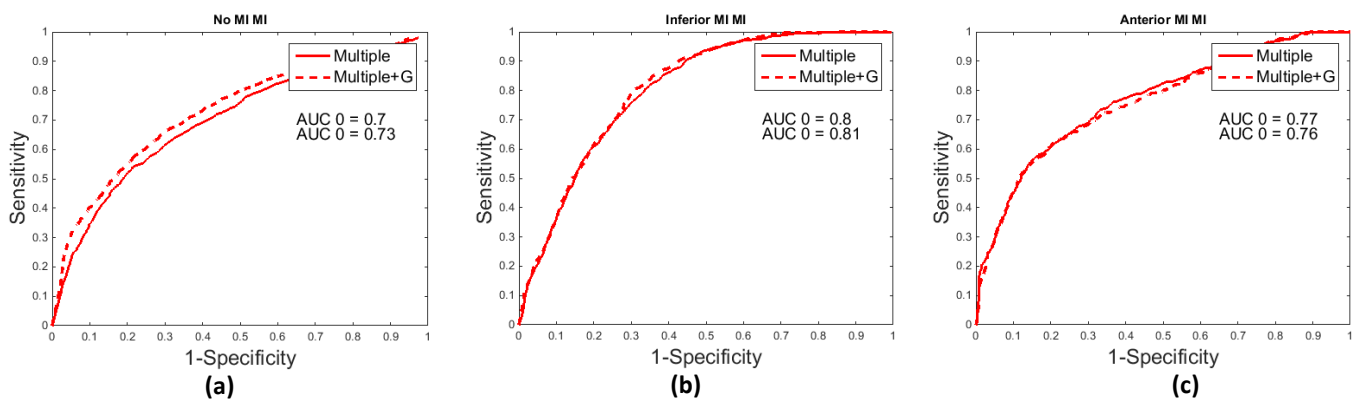


Figure 25. Area under the curve (AUC) for all three classes for the multiple lead model (straight red line) and when gender is added (dotted red line). In (a) the AUC is shown to identify “no myocardial infarction (MI)”, in (b) to identify an “inferior MI” and in (c) to identify an “anterior MI”. G = gender.

From the results of Figure 24 and Figure 25 it can be seen that when gender is included into classification algorithms, the AUC for the identification barely increases on nearly all classes. This applies to both the single lead model and the multiple lead model. On the contrary, the AUC to identify an anterior MI slightly decrease in both models when gender is included, see Figure 24c and Figure 25c.

Discussion / Conclusion

This sub-analysis has shown that in our binary classification problem gender may play an important role. Contrary to expectations, even higher amplitudes in several leads were observed in women with a history of MI compared to women without a history of MI. A possible explanation for this might be the high imbalance in women between inferior (n=4) and anterior (n=12) MIs in the previous MI group, and therefore the anterior MIs may overshadow the inferior ones. According to the multiclass classification, several significant differences in amplitude related characteristics were observed between men and women. In particular, in women amplitude characteristics were higher in limb leads and lower in precordial leads, compared to men. However, they did not reach statistical significance. Consistent with the literature, differences in the precordial leads may be explained by the higher amount of breast tissue and smaller hearts in women, whereas the overall smaller length of women may explain the differences in limb leads.

From the results of the multiclass classification it is shown that among the anterior MIs the AMSAs in the inferior leads in women are higher than in men. Besides the fact that this may be caused by gender related differences, this might be a result of the involved coronary artery as well. According to the coronary anatomy in **Section §2.1**, it might indicate that, in our data set, the infarctions of men concern more proximally occlusions of the LAD (proximal to the septal and diagonal branch) compared to the anterior infarctions in women. More proximally occlusions could affect the inferior part of the heart in some cases as well. Furthermore, more “wraparound” LAD variants may be present in men. This latter is a variant of a LAD that wraps around the apex to supply both the anterior and inferior part of the left ventricle, where an MI might cause ST-elevation in both the precordial and inferior leads.

Although these gender related differences were found, overall increases of the AUCs were quite small when gender was included into our classification algorithm. A possible explanation for this outcome, might be the fact that in our specific chosen lead combination: lead II, V1 and V3 no significant differences were observed between men and women. We may therefore conclude that differences of VF characteristics between men and women were seen, however the added value of gender to our classification algorithm seems to be limited.

§ 5.2 Probabilistic outputs

Introduction

For each model, given sigmoid functions were used to convert the SVM classifications scores into probabilistic outputs, see **Appendix A.2**. Probabilities may be of interest in future perspectives. For example, when the identification of an acute MI based on VF waveform characteristics has been demonstrated in the OHCA setting, these probabilities may give a degree of certainty to the presence or absence of an acute MI. Important to mention is that these probabilities were better known as posterior probabilities. In fact, SVM produces posterior probabilities, which are referred as class membership probabilities and are not induced by probabilistic confidence. Nevertheless, in this sub-analysis they are referred as probabilities.

Method

By converting the SVM scores $s(x)$ using a given sigmoid functions of the model, the probabilities of the outputs were measured. In binary classification we determined for inputs x whether they belong to class 0 (no previous MI) or 1 (previous MI). For each group the probability to their classification class has been determined, either correct or incorrect. As a result, we are able to determine the probabilistic outputs for all four possible classifications (i.e. TN, TP, FN and FP). This has been performed for both the single lead model and the multiple lead model. The results are given in Table 6.

Results

Table 6. Class probabilities for the two different models. Prob. = probabilistic output. TN is referred as true negatives, TP as true positives, FN as false negatives and FP as false positives. Total values are defined as the mean of the correct predicted (TN and TP) and the mean of incorrect predicted (FN and FP). Values are given as mean \pm SD.

	Prob. TN	Prob. TP	Prob. FN	Prob. FP
Single lead	0.71 \pm 0.08 (n=28)	0.61 \pm 0.06 (n=88)	0.66 \pm 0.05 (n=13)	0.59 \pm 0.06 (n=61)
Total	0.66 \pm 0.07		0.63 \pm 0.06	
Multiple lead	0.76 \pm 0.09 (n=42)	0.69 \pm 0.10 (n=85)	0.67 \pm 0.07 (n=16)	0.62 \pm 0.09 (n=46)
Total	0.73 \pm 0.10		0.65 \pm 0.08	

It can be seen from the results in Table 6 that the mean probabilities for correct classifications are higher than for incorrect classifications, for both the single and multiple lead model, 0.66 \pm 0.07 versus 0.63 \pm 0.06 and 0.73 \pm 0.10 versus 0.65 \pm 0.08, respectively. Furthermore, it is given that the most extensive incorrect predicted group FP shows the lowest probability compared to the other groups, for both the single and multiple lead model, 0.59 \pm 0.06 and 0.62 \pm 0.09, respectively.

Discussion / Conclusion

From these results it could be suggested that the use of multiple leads may lead to higher classification probabilities compared to a single lead. Moreover, correct classifications are based on higher probabilities compared to incorrect classifications. Probabilities may be of interest in further perspectives. When the identification of an acute MI based on VF waveform characteristics has been demonstrated in the OHCA setting, these probabilities may give a degree of certainty to the presence or absence of an acute MI. Although, it has been demonstrated for a previous MI that probabilities for correct classifications are higher than incorrect classifications, this should be further investigated and optimized.

§ 5.3 Infarct sizes

Introduction

Early determination of infarct size is important to assess the future risk of patients and for optimization of therapeutic strategies [86]. Nowadays, imaging techniques, such as magnetic resonance imaging (MRI) and single-photon emission computed tomography (SPECT), enable direct visualization of injured myocardium and thus may assess infarct sizes. However, routinely use of these imaging techniques in daily clinical practice is limited by logistics and costs. Therefore, following biochemical markers, as cardiac troponins (i.e. cardiac troponin I and cardiac troponin T) and creatine kinase (CK), remain the most suitable method for infarct size estimation [86]. Troponin is a protein complex that modulate the calcium-mediated interaction between actin and myosin in cardiac muscle cells. In case of necrosis, troponins are released and can be detected in the bloodstream after a few hours. Cardiac troponin as a (high specific) biomarker is particularly suited to both early diagnose myocardial infarction and, over time, assessing the extent of the myocardial necrosis [86, 87]. Over the last decades, several studies have found a positive correlation between cardiac troponins and infarct size determined by both MRI and SPECT.

The mentioned SVM scores in our study reflect the distances between the data points (e.g. patients/subjects) and the hyperplane. It is assumed that the distance is correlated to the likelihood for their determined class. In order to this correlation, a higher score suggest a higher likelihood and vice versa.

In this sub-analysis it is hypothesized that higher scores are more frequently associated with correct classifications compared to lower scores. This implies that for a score close to zero, correct discrimination is more difficult and therefore incorrect classifications are made more frequently for lower scores. In the study of **Chapter 4** no discrimination for previous MIs has been made according to the size of an infarct. Research has shown that the number of leads which present ST elevation is proportional to the size of the infarction [22]. This might be seen as a limitation of our study. In order to investigate this relationship, further analysis has been performed according to the size of infarctions. Patients were analysed who had a negative score and so predicted as having no history of MI, but actually had a history of MI (known as unrecognized infarctions). It is hypothesized that these patients are suffering small infarctions, causing less striking ECG-changes. In light of the above, knowledge of the infarction size may be essential to potentially improve our classification models.

In addition, it was hypothesized that a higher ejection fraction (EF) may be seen in the unrecognized infarctions (e.g. smaller infarctions), because of higher amplitudes, due to higher myocardial contractility. Likewise, it was hypothesized that a higher left ventricular mass (LV mass) may be seen in the unrecognized infarctions, because of higher amplitudes, due to the larger vector through the myocardial tissue.

Method

All patients *with* a history of an MI were analysed. Patients were categorized according to their predicted class (i.e. previous MI (1) or no previous MI (0)). To determine infarct sizes, several biomarkers as CK max, troponin I and troponin T were collected and analysed. These biomarkers were measured during evolvement of the infarction. So, these biomarkers were often indefinitely measured before the ICD implantation. Furthermore, in this analysis we have collected and analysed the following parameters as well; EF and LV mass. The values of these latter parameters, were collected from the last evaluation before the ICD implantation. The results for both recognized and unrecognized infarctions are shown in Table 7.

Results

Table 7. An overview of the parameters for both recognized and unrecognized infarctions. Values are presented as median (IQR). Differences between the two groups were tested using a Mann-Whitney U test. True positives were referred as the correct predicted as having a previous MI, whereas false negatives were predicted as having no previous MI.

Parameter	True positives (n=43)	False negatives (n=16)	p-value
CKmax (U/l) (n=27)	1147 (827 – 3306)	770 (189 – 1690)	0.120
Troponin I (ug/l) (n=14)	99.9 (9.2 – 100.0)	7.32 (1.46 – 15.5)	0.151
Troponin T (ng/l) (n=8)	810 (404 - 1440)	739 (390 – 1759)	1.00
EF (%) (n=47)	32 (25 – 40)	41 (29 – 55)	0.187
LV mass (g/m ²) (n=36)	108.1 (94.3 - 128.3)	108.1 (104.4 – 139.6)	0.491

A total of 59 patients of our database were studied, of whom 43 were correct predicted as having a previous MI (true positives) and 16 were incorrect predicted as having no history of a previous MI (false negatives). Measurements of the CK max were available for 27 patients, troponin I level for 14 patients, troponin T for 8 patients, EF for 47 patients and LV mass for 36 patients. The remaining values were untraceable.

The median CK max of the false negatives was lower compared to the true positives, 770 (189 – 1690) U/l versus 1147 (827 – 3306) U/l, respectively. Likewise, the median of troponin I and troponin T were both lower in the false negative group. However, none of these differences did reach statistical significance. The same applies for the EF and LV mass, were no statistical significance were observed between the two groups.

Discussion / Conclusion

Although, we observed some lower median values for the three cardiac biomarkers, none of these were statistically significant. A possible explanation for this outcome may be the fact that high variances has been observed among the groups and/or a low number of patients were studied. Moreover, cardiac biomarkers of several patients could not be tracked, because these were unknown or patients suffered from infarctions a few decades ago.

To summarize, none of the cardiac biomarkers, EF and LV mass were statistically significant different between the two groups. We may conclude that in our data set no significant correlation between any of these parameters and unrecognized infarctions has been observed. In light of the cardiac biomarkers, this sub-analysis indicate that unrecognized infarctions could not be declared by the fact that these infarctions were smaller than recognized infarctions. Furthermore, higher amplitude values of unrecognized infarction could not be declared be the fact that these patients were familiar with a higher ejection fraction or higher left ventricular mass than recognized infarctions.

§ 5.4 New cohort patients

Introduction

In view of the above, VF-segments of a new cohort of patients was collected and analysed following the determined SVM algorithm. In order to assess the performance measurement of the classifier, a new cohort of VF data has been submitted to determine their classes based on the VF waveform characteristics. Classification was performed according to the used classifier in described in **Section §4.2** and **Section §4.3**.

Method

We identified patients who underwent DFT testing at the Radboud University Medical Center, Nijmegen between January 2014 and July 2017 from a registry of first ICD implantations. The method that has been applied for this analysis corresponds to the method described in **Section §4.2**.

Results

Patients characteristics

In total 37 patients were studied, of whom 18 (49%) had a history of MI. Of the 18 patients with a history of MI, 12 (67%) had an inferior MI and 6 (33%) had an anterior MI. The mean age was 61 ± 13 years and 28 (76%) were men. In 25 (68%) of the patients ICD were implanted for secondary prevention. Baseline characteristics of the study group are presented in Table 16 in **Appendix B.1** on page 76.

VF characteristics

We present the median and IQR values of the analysed VF waveform characteristics of four leads in Table 8. These four leads were used for either our binary or multiclass classification approach. Among these patients, we observed no any significant difference for all VF characteristics in patients with a history of MI compared to those without a history of MI, in all four mentioned leads.

Table 8. An overview of the ventricular fibrillation (VF) characteristics for the four leads, for both study groups. Values are presented as median (IQR).

Characteristic	Lead	No MI (n=19)	MI (n=18)	p-value
MAA	II	0.16 (0.11-0.24)	0.15 (0.08-0.23)	0.429
	V1	0.15 (0.09-0.21)	0.12 (0.10-0.17)	0.784
	V3	0.38 (0.25-0.51)	0.26 (0.17-0.38)	0.089
	V6	0.19 (0.12-0.24)	0.15 (0.11-0.17)	0.068
AMSA	II	8.58 (6.19-12.69)	7.50 (5.50-11.87)	0.605
	V1	7.95 (5.44-10.04)	6.90 (5.58-11.19)	0.671
	V3	19.18 (12.68-24.11)	15.64 (10.35-20.54)	0.181
MF	V6	9.47 (7.79-12.03)	7.63 (6.11-11.18)	0.060
	II	5.37 (5.13-5.86)	5.37 (4.82-5.86)	0.866
	V1	5.37 (4.88-5.86)	5.49 (5.07-5.86)	0.866
	V3	5.62 (5.13-5.86)	5.37 (4.88-5.86)	0.613
Mds	V6	5.37 (5.13-5.86)	5.37 (5.00-5.68)	0.736
	II	4.40 (3.70-7.08)	4.51 (3.01-6.49)	0.362
	V1	4.40 (2.61-5.84)	3.69 (2.71-5.53)	0.671
	V3	10.50 (7.58-16.15)	7.97 (4.87-12.03)	0.064
BW	V6	5.51 (4.00-8.00)	4.37 (3.24-5.35)	0.101
	II	0.20 (0.08-0.36)	0.16 (0.06-0.31)	0.447
	V1	0.16 (0.07-0.25)	0.11 (0.05-0.26)	0.715
	V3	1.09 (0.40-2.00)	0.45 (0.21-1.18)	0.095
	V6	0.27 (0.13-0.41)	0.16 (0.09-0.26)	0.060

DFA α1	II	1.48 (1.28-1.61)	1.47 (1.23-1.60)	0.952
	V1	1.43 (1.11-1.51)	1.37 (1.29-1.47)	0.855
	V3	1.59 (1.43-1.72)	1.54 (1.37-1.64)	0.331
	V6	1.48 (1.30-1.58)	1.40 (1.22-1.48)	0.181
DFA α2	II	0.05 (0.03-0.06)	0.04 (0.03-0.10)	0.855
	V1	0.05 (0.03-0.06)	0.05 (0.03-0.06)	0.903
	V3	0.04 (0.03-0.06)	0.04 (0.03-0.06)	0.715
	V6	0.05 (0.02-0.08)	0.04 (0.03-0.06)	0.738

The performance of the single lead model and multiple lead model on the new cohort data is assessed by the confusion matrices in Table 9 (a) and (b), respectively. From these confusion matrices the performance measures according to those as determined in **Section §4.2** were calculated. The results are presented in Table 10.

Table 9. Assessment of new cohort patients. Performance is presented by the confusion matrix, from which the accuracy and other performance measures can be determined. In (a) the confusion matrix of the single lead model is shown and in (b) the confusion matrix of the multiple lead model.

		True class				True class	
		0	1			0	1
Predicted class	0	4 (TN)	4 (FN)	Predicted class	0	7 (TN)	4 (FN)
	1	15 (FP)	14 (TP)		1	12 (FP)	14 (TP)

(a) (b)

Table 10. Model performance measures on the new cohort data. PPV is the positive predictive value and NPV the negative predictive value.

	Accuracy (%)	Sensitivity (%)	Specificity (%)	PPV	NPV
Single lead model	48.6	77.8	21.2	0.48	0.50
Multiple lead model	56.8	77.8	36.8	0.54	0.64

Discussion / Conclusion

We observed somewhat different performance measures on the new cohort data compared to performance measures of **Chapter 4**. For both single lead and multiple lead model, the sensitivity and specificity were both lower on the new data, and as a result the accuracy, PPV and NPV were both lower as well. These different performance measures could be explained by the optimization problem of overfitting. In fact, the models fit the study data well, but has a worse fit on the new data. Though, different performance measures could even be declared by differences in baseline characteristics, as the number of secondary prevention and percentage of ejection fraction differ between both study data. However, we still observed superior predictive values for the multiple lead model compared to the single lead model.

Moreover, the number of patients (n=37) in the new cohort is substantially lower compared to the number of patients in our main research (n=189). This is an important issue, because even a small number of misclassifications in this sub-analysis will already result in worse performance measures.

§ 5.5 Statistical approach

To compare the machine learning approach with the statistical approach, a multiple regression model has been assessed to predict the presence or absence of a previous MI from the VF characteristics. The goal of a multiple logistic regression model is to find an equation that best predicts the probability of the output Y as a function of the input X . First, in univariate analyses all input predictors X were tested for the association between the predictor X and the output Y (the presence of a previous MI). Secondly, collinearity is tested for the correlation between independent predictors. Thirdly, the performance of the multivariate logistic regression analysis has been performed considering to the included predictors from *Step 1* and *Step 2*. These analysis has been performed for both the single lead model (*lead II*) and multiple lead model (*lead II, V1 and V6*).

Step 1- Univariate analysis

Table 11. Univariate parameters of logistic regression model for the seven predictors of *lead II*. Odd ratios express the likelihood of an event occurring relative to the likelihood an event not occurring, when the predictor has changed one unit. ** Per 0.001 mV increase.

Predictor	Unit	Odds ratio	95 % CI	p-value
MAA	mV	1.0**	0.991-0.998**	0.001
AMSA	mV•Hz	0.89	0.829-0.963	0.003
MF	Hz	0.64	0.388-1.054	0.079
MdS	mV/s	0.82	0.734-0.916	<0.001
BW	Hz	2.30	1.096-4.806	0.028
DFA α1	-	0.49	0.128-1.871	0.297
DFA α2	-	1.00**	0.996-1.008**	0.482

The results of the univariate analyses of *lead II* are shown in Table 11. It should be noted that in univariate analyses statistical significance is achieved at p-values <0.1. In that way, it is shown that the predictors MAA, AMSA, MF, MdS and BW were significantly associated with the presence of an MI, $p=0.001$, $p=0.003$, $p=0.079$, $p<0.001$ and $p=0.028$, respectively. The predictors DFA α 1 and DFA α 2 were not associated with the presence of an MI, $p=0.297$ and $p=0.482$, respectively.

Step 2 - Collinearity

One of the assumptions of logistic regression is that there is no multicollinearity among the predictors [88]. This means that the predictors should not be (highly) correlated to each other. In our study, a correlation analysis shows that the predictors MAA, AMSA and MdS are highly correlated. More specifically, there is a significant positive correlation ($p<0.01$) between the MAA and AMSA, between the MAA and MdS and between the AMSA and MdS, $r=0.896$, $r=0.951$ and $r=0.828$, respectively. Moreover, there is no correlation between the MF and any other predictors.

Since, several predictors are correlated to each other, we omit some of these predictors to perform a logistic regression analysis based on independent predictors. The MdS has the highest significant association and is in our case chosen as the ‘substituted’ predictor for the MAA and AMSA. In addition, DFA α 2 is barely correlated to the other predictors. Specifically, a maximum correlation of -0.386 has been observed between DFA α 2 and MdS. Likewise, the predictor BW is barely correlated to the other predictors, with a maximum correlation of -0.325 with the MdS.

As mentioned before, there is no or barely correlation between MF and other predictors, the BW and other predictors and between DFA $\alpha 2$ and other predictors. Although, DFA $\alpha 2$ is not significantly associated in the univariate analysis, we know that this variable reflects some different dynamics of the signal than those other variables. We therefore include the three predictors in the multivariate analysis as well. In summary, we include the following predictors for the multivariate analyses: MdS, MF, BW and DFA $\alpha 2$.

Step 3 – Multivariate regression analysis

Table 12. Outcomes of multivariate regression analysis for both the single lead model and multiple lead model. OR is referred as the odds ratio. The Nagelkerke R^2 is used to assess the goodness of fit and is defined as the proportion of variance that can be declared by the predictor [88]. ** Per 0.001 mV increase.

Lead	Pred.	Single lead model			Multiple lead model		
		OR	95 % CI	p-value	OR	95 % CI	p-value
Constant		16.869		0.066	11.193		0.189
II	MdS	0.843	0.750-0.948	0.004	0.887	0.760-1.035	0.127
	MF	0.697	0.412-1.181	0.180	1.478	0.254-8.610	0.664
	BW	1.526	0.758-3.073	0.237	1.608	0.740-3.498	0.231
	DFA $\alpha 2$	0.999**	0.992-1.005	0.654	0.996**	0.986-1.007	0.484
V1	MdS				1.283	1.090-1.509	0.003
	MF				1.707	0.486-6.003	0.404
	BW				1.361	0.943-1.966	0.100
	DFA $\alpha 2$				0.998**	0.987-1.010	0.789
V6	MdS				0.769	0.659-0.898	0.001
	MF				0.294	0.049-1.763	0.180
	BW				0.663	0.319-1.375	0.269
	DFA $\alpha 2$				1.006**	0.992-1.019	0.403
Nagelkerke R^2		0.125		0.304			
χ^2		3.589 (18.62)		6.044 (48.73)			

The results of the multivariate regression analysis are shown in Table 12. It is shown that in the single lead model the median slope of *lead II* was significantly associated with the presence of an MI (OR 0.843, 95% CI 0.750-0.948, $p=0.004$) and the median frequency was not significantly associated (OR 0.697, 95% CI 0.412-1.181, $p=0.180$). Likewise, the bandwidth and DFA $\alpha 2$ were not significantly associated with the presence of an MI (OR 1.526, 95% CI 0.758-3.073, $p=0.237$) and (OR 0.999, 95% CI 0.992-1.005, $p=0.654$), respectively.

According to the multiple lead model, only the median slope in *V1* and *V6* were significantly associated with the presence of an MI, (OR 1.283, 95% CI 1.090-1.509, $p=0.003$) and (OR 0.769, 95% CI 0.659-0.898 $p=0.001$), respectively. It is remarkable that the contribution of the median slope in *lead II* was not significant associated with the presence of an MI (OR 0.887, 95% CI 0.760-1.035, $p=0.127$), while this was the case in the single lead model (OR 0.843, 95% CI 0.750-0.948, $p=0.004$). Moreover, the single lead model calculated a Nagelkerke R^2 of 0.125, whereas the multiple lead model calculated a Nagelkerke R^2 of 0.304.

In order to compare the performance of this statistical analysis to the machine learning method, an ROC curve of these regression models were determined and given in Figure 26.

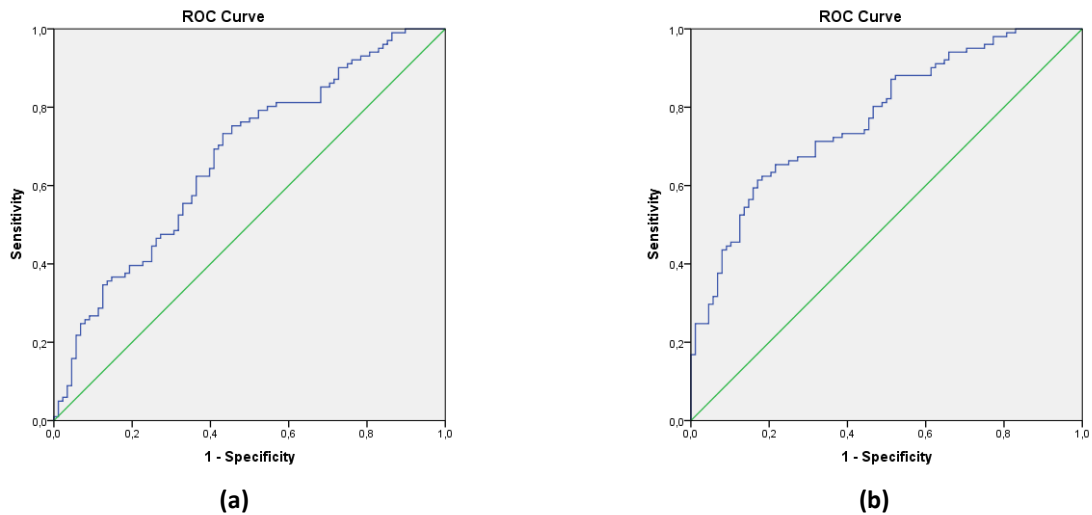


Figure 26. The receiver operating characteristic (ROC) curves are shown, including an area under the curve (AUC). In (a) the ROC is shown for the single lead model, using a single electrocardiogram (ECG)-lead and in (b) the ROC is shown for the multiple lead model, using lead II, V1 and V6.

In Figure 26 the ROC curves for both models to identify a previous MI based on VF characteristics using a statistical approach are shown. It is shown that the AUC of the single lead is 0.67 (95% CI 0.59–0.75) and for the multiple lead model 0.77 (95% CI 0.71 – 0.84).

The performance of the single lead model and multiple lead model is assessed by the confusion matrices in Table 13 (a) and (b), respectively. From these confusion matrices the performance measures according to those as determined in **Section §4.2** were calculated. The results are presented in Table 14.

Table 13. Assessment of new patient data. Performance is presented by the confusion matrix, from which the accuracy and other performance measures can be determined. In (a) the confusion matrix of the single lead model is shown and in (b) the confusion matrix of the multiple lead model.

		True class	
		0	1
Predicted class	0	46 (TN)	23 (FN)
	1	42 (FP)	78 (TP)

(a)

		True class	
		0	1
Predicted class	0	54 (TN)	27 (FN)
	1	34 (FP)	74 (TP)

(b)

Table 14. Model performance measures on statistical analysis. PPV is the positive predictive value and NPV is the negative predictive value.

	Accuracy (%)	Sensitivity (%)	Specificity (%)	PPV	NPV
Single lead model	65.6	77.3	52.3	0.65	0.67
Multiple lead model	67.7	73.3	61.4	0.69	0.67

Conclusion

We observed that identification of a previous myocardial infarction by means of statistical approaches might function fairly well. As a result, we suggest that this statistical approach using multivariate regression analyses, might not be inferior to the machine learning approach. However, for predictive applications and for higher dimensional data sets, machine learning approach is often recommended over the statistical approach.

6. General discussion

In this study we investigated the ability to identify a previous MI using the ventricular fibrillation waveform of a single lead and multiple leads. To investigate this topic, we used VF signals from defibrillation testing of ICD patients in the controlled setting.

The main aims of this thesis were:

- To assess the performance of a single ECG-lead to identify a previous myocardial infarction based on ventricular fibrillation waveform analysis using a machine learning method.
- To assess whether performance increase when more ECG-leads are added.
- To assess the optimal lead combination of ECG-leads to identify a previous myocardial infarction based on ventricular fibrillation waveform analysis using a machine learning method.

In **Chapter 4** we investigated the ability of a single lead model and multiple lead model to identify patients with a history of a myocardial infarction based on ventricular fibrillation waveform characteristics. We have observed that the identification by a single lead model is possible, but only to a limited extent. Moreover, the multiple lead model has shown superior performance compared to the single lead model. Interestingly, the optimal multiple lead combination to identify a previous MI were *lead II, V1* and *V6*. To localise the infarctions more specifically, either inferior or anterior, *lead II, V1* and *V3* might be seen as the optimal lead combination. However, we have assessed short-duration-induced-VF in a controlled setting. For a potential translation to longer-duration-spontaneous-VF in the acute setting, it should be noticed that VF in the acute setting is not similar to VF in the controlled setting. Moreover, induced VF tends to be more organized than spontaneous VF, resulting in incomparable VF characteristics.

Furthermore, performance of our models might be limited by several factors that may affect the VF waveform as well. In order to improve our models, several other factors have been investigated whether they influence the VF waveform. This has been elaborated in the next chapter.

In **Chapter 5** we performed several sub-analyses, in order to provide more insights of the VF waveform and potentially improve our models. Clearly, the performances of VF waveform characteristics for the identification of a previous or acute MI should be further optimized. Since, multiple factors may influence the VF waveform, further investigation is required. In particular, we investigated whether VF waveform characteristics differ according to gender. In this context, remarkable differences in VF characteristics were seen between men and women. Although these gender related differences were found, overall increases of the performance measures were quite small when gender was included into our classification algorithm. Furthermore, we investigated whether (un)recognized infarctions could be clarified by the size of an infarct and how probabilistic outputs are distributed according to (in)correct classifications. In addition, we assessed the performance of our classifications models by analysing VF data of a new cohort. Lastly, a statistical approach to identify a previous MI using the VF characteristics and a multivariate regression analysis has been performed, and might function fairly well. As a result, we suggest that for our data set a statistical approach using multivariate regression analyses, might not be inferior to the machine learning approach.

To summarize, the appearance of the VF waveform might be influenced by multiple factors. Although, identification solely on VF waveform characteristics might be challenging, it certainly offers future prospects. When VF waveform analysis has proven to be able to identify an acute MI in the OHCA setting, resuscitation strategies could be adapted and therefore the survival rates could possibly be improved. This idea has encouraged the development of a “smart” defibrillator system that is able to analyse the VF waveform real-time by multiple leads.

7. General conclusion

In the present study we investigated the ability of ventricular fibrillation waveform characteristics and support vector machine algorithms to differentiate patients with and without a history of a myocardial infarction in a controlled setting. We demonstrated that the identification of underlying aetiology, as myocardial infarction, solely based on VF waveform characteristics seems feasible. Interestingly, a multiple lead approach led to superior predictive values as compared to a single lead approach. The optimal multiple lead combination to identify a previous MI were *lead II, V1* and *V6*. To localise the infarctions more specifically, either inferior or anterior, *lead II, V1 and V3* might be seen as the optimal lead combination. This might implicate that for the identification of a previous or acute MI in the OHCA setting multiple leads may be recommended instead of a single lead approach.

The appearance of the VF waveform on the ECG-leads depends on multiple factors. As we observed that the VF waveform might be influenced by underlying aetiology, several other factors might possibly influence the VF waveform as well, as gender and the size of an infarct. We therefore conclude that the VF waveform might be a potential tool to identify a (previous) myocardial infarction, however several limitations need to be addressed. In follow-up on the experimental studies, in-field studies are eagerly awaited.

8. References

Note: Chapter 3 “Technical Background” has its own reference list, included on page 34 and 35.

1. Berdowski, J., et al., *Global incidences of out-of-hospital cardiac arrest and survival rates: Systematic review of 67 prospective studies*. Resuscitation, 2010. **81**(11): p. 1479-87.
2. Yamaguchi, Y., et al., *Improvements in Out-of-Hospital Cardiac Arrest Survival from 1998 to 2013*. Prehosp Emerg Care, 2017. **21**(5): p. 616-627.
3. Atwood, C., et al., *Incidence of EMS-treated out-of-hospital cardiac arrest in Europe*. Resuscitation, 2005. **67**(1): p. 75-80.
4. Hulleman, M., et al., *Causes for the declining proportion of ventricular fibrillation in out-of-hospital cardiac arrest*. Resuscitation, 2015. **96**: p. 23-9.
5. Nichol, G., et al., *Regional variation in out-of-hospital cardiac arrest incidence and outcome*. JAMA, 2008. **300**(12): p. 1423-1431.
6. Mann, D.L., et al., *Braunwald's Heart Disease E-Book: A Textbook of Cardiovascular Medicine*. 2014: Elsevier Health Sciences.
7. Koplan, B.A. and W.G. Stevenson, *Ventricular tachycardia and sudden cardiac death*. Mayo Clin Proc, 2009. **84**(3): p. 289-97.
8. Priori, S.G., et al., *2015 ESC Guidelines for the management of patients with ventricular arrhythmias and the prevention of sudden cardiac death: The Task Force for the Management of Patients with Ventricular Arrhythmias and the Prevention of Sudden Cardiac Death of the European Society of Cardiology (ESC). Endorsed by: Association for European Paediatric and Congenital Cardiology (AEPC)*. Eur Heart J, 2015. **36**(41): p. 2793-867.
9. Bonnes, J.L., et al., *Ventricular fibrillation waveform characteristics of the surface ECG: Impact of the left ventricular diameter and mass*. Resuscitation, 2017. **115**(Supplement C): p. 82-89.
10. Callaway, C. and J. Menegazzi, *Waveform analysis of ventricular fibrillation to predict defibrillation*. Vol. 11. 2005. 192-9.
11. Hulleman, M., et al., *Predictive value of amplitude spectrum area of ventricular fibrillation waveform in patients with acute or previous myocardial infarction in out-of-hospital cardiac arrest*. Resuscitation, 2017.
12. Bonnes, J.L., et al., *Ventricular fibrillation waveform characteristics differ according to the presence of a previous myocardial infarction: A surface ECG study in ICD-patients*. Resuscitation, 2015. **96**: p. 239-45.
13. Nas, J., *Manuscript: Acute coronary occlusion in out-of-hospital cardiac arrest: A ventricular fibrillation waveform study* 2017.
14. Indik, J.H., et al., *Ventricular fibrillation waveform characteristics are different in ischemic heart failure compared with structurally normal hearts*. Resuscitation, 2006. **69**(3): p. 471-477.
15. Rebergen, D., *Masterthesis: Identification of a Previous Myocardial Infarction During Ventricular Fibrillation: a Machine Learning Based Approach Using the 12-Lead Electrocardiogram*. 2017.
16. Casale, P.N., et al., *Improved sex-specific criteria of left ventricular hypertrophy for clinical and computer interpretation of electrocardiograms: validation with autopsy findings*. Circulation, 1987. **75**(3): p. 565-572.
17. Mieszczanska, H., et al., *Gender Related Differences in Electrocardiographic Parameters and Their Association with Cardiac Events in Patients After Myocardial Infarction*. The American journal of cardiology, 2008. **101**(1): p. 20-24.
18. Simonson, E., et al., *Sex Differences in the Electrocardiogram*. Circulation, 1960. **22**(4): p. 598-601.
19. Taktak, A.F.G., et al., *Clinical Engineering: A Handbook for Clinical and Biomedical Engineers*. 2013: Elsevier Science.
20. *Heart Circulation Diagram*. Available from: <https://humanbodyanatomy.co/heart-circulation-diagram/heart-circulation-diagram-labeled-diagram-of-blood-flow-through-the-heart-endearing/>.
21. Chan-Dewar, F., *The cardiac cycle*. Anaesthesia & Intensive Care Medicine, 2012. **13**(8): p. 391-396.
22. van der Wall, E.E., et al., *Cardiologie*. 2007: Bohn Stafleu van Loghum.
23. Boullin, J. and J.M. Morgan, *The development of cardiac rhythm*. Heart, 2005. **91**(7): p. 874-875.
24. van Weerd, J.H. and V.M. Christoffels, *The formation and function of the cardiac conduction system*. Development, 2016. **143**(2): p. 197-210.

25. Samuel, L. *Heart contraction simplified*. Interactive biology; Available from: <http://www.interactivebiology.com/3619/heart-contractions-simplified/>.
26. Villa, A.D., et al., *Coronary artery anomalies overview: the normal and the abnormal*. World journal of radiology, 2016. **8**(6): p. 537.
27. Patra, S., et al., *Super dominant left anterior descending artery with origin of both posterior descending artery and posterior left ventricular artery from septal branch*. BMJ Case Reports, 2013. **2013**: p. bcr2013010303.
28. Habets, J., et al., *Coronary artery assessment by multidetector computed tomography in patients with prosthetic heart valves*. European radiology, 2012. **22**(6): p. 1278-1286.
29. Fogoros, R.N., *The Electrophysiology Study in the Evaluation and Treatment of Ventricular Arrhythmias*, in *Electrophysiologic Testing*. 2012, John Wiley & Sons, Ltd. p. 160-209.
30. Ikonnikov, G.A.W., *Action potentials and impulse conduction*. 2005; Available from: <http://www.pathophys.org/physiology-of-cardiac-conduction-and-contractility/>
31. Zipes, D.P. and J. Jalife, *Cardiac Electrophysiology: From Cell to Bedside E-Book: Expert Consult*. 2009: Elsevier Health Sciences.
32. Goldberger, A.L., *Electrocardiography*, in *Harrison's Principles of Internal Medicine, 19e*, D. Kasper, et al., Editors. 2015, McGraw-Hill Education: New York, NY.
33. Wesley, K., *Huszar's ECG and 12-Lead Interpretation - E-Book*. 2016: Elsevier Health Sciences.
34. Gargiulo, G.D., *True unipolar ECG machine for Wilson Central Terminal measurements*. BioMed research international, 2015. **2015**.
35. Pourdjabbar, A., et al., *ST-segment elevation interpretation on electrocardiogram: To cath or not to cath?* JAMA Internal Medicine, 2015. **175**(10): p. 1695-1697.
36. Page, R.L., et al., *2015 ACC/AHA/HRS guideline for the management of adult patients with supraventricular tachycardia: a report of the American College of Cardiology/American Heart Association Task Force on Clinical Practice Guidelines and the Heart Rhythm Society*. Heart Rhythm, 2016. **13**(4): p. e136-e221.
37. Tilz, R.R., et al., *Ablation Outcomes and Predictors of Mortality Following Catheter Ablation for Ventricular Tachycardia: Data From the German Multicenter Ablation Registry*. Journal of the American Heart Association, 2018. **7**(6).
38. Katriotis, D.G. and A.J. Camm, *Nonsustained ventricular tachycardia: where do we stand?* European Heart Journal, 2004. **25**(13): p. 1093-1099.
39. Israel, C.W., *Mechanisms of sudden cardiac death*. Indian Heart Journal, 2014. **66**(Suppl 1): p. S10-S17.
40. Bonow, R.O., et al., *Braunwald's Heart Disease E-Book: A Textbook of Cardiovascular Medicine*. 2011: Elsevier Health Sciences.
41. Jalife, J., *Ventricular fibrillation: mechanisms of initiation and maintenance*. Annu Rev Physiol, 2000. **62**: p. 25-50.
42. van Hemel, N.M., et al., *Klinische elektrocardiografie: Een handleiding voor zelfstandige beoordeling van het ECG*. 2012: Bohn Stafleu van Loghum.
43. Lee, S.H., *Development of Ventricular Fibrillation Diagnosis Method Based on Neuro-fuzzy Systems for Automated External Defibrillators*. International Journal of Fuzzy Systems, 2016. **19**(2): p. 440-451.
44. Thygesen, K., et al., *Third Universal Definition of Myocardial Infarction*. Circulation, 2012. **126**(16): p. 2020-2035.
45. Rutten, F., et al., *NHG-Standaard Acut coronair syndroom*, in *NHG-Standaarden 2009*. 2009, Springer. p. 3-24.
46. Hreybe, H. and S. Saba, *Location of Acute Myocardial Infarction and Associated Arrhythmias and Outcome*. Clinical Cardiology, 2009. **32**(5): p. 274-277.
47. Stone, P.H., et al., *Prognostic significance of location and type of myocardial infarction: independent adverse outcome associated with anterior location*. J Am Coll Cardiol, 1988. **11**(3): p. 453-63.
48. Al-Khatib, S.M., et al., *Sustained Ventricular Arrhythmias Among Patients With Acute Coronary Syndromes With No ST-Segment Elevation*. Incidence, Predictors, and Outcomes, 2002. **106**(3): p. 309-312.
49. Newby, K.H., et al., *Sustained ventricular arrhythmias in patients receiving thrombolytic therapy: incidence and outcomes*. The GUSTO Investigators. Circulation, 1998. **98**(23): p. 2567-73.
50. Eichlerová, T., et al., *Ventricular fibrillation as a primary manifestation of Wolff-Parkinson-White syndrome*. Cor et Vasa, 2017.
51. Mazur, A., et al., *Bundle Branch Reentrant Ventricular Tachycardia*. Indian Pacing and Electrophysiology Journal, 2005. **5**(2): p. 86-95.

52. Viskin, S. and B. Belhassen, *Idiopathic ventricular fibrillation*. American heart journal, 1990. **120**(3): p. 661-671.
53. Tiltz, R.R., et al., *Idiopathic ventricular fibrillation*. Herz Kardiovaskuläre Erkrankungen, 2007. **32**(3): p. 233-239.
54. Mani, G., et al., *Bystander cardiopulmonary resuscitation in out of hospital cardiac arrest: need of the hour*. Afr Health Sci, 2015. **15**(1): p. 307-9.
55. Oksuz, F., et al., *The classical "R-on-T" phenomenon*. Indian Heart Journal, 2015. **67**(4): p. 392-394.
56. Zaqqqa, M., *Defibrillator Threshold Testing*, in *Cardiac Defibrillation*. 2013, InTech.
57. Williams, E.S. and M.N. Viswanathan, *Current and Emerging Antiarrhythmic Drug Therapy for Ventricular Tachycardia*. Cardiology and Therapy, 2013. **2**(1): p. 27-46.
58. Salcido, D.D., et al., *Association of intramyocardial high energy phosphate concentrations with quantitative measures of the ventricular fibrillation electrocardiogram waveform*. Resuscitation, 2009. **80**(8): p. 946-950.
59. Indik, J.H., et al., *The influence of myocardial substrate on ventricular fibrillation waveform: A swine model of acute and postmyocardial infarction*. Critical care medicine, 2008. **36**(7): p. 2136-2142.
60. Jones, D.L. and G.J. Klein, *Ventricular fibrillation: The importance of being coarse?* Journal of Electrocardiology, 1984. **17**(4): p. 393-399.
61. Weaver, W., et al., *Amplitude of ventricular fibrillation waveform and outcome after cardiac arrest*. Annals of Internal Medicine, 1985. **102**(1): p. 53-55.
62. Ristagno, G., et al., *Amplitude spectrum area to guide resuscitation-a retrospective analysis during out-of-hospital cardiopulmonary resuscitation in 609 patients with ventricular fibrillation cardiac arrest*. Resuscitation, 2013. **84**(12): p. 1697-703.
63. Eftestøl, T., et al., *Effects of Cardiopulmonary Resuscitation on Predictors of Ventricular Fibrillation Defibrillation Success During Out-of-Hospital Cardiac Arrest*. Circulation, 2004. **110**(1): p. 10-15.
64. Wik, L., et al., *Delaying defibrillation to give basic cardiopulmonary resuscitation to patients with out-of-hospital ventricular fibrillation: a randomized trial*. Jama, 2003. **289**(11): p. 1389-95.
65. Cobb, L.A., et al., *Influence of cardiopulmonary resuscitation prior to defibrillation in patients with out-of-hospital ventricular fibrillation*. JAMA, 1999. **281**(13): p. 1182-1188.
66. Freese, J.P., et al., *Waveform analysis-guided treatment versus a standard shock-first protocol for the treatment of out-of-hospital cardiac arrest presenting in ventricular fibrillation: results of an international randomized, controlled trial*. Circulation, 2013. **128**(9): p. 995-1002.
67. Indik, J.H., et al., *Ventricular fibrillation waveform characteristics are different in ischemic heart failure compared with structurally normal hearts*. Resuscitation, 2006. **69**(3): p. 471-7.
68. Friedman, J., et al., *The elements of statistical learning*. Vol. 1. 2001: Springer series in statistics New York.
69. Li, Q., et al., *Ventricular fibrillation and tachycardia classification using a machine learning approach*. IEEE Trans Biomed Eng, 2014. **61**(6): p. 1607-13.
70. Song, B., et al., *ROC operating point selection for classification of imbalanced data with application to computer-aided polyp detection in CT colonography*. International journal of computer assisted radiology and surgery, 2014. **9**(1): p. 79-89.
71. Povoas, H.P., et al., *Predicting the success of defibrillation by electrocardiographic analysis*. Resuscitation, 2002. **53**(1): p. 77-82.
72. Marn-Pernat, A., et al., *Optimizing timing of ventricular defibrillation*. Crit Care Med, 2001. **29**(12): p. 2360-5.
73. Jacobson, J.T., et al., *Effect of underlying heart disease on the frequency content of ventricular fibrillation in the dog heart*. Pacing Clin Electrophysiol, 2000. **23**(2): p. 243-52.
74. Indik, J.H., et al., *Ventricular fibrillation frequency characteristics are altered in acute myocardial infarction*. Crit Care Med, 2007. **35**(4): p. 1133-8.
75. Indik, J.H., et al., *Utility of the Ventricular Fibrillation Waveform to Predict a Return of Spontaneous Circulation and Distinguish Acute From Post Myocardial Infarction or Normal Swine in Ventricular Fibrillation Cardiac Arrest*. *Clinical Perspective*. Circulation: Arrhythmia and Electrophysiology, 2011. **4**(3): p. 337-343.
76. Olasveengen, T.M., et al., *Acute ischemic heart disease alters ventricular fibrillation waveform characteristics in out-of hospital cardiac arrest*. Resuscitation, 2009. **80**(4): p. 412-7.
77. Alonso-Atienza, F., et al., *Detection of life-threatening arrhythmias using feature selection and support vector machines*. IEEE Trans Biomed Eng, 2014. **61**(3): p. 832-40.

78. Alonso-Atienza, F., et al., *Feature selection using support vector machines and bootstrap methods for ventricular fibrillation detection*. Expert Systems with Applications, 2012. **39**(2): p. 1956-1967.
79. Mjahad, A., et al., *Ventricular Fibrillation and Tachycardia detection from surface ECG using time-frequency representation images as input dataset for machine learning*. Comput Methods Programs Biomed, 2017. **141**: p. 119-127.
80. Lee, H., et al., *Prediction of Ventricular Tachycardia One Hour before Occurrence Using Artificial Neural Networks*. Scientific Reports, 2016. **6**: p. 32390.
81. Howe, A., et al., *A support vector machine for predicting defibrillation outcomes from waveform metrics*. Resuscitation, 2014. **85**(3): p. 343-9.
82. Maldonado, H., et al., *Post myocardial infarct detection with support vector machine and ECG intervals ratios JTp/JT, Tpe/JTp and Tpe/JT*. 2016. 1-4.
83. Dohare, A.K., et al., *Detection of myocardial infarction in 12 lead ECG using support vector machine*. Applied Soft Computing, 2018. **64**: p. 138-147.
84. Hedén, B., et al., *Acute Myocardial Infarction Detected in the 12-Lead ECG by Artificial Neural Networks*. Circulation, 1997. **96**(6): p. 1798-1802.
85. Lewis, K.M. and K.A. Handal, *Sensible Analysis of the 12-lead ECG*. 2000: Delmar Cengage Learning.
86. Hallen, J., *Troponin for the estimation of infarct size: what have we learned?* Cardiology, 2012. **121**(3): p. 204-12.
87. Hajar, R., *Evolution of Myocardial Infarction and its Biomarkers: A Historical Perspective*. Heart Views : The Official Journal of the Gulf Heart Association, 2016. **17**(4): p. 167-172.
88. Field, A., *Discovering statistics using IBM SPSS statistics*. 2013: sage.
89. Xia, D., et al. *Classification of ventricular tachycardia and fibrillation based on the lempel-ziv complexity and EMD*. in *International Conference on Intelligent Computing*. 2014. Springer.
90. Samie, F.H. and J. Jalife, *Mechanisms underlying ventricular tachycardia and its transition to ventricular fibrillation in the structurally normal heart*. Cardiovascular Research, 2001. **50**(2): p. 242-250.
91. Kantelhardt, J.W., et al., *Multifractal detrended fluctuation analysis of nonstationary time series*. Physica A: Statistical Mechanics and its Applications, 2002. **316**(1): p. 87-114.
92. Van der Waal, J., *Masterthesis - Detrended fluctuation analysis*.
93. Platt, J., *Probabilistic Outputs for Support Vector Machines and Comparisons to Regularized Likelihood Methods*. Vol. 10. 2000.
94. Park, S.H., et al., *Receiver Operating Characteristic (ROC) Curve: Practical Review for Radiologists*. Korean Journal of Radiology, 2004. **5**(1): p. 11-18.
95. Fawcett, T., *An introduction to ROC analysis*. Pattern recognition letters, 2006. **27**(8): p. 861-874.
96. Franc, V., *Support Vector Machines as Probabilistic Models*. Proceedings of the 28th International Conference on Machine Learning (2011), 2011.
97. Mathworks. *perfcurve*. Available from: <https://nl.mathworks.com/help/stats/perfcurve.html>.
98. Schisterman, E.F., et al., *Optimal cut-point and its corresponding Youden Index to discriminate individuals using pooled blood samples*. Epidemiology, 2005. **16**(1): p. 73-81.

Appendix

Part A

<i>A.1 Detrended fluctuation analysis</i>	68
<i>A.2 Probabilistic outcomes SVM</i>	70
<i>A.3 ROC curve</i>	72

Part B

<i>B.1 Baseline characteristics</i>	75
<i>B.2 VF characteristics for two study groups</i>	77
<i>B.3 Multiclass lead performances</i>	78
<i>B.4 VF characteristics - Gender</i>	80

Part A

A.1 Detrended fluctuation analysis

Several studies have shown that changes in VF waveform characteristics give information about the underlying aetiology and survival. It will be assumed that VF signals during resuscitation seems to be non-stationary [89, 90]. In the recent years detrended fluctuation analysis has become a widely used technique to analyse scaling properties and long-range correlation in non-stationary time series [91]. For this approach the root mean square of an integrated signal is introduced. The DFA procedure consists of six steps, see Figure 27.

1. First the global trend or profile of the original time series is determined by subtracting the mean of the signal.
2. Thereafter, the signal is integrated by taking the cumulative sum of the signal.
3. The resulting signal is divided into non-overlapping equal boxes of length n .
4. In each box the local linear trend is calculated and subtracted from the integrated time series. The signal is now 'detrended'.
5. The root mean square of the detrended signal is calculated, which represents the fluctuation in that box size.
6. This is repeated for several box sizes n .

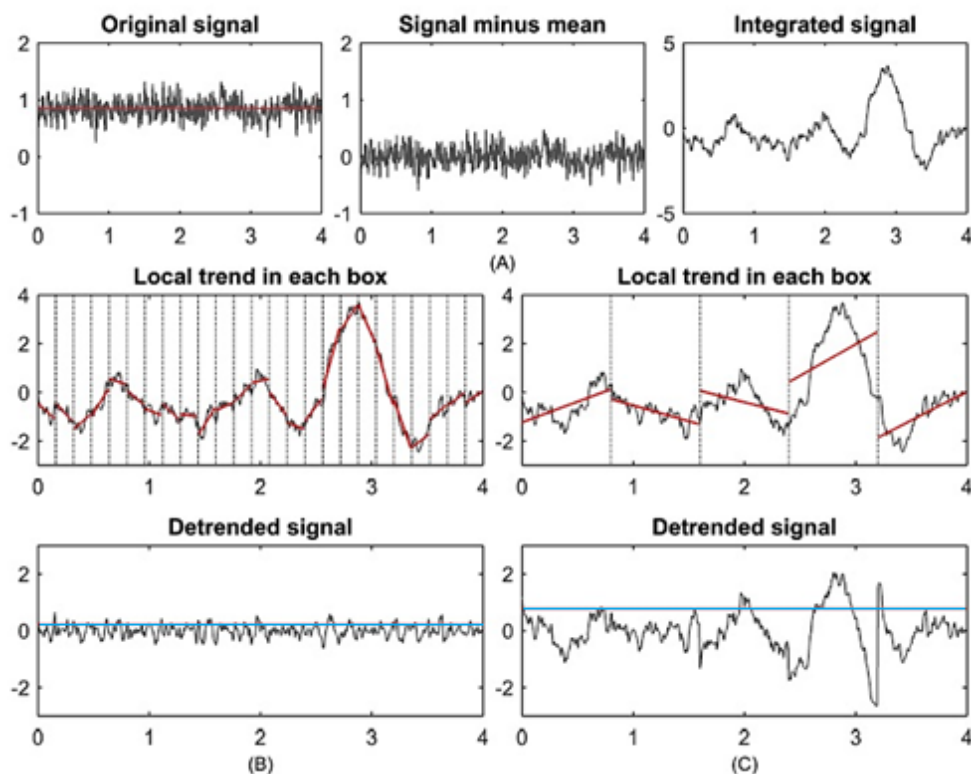


Figure 27. Step-wise approach of detrended fluctuation analysis. In (A) the original signal is shown on the left, whereafter the signal is pre-processed and integrated (mid and right). In (B) and (C) the local trend and detrended signal is determined for smaller box sizes (B) and larger box sizes (C), respectively. The root mean square is represented by the blue line in the bottom figure of (B) and (C). Adapted from [92].

The relation between the fluctuation and box size n is plotted on logarithmic axis. The DFA scaling exponent α is the slope of the trend line of this function. In general, the slope of the DFA curve will give information about the smoothness of the signal (i.e. if α is near 2, the signal is assumed to be smooth and if α is near 0.5 the signal is assumed to be random) [92].

Moreover, different scaling exponents are required for different part of the slope. In case of oscillating signals, the slope should be separated in two slopes for smaller and larger box sizes, α_1 and α_2 , respectively. It is given that the first DFA exponent α_1 gives information about the smoothness for smaller box sizes. When the signal is more noisy or more complex, the exponent α_1 will be smaller than for homogenous signals. In contrast, the second DFA exponent α_2 gives information about the signal for larger box sizes. In case of more noisy or complex signals, the α_2 will be higher than for more homogenous signals. An example for both study groups (no previous MI and previous MI) of the 4.1 second VF segments and corresponding DFA components of lead V5 are shown in Figure 28.

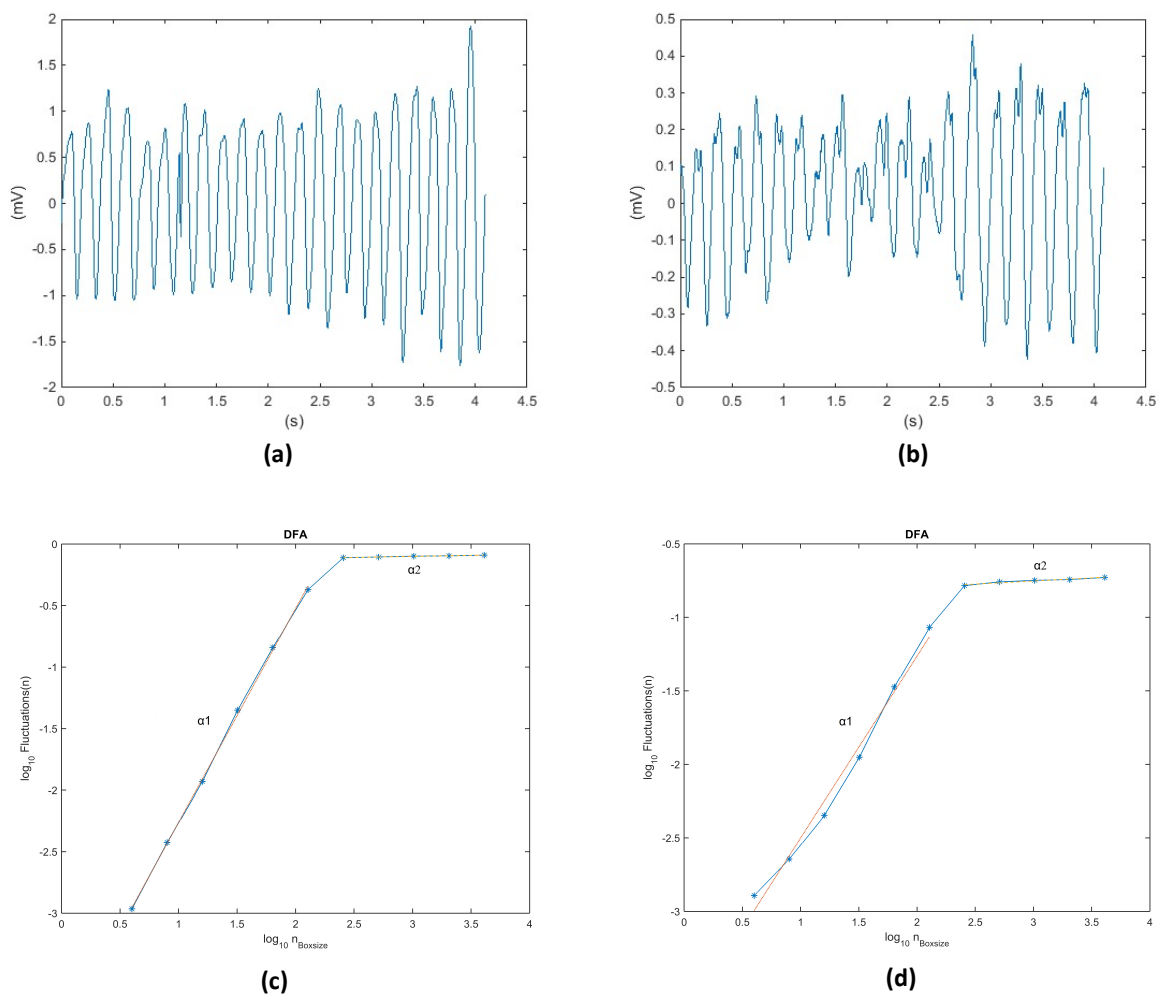


Figure 28. Ventricular fibrillation signal in time domain (above) and corresponding detrended fluctuation analysis (DFA) components α_1 and α_2 (below). In (a) and (c) an example for a patient without previous myocardial (MI) is shown, whereas in (b) and (d) an example for a patient with a history of MI is shown. The mean absolute amplitude (MAA) in the patient without a history of MI (a) is 0.71 mV and in the patient with a previous MI (b) the MAA is 0.15 mV. In (c) the $\alpha_1=1.74$ and $\alpha_2=0.02$, whereas in (d) the $\alpha_1=1.25$ and $\alpha_2=0.04$.

A.2 Probabilistic outcomes SVM

The sigmoid function

The logistic regression function uses a sigmoid function that converts an input into a “probability” value between 0 and 1. To decide whether an output belongs to one of the two possible classes, the model uses a threshold typically at 0.5. Consequently, it follows that outputs $P(x) \geq 0.5$ corresponds to class $y=1$ and $P(x) \leq 0.5$ corresponds to class $y=0$. A sigmoid function is defined following formula (17).

$$P(x, a, c) = \frac{1}{1+e^{a(x-c)}}, \quad P \in [0,1] \quad (17)$$

where P is interpreted as a probability which depends on the parameters x , a and c . The sigmoid function is increasing or decreasing, depending on the sign of the parameter a . A plus sign of a means that the sigmoid function is decreasing, see Figure 29. In contrast, a minus sign of parameter a means the function is increasing. The value of a reflects the slope of the function at c , where c is the inflection at $P=0.5$. Moreover, a higher slope a means a smaller range of possibilities P in which the data will be classified, so in that case higher probabilities will be achieved more easily. The inflection point c refers to output ranges to which class they belong, whether $P>0.5$ or $P<0.5$.

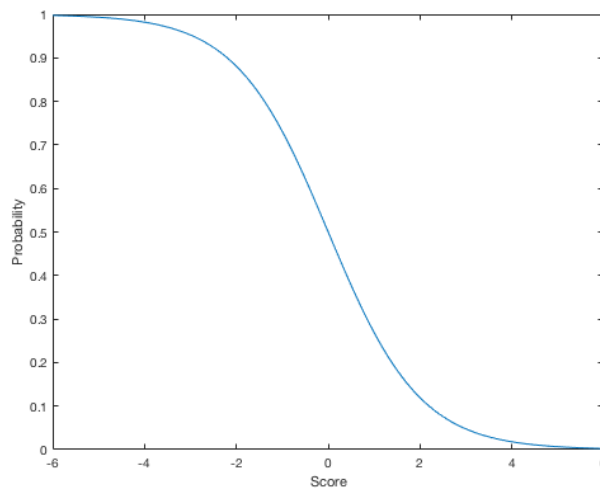


Figure 29. General S-shaped sigmoid function, with probability $P \in [0,1]$.

SVM probabilistic outputs

Constructing a classifier to produce a "probability" to a class can be useful for classification post-processing. However, SVM produces "uncalibrated" output values, known as classification scores. Thus, these classification scores are not probabilities.[93] As previously mentioned; SVM produces from these scores posterior probabilities, which are referred as class membership probabilities and are not induced by probabilistic confidence. Nevertheless, in this sub-analysis they are referred as probabilities. Assume the "uncalibrated" SVM classification scores as:

$$s(x) = h(x) + \beta \quad (18)$$

where

$$h(x, x') = \sum_{i=1}^N \alpha_i y_i \langle \phi(x), \phi(x') \rangle \quad (19)$$

In short, the score for predicting an observation x into the positive class, $s(x)$, is the trained SVM classification function:

$$s(x, x') = \sum_{i=1}^N \alpha_i y_i \langle \phi(x), \phi(x') \rangle + \beta \quad (20)$$

where $(\alpha_1, \dots, \alpha_N)$ are the coefficients of the Lagrange multiplier, where $\alpha_i \in \{0, 1\}$, y is the output, $y \in \{-1, +1\}$, $\langle \phi(x), \phi(x') \rangle$ is the dot product in the feature space between the observation x , where $x \in \mathbb{R}^p$ and the support vectors x' , where $x' \in \mathbb{R}^p$ and β a scalar of the bias of the hyperplane. The sum includes the training set of observations. The SVM classification score for the negative class is $-s(x)$. The SVM classification score for an observation x is the signed distance from x to the hyperplane ranging from $-\infty$ to $+\infty$. Thereby, a positive score indicated that the observation x is predicted to be in that class. A negative score indicates otherwise.

In machine learning *Platt* scaling is a way of transforming the classification score outputs into a probability $P(\text{class}|\text{input})$ distribution over classes, using formula (21) [93]. Platt scaling is based on a logistic regression model of the SVM classification scores and has been shown to be effective for SVM models. For example, in binary classification we determined for inputs $h(x)$ whether they belong to class 0 (no MI) or 1 (MI), arbitrarily labelled as +1 and -1:

$$P(\text{class}|\text{input}) = P(y = 1|x) = \frac{1}{1 + e^{-a(s(x)-c)}} \quad (21)$$

By converting the SVM scores $s(x)$ using a given sigmoid function of the model, the probabilities of the outputs can be measured following formula (21).

A.3 ROC curve

Introduction

To evaluate model performances, the receiver operating characteristics (ROC) curve will be introduced. The ROC curve is defined as a plot of the relation between the sensitivity and the 1 -specificity. Thereby the sensitivity is plotted on the y -axis and the 1 -specificity (also known as false positive rate) on the x -axis. The x -axis and y -axis both have values ranging from 0 to 1. The ROC curve is an effective method of evaluating the performance of diagnostic tests [94, 95]. To describe the full variation in diagnostic performance of a test, multiple pairs of sensitivity and specificity are required. Every pair has their own cut-off level to define the positive and negative test results. As the cut-off level decreases, the sensitivity increases while the specificity decreases and vice versa. To deal with these multiple pairs of sensitivity and specificity, a graph can be drawn using these sensitivities and specificities [94]. Each point on the graph is called an operating point. The ROC curve display the sensitivity and specificity at all cut-off levels and can therefore assess the performance of a test independently of the decision threshold.

One of the most used quantitative indices associated with the ROC curve is the AUC. The AUC is a measure of the overall performance of a test. Trapezoidal integration is used to calculate the AUC. The closer the AUC is to 1, the better the performance of the test.

SVM classifier

By varying the cut-off levels of the classification scores from the minimum to the maximum score, a ROC can be performed for the classification of a previous MI. Since the ROC curve is built up from all cut-off levels, the number of steps in the curve is equal to the number of patients. By running the model several (x) times, the ROC curve will get smoother.

Optimal operating point

Since a high AUC does not guarantee high accuracy of the prediction, an optimal operating point is introduced. Logically, the point on the ROC curve closest to (0,1) tends to have high sensitivity and specificity. In general, the point on the ROC curve with the minimum distance to the point (0,1) corresponds to the “optimal” operating point. [70] Nevertheless, SVM assumes another point to be optimal, in case of imbalanced data. This will be further explained in this section.

In general, classification algorithms assume balanced class distributions and equal misclassification costs. However, recent years there has been interest in class-imbalanced data. As the name suggests, class-imbalanced data refer to a dataset where the number of samples in each class differs. Consider a dataset with P positive cases and N negative cases. Define $\beta = P/(P+N)$ as the proportion of positive class in the dataset, $\beta \in [0,1]$. For balanced data β is equal to 0.5, which is equivalent to maximizing the sensitivity and specificity on the ROC curve. However, for imbalanced data the overall accuracy will be biased due to maximizing the specificity more than the sensitivity or vice versa. For example, when β approaches 0 (e.g. in case of low prevalence), the specificity will be maximized more than the sensitivity, and vice versa as β approaches 1. [70] In view of the above, a cost function is introduced. A cost function is defined as the costs for correct and incorrect classifications and defined as

$$\text{cost for } \begin{bmatrix} TN & FP \\ FN & TP \end{bmatrix} \quad (22)$$

The SVM default assumes that the costs for both classes are equal and no costs are given to correct classifications, in other words

$$\text{cost} \begin{bmatrix} TN & FP \\ FN & TP \end{bmatrix} = \begin{bmatrix} 0 & 1 \\ 1 & 0 \end{bmatrix} \quad (23)$$

In order to this equal costs, it implies balanced data and therefore the (posterior) probability of the model as uniform (i.e. $P(x|y)=0.5$, see **Appendix A.2**). It is known that SVM often do not work if class distribution is highly imbalanced. To deal with this, SVM use higher costs for the class which is less represented in the data [96]. In view of this, the optimal operating point for imbalanced data differ from that of balanced data.

To overcome the class imbalance data problem, the SVM classifier uses another strategy to select the optimal operating point, using formula (24). The optimal operating point of the ROC curve is returned as a 1-by-2 array as the sensitivity and 1-specificity on the ROC curve. To obtain the optimal operating point, first a slope S is found, using formula (24) [97]:

$$S = \frac{\text{cost}(FP) - \text{cost}(TN)}{\text{cost}(FN) - \text{cost}(TP)} \cdot \frac{N}{P} \quad (24)$$

where $\text{cost}(FN)$ is the cost of misclassifying a positive class as a negative class and $\text{cost}(FP)$ is the cost of misclassifying a negative class as a positive class. P are the total samples in the positive class ($TP + FN$) and N the samples in the negative class ($TN + FP$). Usually, no costs are given to correct classifications, therefore, $\text{cost}(TP)=0$ and $\text{cost}(TN)=0$.

Now the optimal operating point is found by moving a straight line with slope S from the upper left corner (0,1) down to the right, until it intersects the ROC curve. This intersection is defined as the optimal operating point. [97] Moreover, using a default slope $S=1$, the optimal operating point is the defined as the smallest distance to the upper left corner. The first intersect with the ROC curve for a slope S of 1 is known as the Youden's index [98]. This index gives equal costs to false positive and false negative values and suggested only in case of balanced data. Furthermore, from formula (24) it can be seen that in case of equal costs of the FN and FP, the prevalence of the positives may play an important role. Generally, it can be concluded that higher values of the slope S lead to higher specificity, but lower sensitivity and vice versa. In other words, a higher slope results in a lower number of false positives (FP), but at the expense of more false negatives (FN).

In our study the cost(FP) and cost(FN) are set equal. Hence, the ratio of numbers of N and P play a role in the optimal operating point approach. From the formula (24) it can be derived that the slope in our study is $S= N/P = 88/101 = 0.87$. Since, there is a minority of negatives, the sensitivity may be more relevant compared to the case of balanced negatives and positives, see Figure 30. We want to avoid a **previous MI** classified as **no MI**, thus we want the sensitivity to be very high. In addition, the slope for balanced data ($S=1$) is given in Figure 30.

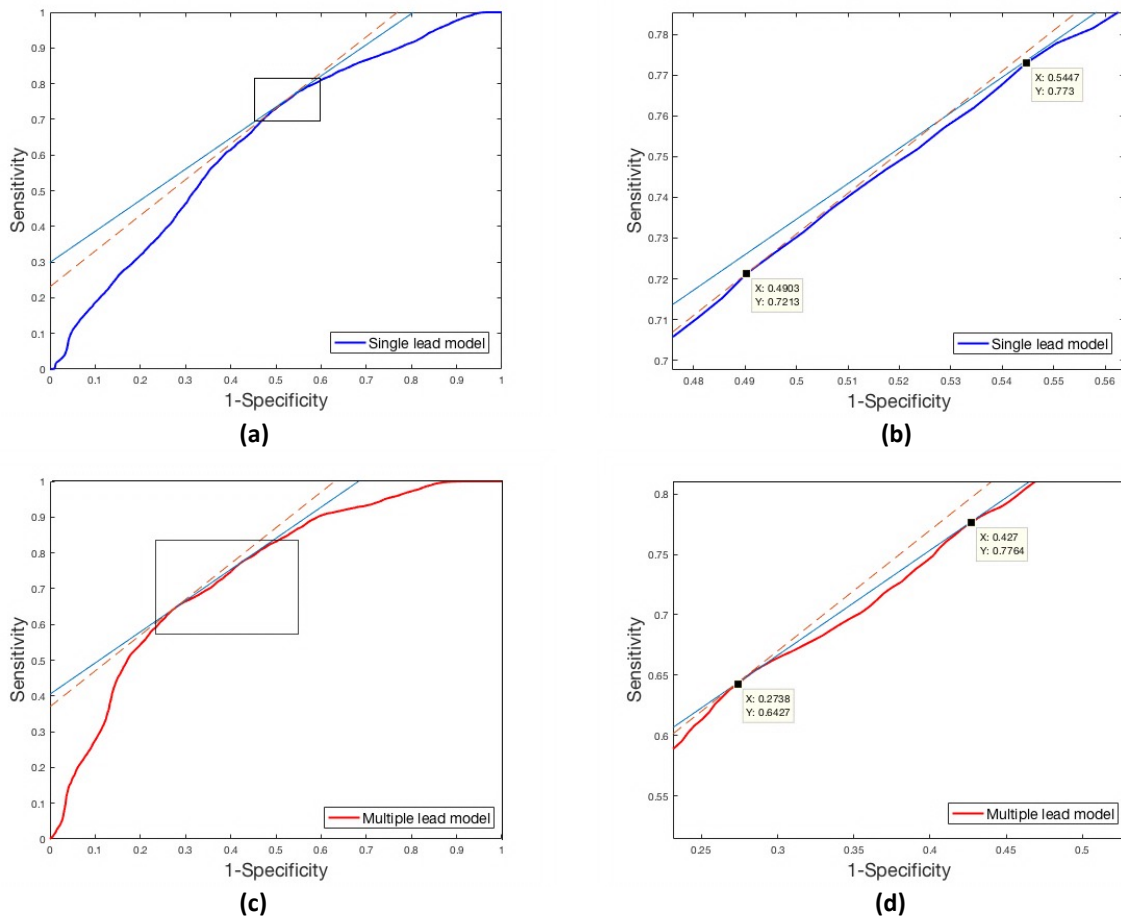


Figure 30. Slopes measuring the operating points on the receiver operating characteristic (ROC) curves of the single lead model (above) and multiple lead model (below). In (a) and (c) our chosen slope $S=0.87$ (blue straight line) and the default slope $S=1$ (dotted orange line) are both shown. In (b) and (d) a zoomed window is shown to specify the optimal operating points on the ROC curve for both slopes $S=0.87$ and $S=1$.

Part B

B.1 Baseline characteristics

Study patients

Table 15. Baseline characteristics of the study patients. Values are presented as N (%), median (IQR), mean \pm SD or median \pm IQR. Differences were tested using the Student t-test or Mann-Whitney U test, whichever appropriate.

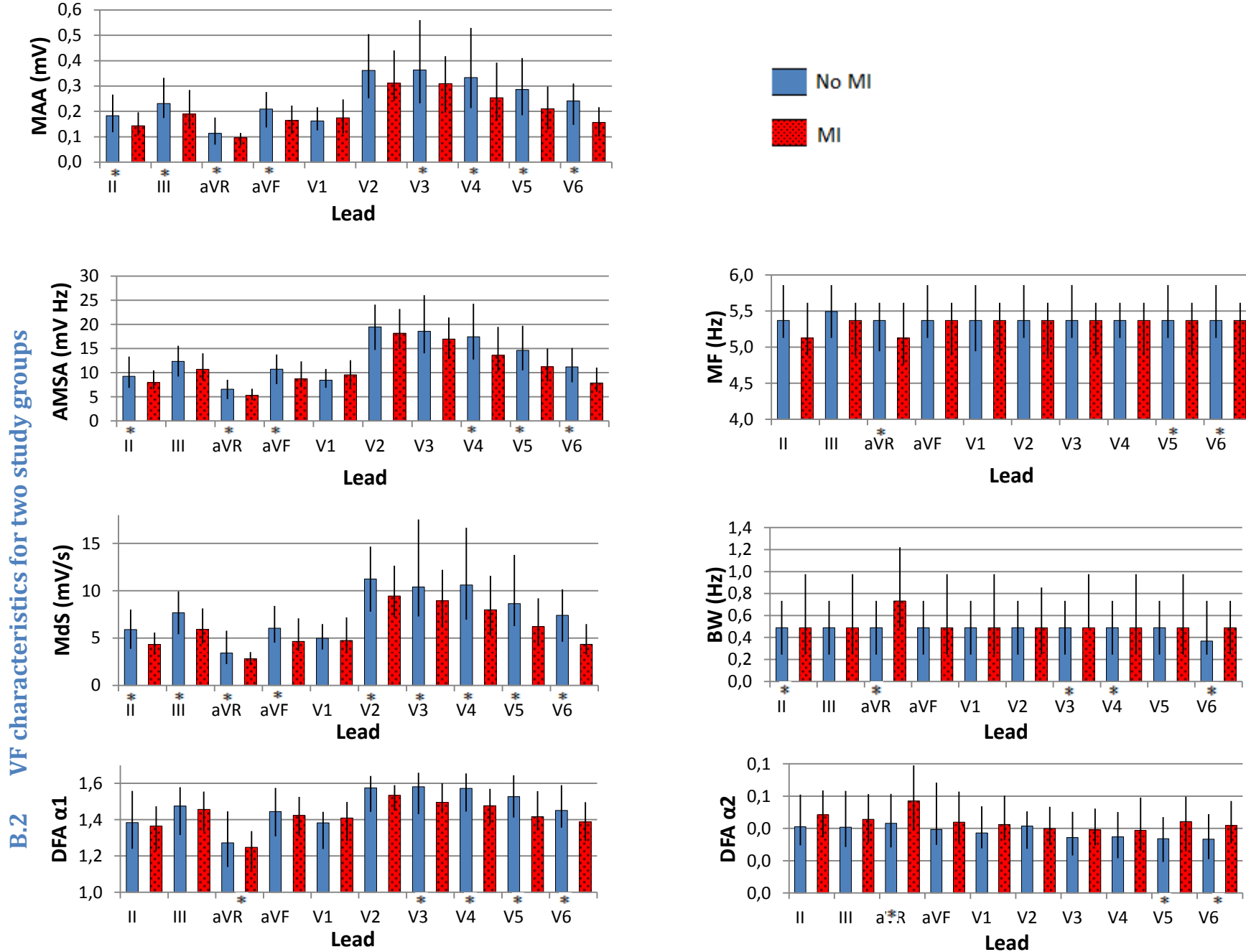
Baseline characteristics – Study patients			
	No previous MI (n=88)	Previous MI (n=101)	p-value
Sex			
Men	56 (64%)	85 (84%)	0.001
Female	32 (36%)	16 (16%)	
Age at DFT (yr)	59 (48-68)	67 (60-75)	<0.001
Length (cm)	174 \pm 10	173 \pm 8	0.465
Weight (kg)	76 (65-89)	80 (73-88)	0.133
BMI (kg/m ²)	26 \pm 4	27 \pm 4	0.073
LVEF (%)	33 (26-46)	35 (29-44)	0.409
Prevention			
Primary	64 (73%)	58 (57%)	0.027
Secondary	24 (27%)	43 (43%)	
VF	16 (18%)	36 (36%)	0.006
Shock success			
Unsuccessful	19 (22%)	13 (13%)	0.117
Successful	69 (78%)	88 (87%)	
Hypertension	30 (34%)	41 (41%)	0.332
Diabetes	17 (19%)	26 (26%)	0.276
Atrial fibrillation	26 (30%)	31 (31%)	0.865
Coronary heart disease	6 (7%)	96 (95%)	<0.001
Medication			
Beta blocker	76 (86%)	93 (92%)	0.212
ACE inhibitor	59 (67%)	83 (82%)	0.018
ARB	15 (17%)	9 (9%)	0.101
Aldosteron antagonist	31 (35%)	43 (43%)	0.303
Diuretics	41 (47%)	50 (50%)	0.691
Calcium channel blockers	6 (7%)	7 (7%)	0.976
ASA	30 (34%)	73 (72%)	<0.001
Clopidogrel	8 (9%)	32 (32%)	<0.001
Antiplatelet therapy	33 (38%)	78 (77%)	<0.001
Anticoagulation	35 (40%)	41 (41%)	0.909
Anti thrombotics	60 (68%)	100 (99%)	<0.001
Cholesterol reducer	35 (40%)	89 (88%)	<0.001
Antiarrhythmics	10 (11%)	17 (17%)	0.281
Sotalol	1 (1%)	2 (2%)	0.645

New cohort patients

Table 16. Baseline characteristics of new cohort of patients. Values are presented as N (%), median (IQR), mean \pm SD or median \pm IQR. Differences were tested using the Student t-test or Mann-Whitney U test, whichever appropriate.

Baseline characteristics – New cohort patients			
	No previous MI (n=19)	Previous MI (n=18)	p-value
Sex			
Men	16 (84%)	12 (67%)	0.229
Female	3 (16%)	6 (33%)	
Age at DFT (yr)	62 (55-69)	69 (57-74)	0.019
Length (cm)	178 \pm 8	172 \pm 8	0.070
Weight (kg)	83 (70-98)	84 (80-93)	0.949
BMI (kg/m²)	27 \pm 5	29 \pm 6	0.436
LVEF (%)	35 (28-58)	43 (35-54)	0.662
Prevention			
Primary	8 (42%)	4 (22%)	0.205
Secondary	9 (58%)	14 (78%)	
VF	6 (32%)	8 (44%)	0.434
Shock success			
Unsuccessful	0	0 (0%)	-
Successful	19 (100%)	17 (100%)	
Hypertension	7 (37%)	11 (61%)	
Diabetes	2 (11%)	5 (28%)	0.196
Atrial fibrillation	1 (5%)	4 (22%)	0.148
Coronary heart disease	1 (5%)	17 (94%)	<0.001
Medication			
Beta blocker	16 (84%)	15 (83%)	0.994
ACE inhibitor	10 (53%)	12 (67%)	0.399
ARB	3 (16%)	2 (11%)	0.688
Aldosteron antagonist	8 (42%)	4 (22%)	0.205
Diuretics	7 (37%)	6 (33%)	0.829
Calcium channel blockers	1 (5%)	2 (11%)	0.528
ASA	7 (37%)	5 (28%)	0.569
Clopidogrel	1 (5%)	4 (22%)	0.148
Antiplatelet therapy	0	8 (44%)	<0.001
Anticoagulation	7 (37%)	11 (61%)	0.148
Anti thrombotics	1 (5%)	0	0.331
Cholesterol reducer	9 (47%)	14 (78%)	0.058
Antiarrhythmics	1 (5%)	3 (17%)	0.285
Sotalol	0	0	-

Figure 31. VF characteristics of all 10 leads for the two study groups. Values are presented as median (IQR). Differences between the groups were tested using a Mann-Whitney U test. * = P<0.05



B.3 Multiclass lead performances

One-vs-one approach

Table 17. One-versus-one approach for multiclass classification for both, a linear and a Gaussian SVM model. For the Gaussian SVM, the optimal SVM is a medium Gaussian SVM ($K=VP$), where P is set to be 2.6, 3.7, 4.6 and 8.4 for the single lead, two leads, three leads and ten leads, respectively.

Performances – One-vs-one approach

Inferior lead	Anterior lead	Right side	AUC Linear SVM model			AUC Gaussian SVM model		
			No MI	Inf MI	Ant MI	No MI	Inf MI	Ant MI
II			0.58	0.75	0.55	0.59	0.73	0.59
II	V3		0.63	0.73	0.78	0.65	0.75	0.79
II	V2	V1	0.66	0.77	0.67	0.64	0.75	0.61
	V2	aVR	0.64	0.75	0.68	0.65	0.73	0.65
	V3	V1	0.72	0.76	0.78	0.70	0.80	0.77
	V3	aVR	0.66	0.77	0.72	0.67	0.75	0.75
	V4	V1	0.71	0.74	0.73	0.72	0.74	0.74
	V4	aVR	0.66	0.73	0.73	0.67	0.74	0.77
	V5	V1	0.70	0.77	0.73	0.69	0.72	0.72
	V5	aVR	0.63	0.71	0.72	0.66	0.72	0.73
	V6	V1	0.72	0.72	0.64	0.73	0.70	0.64
	V6	aVR	0.68	0.74	0.71	0.69	0.70	0.72
III	V2	V1	0.57	0.72	0.69	0.56	0.67	0.63
	V2	aVR	0.59	0.72	0.70	0.64	0.71	0.62
	V3	V1	0.63	0.71	0.80	0.62	0.69	0.75
	V3	aVR	0.61	0.75	0.78	0.60	0.72	0.73
	V4	V1	0.67	0.69	0.76	0.65	0.68	0.72
	V4	aVR	0.66	0.70	0.78	0.64	0.70	0.74
	V5	V1	0.70	0.70	0.75	0.68	0.60	0.68
	V5	aVR	0.65	0.66	0.72	0.65	0.66	0.67
	V6	V1	0.69	0.68	0.71	0.68	0.65	0.66
	V6	aVR	0.65	0.65	0.69	0.65	0.63	0.66
aVF	V2	V1	0.67	0.77	0.70	0.64	0.73	0.63
	V2	aVR	0.61	0.76	0.69	0.66	0.75	0.67
	V3	V1	0.72	0.75	0.81	0.70	0.75	0.78
	V3	aVR	0.67	0.74	0.81	0.63	0.71	0.80
	V4	V1	0.66	0.75	0.74	0.67	0.71	0.73
	V4	aVR	0.68	0.72	0.77	0.63	0.69	0.75
	V5	V1	0.68	0.71	0.75	0.66	0.65	0.71
	V5	aVR	0.68	0.74	0.77	0.67	0.69	0.76
	V6	V1	0.69	0.72	0.66	0.70	0.68	0.65
	V6	aVR	0.68	0.68	0.67	0.69	0.66	0.68
10-Lead		K=8,4 K=33	0.71	0.73	0.75	0.70 0.67	0.72 0.76	0.77 0.78

One-vs-all approach

Table 18. One-versus-all approach for multiclass classification for both, a linear and a Gaussian SVM model. For the Gaussian SVM, the optimal SVM is a medium Gaussian SVM ($K=VP$), where P is set to be 2.6, 3.7, 4.6 and 8.4 for the single lead, two leads, three leads and ten leads, respectively.

Performances – One-vs-all approach

Inferior lead	Anterior lead	Right side	AUC Linear SVM model			AUC Gaussian SVM model		
			No MI	Inf MI	Ant MI	No MI	Inf MI	Ant MI
II			0.62	0.71	0.46	0.59	0.69	0.46
II	V3		0.66	0.73	0.74	0.64	0.72	0.76
II	V2	V1	0.71	0.75	0.68	0.72	0.78	0.62
	V2	aVR	0.69	0.78	0.69	0.68	0.77	0.64
	V3	V1	0.73	0.73	0.76	0.73	0.76	0.73
	V3	aVR	0.64	0.72	0.66	0.63	0.73	0.70
	V4	V1	0.71	0.73	0.71	0.72	0.75	0.68
	V4	aVR	0.67	0.70	0.71	0.66	0.71	0.73
	V5	V1	0.72	0.72	0.71	0.71	0.71	0.68
	V5	aVR	0.68	0.70	0.68	0.68	0.73	0.69
	V6	V1	0.75	0.69	0.61	0.73	0.68	0.62
	V6	aVR	0.66	0.72	0.68	0.67	0.66	0.71
III	V2	V1	0.59	0.69	0.64	0.65	0.68	0.60
	V2	aVR	0.62	0.70	0.67	0.65	0.73	0.59
	V3	V1	0.66	0.70	0.79	0.66	0.68	0.74
	V3	aVR	0.63	0.74	0.74	0.62	0.71	0.69
	V4	V1	0.67	0.67	0.76	0.66	0.65	0.70
	V4	aVR	0.67	0.7	0.74	0.66	0.69	0.72
	V5	V1	0.72	0.67	0.73	0.69	0.58	0.66
	V5	aVR	0.65	0.66	0.71	0.65	0.66	0.67
	V6	V1	0.69	0.66	0.70	0.69	0.65	0.62
	V6	aVR	0.62	0.63	0.68	0.65	0.59	0.66
aVF	V2	V1	0.69	0.76	0.66	0.68	0.73	0.57
	V2	aVR	0.63	0.74	0.64	0.66	0.75	0.63
	V3	V1	0.72	0.73	0.78	0.71	0.76	0.75
	V3	aVR	0.66	0.72	0.76	0.64	0.72	0.78
	V4	V1	0.67	0.72	0.72	0.69	0.70	0.71
	V4	aVR	0.66	0.66	0.69	0.63	0.68	0.71
	V5	V1	0.68	0.67	0.74	0.7	0.64	0.71
	V5	aVR	0.69	0.74	0.73	0.7	0.71	0.73
	V6	V1	0.70	0.68	0.67	0.73	0.68	0.64
	V6	aVR	0.68	0.68	0.64	0.71	0.65	0.69
10-Lead		K=8,4 K=33	0.73	0.72	0.75	0.70 0.63	0.70 0.68	0.73 0.67

B.4 VF characteristics - Gender

Binary classification

Table 19. Amplitude characteristics of all 10 leads for the two study groups for both men and women. Differences were analysed using a Mann-Whitney U-test, * = P<0.05.

Amplitude characteristics – Binary - Gender						
Study groups						
	No MI			MI		
	<i>Men (n=56)</i>	<i>Women (n=32)</i>		<i>Men (n=85)</i>	<i>Women (n=16)</i>	
	<i>Median</i>	<i>Median</i>	<i>p-value</i>	<i>Median</i>	<i>Median</i>	<i>p-value</i>
MAA_II	.18 (.11-.27)	.19 (.14-.27)	.319	.14 (.10-.18)	.21 (.13-.26)	.048*
AMSA_II	8.89 (6.74-13.08)	11.01 (7.92-13.85)	.182	7.70 (6.52-9.47)	10.85 (7.97-12.97)	.009*
MAA_III	.22 (.17-.30)	.25 (.19-.36)	.160	.18 (.13-.26)	.30 (.18-.38)	.009*
AMSA_III	11.86 (9.09-14.87)	13.45 (9.21-18.60)	.152	10.29 (8.08-13.00)	15.57 (10.33-17.84)	.004*
MAA_aVR	.11 (.07-.17)	.12 (.08-.19)	.349	.09 (.07-.11)	.10 (.07-.12)	.527
AMSA_aVR	5.83 (4.28-8.56)	7.28 (4.84-8.54)	.290	5.25 (4.26-6.63)	5.87 (5.02-6.66)	.157
MAA_aVF	.21 (.13-.27)	.21 (.16-.30)	.212	.15 (.11-.21)	.26 (.15-.32)	.014*
AMSA_aVF	9.68 (7.45-13.29)	11.92 (8.12-16.26)	.171	8.31 (6.66-10.81)	13.35 (8.52-15.15)	.003
MAA_V1	.17 (.13-.22)	.16 (.12-.22)	.931	.18 (.11-.25)	.14 (.11-.19)	.324
AMSA_V1	8.48 (7.06-10.27)	7.85 (6.69-11.09)	.555	9.74 (7.14-13.20)	8.82 (7.14-10.10)	.367
MAA_V2	.37 (.26-.51)	.33 (.23-.46)	.314	.31 (.25-.44)	.32 (.21-.39)	.503
AMSA_V2	20.43 (15.80-24.19)	17.13 (14.24-23.80)	.152	18.68 (15.22-23.12)	17.87 (13.70-23.03)	.615
MAA_V3	.37 (.24-.56)	.32 (.21-.58)	.440	.32 (.21-.43)	.19 (.14-.32)	.002*
AMSA_V3	19.92 (14.44-27.16)	16.74 (12.30-22.20)	.179	18.45 (13.93-21.74)	12.16 (9.81-18.97)	.011*
MAA_V4	.36 (.22-.53)	.30 (.21-.53)	.532	.28 (.19-.41)	.16 (.12-.24)	.001*
AMSA_V4	19.23 (13.79-24.76)	16.09 (11.93-22.11)	.138	15.14 (11.04-19.68)	9.97 (7.49-13.02)	.003*
MAA_V5	.31 (.20-.40)	.27 (.18-.42)	.430	.23 (.16-.33)	.15 (.10-.21)	.003*
AMSA_V5	15.24 (10.93-20.99)	13.28 (10.24-18.21)	.112	11.77 (8.42-15.96)	8.18 (6.71-10.53)	.011*
MAA_V6	.24 (.15-.32)	.24 (.14-.31)	.696	.16 (.11-.22)	.14 (.09-.16)	.104
AMSA_V6	11.61 (8.14-15.29)	10.27 (7.63-14.17)	.302	8.01 (6.09-11.20)	7.16 (5.51-8.65)	.213

Multiclass classification - Men

Table 20. Amplitude characteristics of all 10 leads for the three study groups in men. Values are presented as median (IQR). α = p-value between No MI and Inferior MI (column 1 versus column 2) using a Mann-Whitney U-test; β = p-value between No MI and Anterior MI (column 1 versus column 3) using a Mann-Whitney U-test. * = P<0.05

Men	Amplitude characteristics – Multiclass - Men				
	Study groups			α	β
	No MI (n= 56)	Inferior MI (n=50)	Anterior MI (n=35)		
<i>Median (IQR)</i>	<i>Median (IQR)</i>	<i>Median (IQR)</i>	<i>p-value</i>	<i>p-value</i>	
MAA_II	.18 (.11-.27)	.12 (.09-.15)	.18 (.14-.25)	.000*	.877
AMSA_II	8.89 (6.74-13.08)	7.20 (5.59-8.64)	8.98 (7.70-13.29)	.002*	.870
MAA_III	.22 (.17-.30)	.15 (.12-.23)	.25 (.17-.36)	.001*	.800
AMSA_III	11.86 (9.09-14.87)	9.65 (8.01-11.41)	12.64 (10.11-17.18)	.011*	.794
MAA_aVR	.11 (.07-.17)	.09 (.06-.11)	.10 (.07-.12)	.006*	.348
AMSA_aVR	5.83 (4.28-8.56)	5.06 (3.89-6.33)	5.78 (4.76-7.16)	.022*	.324
MAA_aVF	.21 (.13-.27)	.13 (.11-.18)	.21 (.15-.30)	.000*	.782
AMSA_aVF	9.68 (7.45-13.29)	7.59 (6.55-9.67)	10.22 (8.72-14.43)	.003*	.993
MAA_V1	.17 (.13-.22)	.18 (.11-.22)	.17 (.12-.28)	.879	.387
AMSA_V1	8.48 (7.06-10.27)	9.44 (7.28-11.88)	10.03 (6.79-12.67)	.172	.123
MAA_V2	.37 (.26-.51)	.34 (.26-.45)	.27 (.22-.40)	.455	.010*
AMSA_V2	20.43 (15.80-24.19)	18.85 (15.37-24.80)	17.71 (13.87-20.87)	.859	.088
MAA_V3	.37 (.24-.56)	.35 (.24-.47)	.24 (.17-.34)	.578	.001*
AMSA_V3	19.92 (14.44-27.16)	19.49 (14.41-23.56)	14.71 (10.97-19.10)	.835	.002*
MAA_V4	.36 (.22-.53)	.30 (.20-.43)	.24 (.14-.29)	.197	.002*
AMSA_V4	19.23 (13.79-24.76)	16.27 (12.16-21.93)	12.73 (9.54-15.72)	.222	.000*
MAA_V5	.31 (.20-.40)	.23 (.15-.33)	.18 (.12-.26)	.016*	.003*
AMSA_V5	15.24 (10.93-20.99)	12.33 (8.26-16.35)	10.53 (7.91-13.68)	.015*	.001*
MAA_V6	.24 (.15-.32)	.15 (.10-.22)	.16 (.11-.22)	.001*	.004*
AMSA_V6	11.61 (8.14-15.29)	7.94 (6.00-11.20)	7.77 (6.19-10.57)	.001*	.002*

Multiclass classification - Women

Table 21. Amplitude characteristics of all 10 leads for the three study groups in women. Values are presented as median (IQR). α = p-value between No MI and Inferior MI (column 1 versus column 2) using a Mann-Whitney U-test; β = p-value between No MI and Anterior MI (column 1 versus column 3) using a Mann-Whitney U-test. * = $P < 0.05$

Amplitude characteristics – Multiclass - Women					
Women	Study groups				
	No MI (n=32)	Inferior MI (n=4)	Anterior MI (n=12)	α	β
	<i>Median (IQR)</i>	<i>Median (IQR)</i>	<i>Median (IQR)</i>	<i>p-value</i>	<i>p-value</i>
MAA_II	.19 (.14-.27)	.10 (.07-.13)	.24 (.17-.30)	.010*	.317
AMSA_II	11.01 (7.92-13.85)	7.11 (5.88-7.28)	12.25 (9.33-14.21)	.035*	.370
MAA_III	.25 (.19-.36)	.18 (.13-.23)	.36 (.25-.40)	.087	.216
AMSA_III	13.45 (9.21-18.60)	10.19 (9.74-10.71)	17.01 (14.56-18.43)	.191	.225
MAA_aVR	.12 (.08-.19)	.07 (.06-.08)	.11 (.09-.12)	.039*	.280
AMSA_aVR	7.28 (4.84-8.54)	4.94 (4.22-5.14)	6.24 (5.67-7.38)	.078	.510
MAA_aVF	.21 (.16-.30)	.14 (.09-.17)	.28 (.21-.35)	.024*	.257
AMSA_aVF	11.92 (8.12-16.26)	8.25 (7.42-8.30)	14.05 (11.91-15.79)	.070	.206
MAA_V1	.16 (.12-.22)	.12 (.10-.16)	.15 (.11-.23)	.208	.693
AMSA_V1	7.85 (6.69-11.09)	8.16 (6.16-9.32)	9.34 (7.37-11.01)	.725	.562
MAA_V2	.33 (.23-.46)	.37 (.35-.41)	.28 (.17-.37)	.546	.225
AMSA_V2	17.13 (14.24-23.80)	21.21 (16.18-26.08)	17.35 (12.31-21.39)	.392	.854
MAA_V3	.32 (.21-.58)	.26 (.16-.39)	.18 (.14-.29)	.365	.008*
AMSA_V3	16.74 (12.30-22.20)	16.04 (10.29-22.15)	12.16 (9.53-16.75)	.615	.040*
MAA_V4	.30 (.21-.58)	.15 (.11-.24)	.16 (.12-.24)	.063	.003*
AMSA_V4	16.09 (11.93-22.11)	10.05 (7.35-16.95)	9.97 (7.67-12.29)	.174	.006*
MAA_V5	.27 (.18-.42)	.11 (.09-.20)	.16 (.11-.21)	.050	.002*
AMSA_V5	13.28 (10.24-18.21)	7.03 (6.65-10.94)	8.71 (7.24-10.53)	.050	.012*
MAA_V6	.24 (.14-.31)	.09 (.07-.13)	.15 (.11-.19)	.018*	.018*
AMSA_V6	10.27 (7.63-14.17)	5.64 (5.03-6.54)	7.87 (6.29-9.63)	.010*	.054

